

WestminsterResearch

<http://www.westminster.ac.uk/research/westminsterresearch>

Structure-function studies of the Parkinsonism-linked protein DJ-1

Marc Rhyan Anthony Puno

Faculty of Science and Technology

This is an electronic version of a PhD thesis awarded by the University of Westminster. © The Author, 2014.

This is an exact reproduction of the paper copy held by the University of Westminster library.

The WestminsterResearch online digital archive at the University of Westminster aims to make the research output of the University available to a wider audience. Copyright and Moral Rights remain with the authors and/or copyright owners.

Users are permitted to download and/or print one copy for non-commercial private study or research. Further distribution and any use of material from within this archive for profit-making enterprises or for commercial gain is strictly forbidden.

Whilst further distribution of specific materials from within this archive is forbidden, you may freely distribute the URL of WestminsterResearch: (<http://westminsterresearch.wmin.ac.uk/>).

In case of abuse or copyright appearing without permission e-mail repository@westminster.ac.uk

Structure-function studies of the
Parkinsonism-linked protein DJ-1

Marc Rhyan Anthony Puno

A thesis submitted in partial fulfilment of the
requirements of the University of Westminster
for the degree of Doctor of Philosophy

March 2014

Abstract

DJ-1 is a multifunctional protein linked to familial Parkinson's disease. DJ-1 has been suggested to exert its cytoprotective function, in part, by acting as a copper carrier that can sequester the reactive metal and/or provide the copper cofactor for the activation of the Cu-Zn superoxide dismutase (SOD1). Using absorption spectroscopy and mass spectrometry, we found that DJ-1 binds one Cu(I) ion per DJ-1 homodimer. The structure of Cu(I)-bound DJ-1 reveals a new biscysteinate metal binding motif formed by juxtaposed Cys-53 at the homodimer interface. We calculated a subfemtomolar dissociation constant ($K_d = 6.41 \times 10^{-16}$ M) for Cu(I) that supports the physiological intracellular retention of the metal. Cu(I)-bound DJ-1 was not capable of interacting and activating SOD1 *in vitro*. We posit that DJ-1 sequester copper to protect against metal-induced cytotoxicity. Our results illuminate the molecular basis on how disease-linked mutations that impairs homodimerisation could disrupt the metal binding site.

In the second part of this dissertation, we sought to determine the impact of a Parkinsonism-linked A107P mutation on DJ-1 structure and glyoxalase activity. The A107P variant abrogates the ability of DJ-1 to protect against glyoxal-induced cytotoxicity and carboxymethyllysine protein modification. A crystal structure of DJ-1 C106S variant with glycerol and sulphate bound in the active site suggests that Ala-107 is critical for the stabilization of the transition state of the nucleophilic addition step. In our hands, the protein levels of DJ-1 A107P mutant in SH-SH5Y cells were ostensibly similar to the wild-type level but reduced levels were found in HEK 293E and MEF cells. Using CD and NMR spectroscopy, we found that the structural defect caused by the mutation extends beyond the active site. The A107P mutation resulted in a remarkable misfolding of the protein providing a basis for the reduced intracellular protein level and the abrogation of enzymatic activity.

List of publications

1. Puno, M.R., Patel, N.A., Moller, S.G., Robinson, C.V., Moody, P.C.E., and Odell, M. (2013) 'Structure of Cu(I)-bound DJ-1 reveals a biscysteinate metal binding site at the homodimer interface: insights into functional inactivation of DJ-1 in Parkinsonism' *Journal of the American Chemical Society*, 135 (43), 15974 – 15977.
2. Puno, M.R., Rannikko, E., Peiris, D., Sula, A., Moller, S.G., Moody, P.C.E., Kahle, P. and Odell, M. 'Structural and functional analysis of the Parkinsonism-linked A107P mutation of DJ-1' *Journal of Biological Chemistry*, to be submitted.
3. Piston, D., Alvarez-Erviti, L., Gargano, D., Yao, Z., Szabadkai, G., Taanman, J.W., Odell, M., Puno, M.R., Bjorkblom, B., Maple-Groden, J., Larsen, J.P., Moller, S.G., Schapira, A.H.V., Gegg, M.E. 'DJ-1 forms redox sensitive high molecular weight protein complexes involved in RNA metabolism' manuscript in preparation.
4. Puno, M.R., Bjorkblom B., Patel, N.A., Moody, P.C.E., Milton, N.G.N., Robinson, C.V., Moller, S.G., and Odell, M. 'On the role of DJ-1 in metal sequestration and SOD1 activation' manuscript in preparation.

Table of Contents

Abstract	2
List of publications	3
List of Abbreviations	7
List of Figures	10
List of Tables	12
Acknowledgement	13
Author's declaration	15
Chapter 1 General Introduction	16
1.1 Introduction to Parkinson's disease	17
1.1.1 Parkinson's disease	17
1.1.2 Pathophysiology of PD	17
1.1.3 Pathways associated with PD pathogenesis	19
1.1.3.1 Oxidative Stress	20
1.1.3.2 Mitochondrial dysfunction	21
1.1.3.3 Proteotoxic stress	21
1.1.4 Causative agents and risk factors	22
1.1.4.1 Exposure to agricultural chemicals	22
1.1.4.2 Exposure to metals	23
1.1.4.3 Genetics	24
1.2 Introduction to DJ-1	26
1.2.1 The <i>DJ-1</i> gene and its product	26
1.2.2. DJ-1 and PD	29
1.2.3 Biological activities of DJ-1	30
1.2.3.1 Peroxiredoxin-like peroxidase	30
1.2.3.2 Transcriptional regulation	31
1.2.3.3 Molecular chaperone	33
1.2.3.4 RNA binding	34
1.2.3.5 Weak protease activity	34
1.2.3.6 Copper binding and activation of SOD1	34
1.2.3.7 Cofactor-independent glyoxalase	36
1.3 Aims	41
Chapter 2 Structural basis for the interaction of DJ-1 with Cu(I)	42
2.1 Introduction	43
2.2 Results	45
2.2.1 Recombinant protein expression and purification of human DJ-1	45
2.2.2 Electronic absorption spectroscopy indicates that Cu(I) is coordinated through S_{γ}	46
2.2.3 DJ-1 interacts with Cu(I) as a $Cu^I(DJ-1)_2$ complex	47
2.2.4 Crystal structure of Cu(I)-bound DJ-1 reveals a new copper binding motif	51
2.2.5 DJ-1 binds Cu(I) with subfemtomolar affinity	58
2.2.6 DJ-1 does not stimulate the activity of SOD1 <i>in vitro</i>	59

2.2.7 DJ-1 does not interact with SOD1	61
2.3 Discussion	65
Chapter 3 Structural and functional characterisation of the Parkinsonism-linked DJ-1 A107P mutation	71
3.1 Introduction	72
3.2 Results	75
3.2.1 Bacterial expression of DJ-1 A107P variant	75
3.2.2 A107P mutation abolishes DJ-1 glyoxalase activity	77
3.2.3 Clues on the catalytic role of Ala-107 from <i>in silico</i> analysis and the crystal structure of DJ-1 bound to SO ₄ ²⁻ and glycerol	81
3.2.4 Intracellular steady-state levels of DJ-1 ^{A107P}	87
3.2.5 The A107P mutation leads to DJ-1 misfolding	89
3.3 Discussion	92
Chapter 4 Discussion and Outlook	97
4.1 Biological role of the copper binding site	98
4.2 Structure of Cu(I)-bound DJ-1 establishes the role for DJ-1 homodimerisation in copper sequestration: insights into mutational inactivation of DJ-1 in PD	101
4.3 Molecular basis for the pathogenicity of the DJ-1 A107P mutation	104
4.5 Role of the nucleophile elbow motif in the structural integrity of the DJ-1 fold	106
4.4 Crystal structure of DJ-1 C106S bound to a sulphate anion and glycerol illuminates the mechanism of substrate recruitment and hemithioacetal intermediate formation	110
4.5 Future work	114
Chapter 5 Materials and Methods	116
5.1 Bacterial strains	116
5.2 Plasmid constructs and primers	117
5.3 Media, buffers, and solutions	119
5.4 Molecular biology methods	119
5.4.1 Preparation of chemically competent cells	119
5.4.2 Transformation of chemically competent cells	119
5.4.3 Agarose gel electrophoresis	119
5.4.4 Molecular cloning	121
5.5 Protein production and analysis	121
5.5.1 Recombinant DJ-1 production in <i>E. coli</i> (applies to all DJ-1 constructs)	121
5.5.2 Preparation of ¹⁵ N-labelled DJ-1 proteins	122
5.5.3 DJ-1 protein extraction and purification (applies to all DJ-1 constructs)	123
5.5.4 Preparation of apo-SOD1 and variants	124
5.5.5 Determination of protein concentration	124
5.5.6 SDS-PAGE	125

5.6 Chemical and biophysical techniques	126
5.6.1 Electronic absorption spectroscopy	127
5.6.2 MALDI-TOF	126
5.6.3 nESI-MS	126
5.6.4 Estimation of copper affinity	127
5.6.5 Crystallisation and structure determination of Cu(I)-bound DJ-1	127
5.6.6 Crystallisation and structure determination of DJ-1 C106S bound to glycerol and sulphate anion	128
5.6.7 Single crystal spectroscopy of Cu(I)-bound DJ-1	129
5.6.8 Circular dichroism (CD) spectroscopy	129
5.6.9 Nuclear magnetic resonance (NMR) spectroscopy	129
5.6.10 <i>In vitro</i> SOD1 activation assay	130
5.6.11 <i>In vitro</i> glyoxalase activity assay	131
5.7 Cell-based assays	132
5.7.1 Cell culture, transfections, and transductions	132
5.7.2 Cell viability assays	132
5.7.3 Immunoblotting	133
5.7.4 Immunofluorescence	134
5.7.5 Measurement of intracellular superoxide levels and SOD1 activity	
5.7.6 Statistical analysis	134
Appendices	135
References	146

List of Abbreviations

Atox1	Antioxidant 1
AR	Androgen receptor
Bca	Bicinchoninic acid
BSA	Bovine serum albumin
CCS	Copper chaperone for superoxide dismutase
CD	Circular dichroism
CEL	Carboxyethyllysine
CML	Carboxymethyllysine
cyt c	Cytochrome c
DJ-1 ^{A107P}	DJ-1 A107P variant
DJ-1 ^{C106A}	DJ-1 C106A variant
DJ-1 ^{C53A}	DJ-1 C53A variant
DJBP	DJ-1 binding protein
DNA	Deoxyribonucleic acid
DNPH	Dinitrophenylhydrazine
DTT	Dithiothreitol
DUSP1	Dual specificity phosphate 1
EDTA	Ethylenediaminetetraacetic acid
GLO1	Glyoxalase I
GLO2	Glyoxalase II
GO	Glyoxal
GPe	<i>Globus Pallidus externus</i>
GPi	<i>Globus Pallidus internus</i>
GSH	Glutathione
HDAC	Histone deacetylase complex
HEK	Human embryonic kidney
HEPES	4-(2-hydroxyethyl)-1-piperazineethanesulphonic acid
His ₆	Hexahistidine
HSQC	Heteronuclear single quantum coherence
IPTG	Isopropyl β -D-1-thiogalactopyranoside
k _{cat}	Catalytic turnover
LB	Lewy body
LB broth	Luria-Bertani broth

LRRK2	Leucine-rich repeat kinase 2
MALDI-TOF	Matrix-assisted laser desorption/ionisation time-of-flight
MEF	Mouse embryonic fibroblast
MGO	Methylglyoxal
MPP+	1-methyl-4-phenylpyridinium
MPTP	1-methyl-4-phenyl-1,2,3,6-tetrahydropyridine
mRNA	messenger ribonucleic acid
nESI-MS	nanoflow electrospray ionization mass spectrometry
OD ₅₉₅	Optical density at 595 nm
OHDA	6-hydroxydopamine
PBS	Phosphate-buffered saline
PCR	Polymerase chain reaction
PD	Parkinson's disease
PEG	Polyethylene glycol
PET	Positron emission tomography
PIASx α	Protein inhibitor of activated STAT x isoform α
PINK1	PTEN-induced kinase 1
PGC-1 α	Peroxisome proliferator-activated receptor γ coactivator 1 α
PSF	Pyrimidine tract-binding protein-associated splicing factor
R _{free}	R-factor of free data set
RMSD	Root-mean squared deviation
ROS	Reactive oxygen species
RT-PCR	Reverse-transcriptase polymerase chain reaction
R _{work}	R-factor of working data set
SD	Standard deviation
SDS-PAGE	Sodium dodecyl sulphate polyacrylamide gel electrophoresis
SEM	Standard error of the mean
SNpc	Substantia Nigra pars compacta
SOD1	Superoxide dismutase 1
SUMO-1	Small ubiquitin-like modifier 1
TBS	Tris-buffered saline
TBS-T	Tris-buffered saline with Tween 20
TEV	Tobacco etch virus
TH	Tyrosine hydroxylase

Tris	Tris(hydroxymethyl)aminomethane
UV	Ultraviolet
WLN	Wilson disease protein
Zn-SOD	Zn-loaded superoxide dismutase

List of Figures

- Figure 1 Nigrostriatal pathway
- Figure 2 Chromosome location and gene structure of *DJ-1*
- Figure 3 Protein sequence and structure of DJ-1
- Figure 4 PD-linked mutations in DJ-1
- Figure 5 Enzymatic reactions of peroxiredoxins
- Figure 6 Cu-Zn superoxide dismutase
- Figure 7 GO and MGO modifications of lysine residues lead to formation of AGEs
- Figure 8 Glyoxalase reactions of GLO1/GLO2, Hsp31, and DJ-1
- Figure 9 Proposed reaction mechanism for DJ-1 glyoxalase activity
- Figure 10 Crystal structure of the yeast CCS
- Figure 11 SDS-PAGE analysis of purified DJ-1
- Figure 12 Absorption spectrum of Cu(I)-titrated DJ-1
- Figure 13 Cu(I) interaction of DJ-1 probed by MALDI-TOF
- Figure 14 Cu(I) interaction of DJ-1 probed by nESI-MS
- Figure 15 Crystal structure of the metal-bound DJ-1
- Figure 16 Structural alignment of apo- and Cu(I)-bound DJ-1
- Figure 17 Spectroscopic analysis of Cu(I)-bound DJ-1 *in crystallo*
- Figure 18 Cu(I) binding of recombinant DJ-1^{C53A}
- Figure 19 SDS-PAGE analysis of purified SOD1
- Figure 20 SOD1 activity assays *in vitro*
- Figure 21 nESI analysis of interaction between DJ-1 and SOD1
- Figure 22 SDS-PAGE analysis of purified HCV
- Figure 23 Cu(II)-induced aggregation of DJ-1
- Figure 24 Cys-53 role in superoxide level modulation and SOD1 activation *in vivo*
- Figure 25 Protein sequence alignment of DJ-1 homologues
- Figure 26 The nucleophile elbow motif of DJ-1
- Figure 27 Purified recombinant DJ-1 proteins produced in bacteria
- Figure 28 Comparative size exclusion chromatography analysis of wild-type DJ-1 and DJ-1^{A107P}
- Figure 29 The A107P mutation abrogates the ability of DJ-1 to protect against gloxal cytotoxicity and accumulation of CML
- Figure 30 Immunoblot analysis of transduced proteins in MEF and SH-SY5Y cells
- Figure 31 *In silico* structural analysis of the A107P mutation

Figure 32	The glyoxalase active site of DJ-1 with sulphate anion and glycerol bound
Figure 33	Steady-state levels of the DJ-1 ^{A107P} as determined by immunoblot analysis
Figure 34	Subcellular localisation of DJ-1 ^{A107P}
Figure 35	CD spectra of wild-type DJ-1 and DJ-1 ^{A107P}
Figure 36	¹ H- ¹⁵ N HSQC of wild-type DJ-1 and DJ-1 ^{A107P}
Figure 37	Overlay of the ¹ H- ¹⁵ N HSQC spectra of wild-type DJ-1 and DJ-1 ^{A107P}
Figure 38	Proposed biological roles of the copper binding site of DJ-1
Figure 39	Location of Parkinsonism-linked mutations that reduce DJ-1 dimerisation
Figure 40	Structural analysis of the human DJ-1 nucleophile elbow motif
Figure 41	Conserved motifs interacting with the nucleophile elbow motif in DJ-1
Figure 42	Proposed mechanism of the hemithioacetal intermediate formation of the DJ-1 glyoxalase activity
Figure 43	Glyoxalase catalytic turnover constants of DJ-1 variants
Figure 44	Chemical basis for the SOD1 activity assay

List of Tables

Table 1	Reactive oxygen species
Table 2	Data collection and refinement statistics for Cu(I)-bound DJ-1.
Table 3	Dissociation constant for $\text{Cu}^{\text{I}}(\text{DJ-1})_2$ complex based on competition with bicinchoninic acid (Bca).
Table 4	Data collection and refinement statistics for DJ-1 C106S variant with glycerol and sulphate bound.
Table 5	<i>E. coli</i> strains for cloning and protein expression
Table 6	Plasmid constructs
Table 7	Cloning and sequencing primers
Table 8	Media and media supplements
Table 9	Antibiotics
Table 10	General buffers and solutions
Table 11	Buffers used in protein purification
Table 12	Preparation of reaction mixtures for SOD1 assay

Acknowledgement

I would like to thank my Director of Studies, Dr. Mark Odell for giving me the opportunity to undertake my doctoral studies under his supervision. Mark has given me a tremendous amount of freedom in pursuing my own ideas rather than his, which I especially thank him for. He has not put me under pressure for the sake of meeting deadlines but has understood the challenge of doing good science. His enthusiasm for science is infectious.

I would like to thank the members of my supervisory team, Prof. Peter Moody for sharing his expertise in protein crystallisation and X-ray crystallography, Dr. Nat Milton and Prof. Simon Moller for their advice on cell-based assays and for sharing reagents critical for my work. I'd also like to thank Dr. Alastair Barr for his helpful comments during the transfer viva. I am very grateful to our collaborators Dr. Nisha Patel, Prof. Carol Robinson, Mr. Altin Sula, Dr. Mark Williams, Dr. Dave Scott, Dr. Dominik Piston, Ms. Emmy Rannikko and Prof. Philipp Kahle for providing reagents and equipment access and for sharing data generated in their respective labs. I am indebted to the Scholarships Office of the University of Westminster, especially to the former Scholarships Director, Colin Matheson, for the generous financial support they have endowed me.

I cannot thank my friends enough, Altin, Amrutha, Amor, Beya, Danica, Diluka, Dory, Elvie, Genevieve, Grethel, Isabelle, Jude, Karima, Keinza, Melanie, Maricel, Michael, Patty and Sedney for the fun times and for being there for me when I am down. I remain sane because of you all!

Lastly, I am indebted to my family for their unconditional love and support and for giving me an inspiration to succeed in my career. To them I dedicate this work.

Author's declaration

The nESI-MS data was collected by Dr. Nisha Patel under the supervision of Prof. Carol Robinson at the Chemistry Department of the University of Oxford. NMR data was collected by Mr. Altin Sula under the supervision of Dr. Mark Williams. I hereby declare that all the material contained in this thesis is my own. Where information has been derived from other sources, I confirm that this has been indicated in the text.

Marc Rhyan Anthony Puno

March, 2014

Chapter 1

General introduction

1.1 Introduction to Parkinson's disease

1.1.1 Parkinson's disease

In 1817, James Parkinson, a surgeon in London, wrote the famous monograph "An Essay of Shaking Palsy" where he defined a pathological condition that affected six patients with a progressive deficit in controlling bodily movements (reviewed by Critchley, 1955). His description of the malady states:

"Involuntary tremulous motion, with lessened muscular power, in parts not in action and even when supported; with a propensity to bend the trunk forwards, and to pass from walking to a running pace; the senses and intellects being uninjured".

Most of these classical motor symptoms *e.g.* tremor at rest, rigidity (increased muscular tone), bradykinesia (slowness of movement) and postural instability remain as the cardinal basis for the diagnosis of a spectrum of chronic movement disorders termed parkinsonism, with Parkinson's disease (PD) or primary parkinsonism being the most common form (Dauer and Przedborski, 2003).

PD affects at least 4 million people worldwide (Dorsey *et al.*, 2007). Its incidence increases with age, with 1 - 2% of the population aged over 65 years likely to be affected by the disease (Eriksen *et al.*, 2005a). PD remains incurable and current treatments have limitations. The development of new therapies is held back by our inadequate knowledge of physiological pathways that trigger the onset of the disease. As the ageing population expands, many countries realise the need for fundamental understanding of PD pathogenesis and the development of new therapies that can improve symptoms and delay disease progression.

1.1.2 Pathophysiology of PD

Pathological studies of PD gained impetus when Nobel Laureate Arvid Carlsson discovered dopamine (Carlsson *et al.*, 1957). Dopamine is a neurotransmitter

synthesised from L-tyrosine by specific sets of neurons to signal either an excitatory or inhibitory output. PD is a neurodegenerative disease caused by the marked deterioration of dopamine-producing neurons in the specific area of the midbrain called the *Substantia Nigra pars compacta* (SNpc).

The SNpc is part of the basal ganglia motor circuitry that modulates movement *e.g.* muscle contraction, multi-joint movements, muscle force and the sequence of movements (Dauer and Przedborski, 2003; Lewis *et al.*, 2003). SNpc neurons form the nigrostriatal pathway that connects the *substantia nigra* to the striatum (Figure 1). Their synapses mainly provide dopaminergic input to the putamen through direct and indirect pathways to produce a regulated motor output. In the direct pathway, dopamine acts as an excitatory neurotransmitter to the putamen through D2 dopamine receptors. The putamen directly inhibits the *Globus Pallidus internus* (GPi) allowing the motor cortex to signal movement. In the indirect pathway, dopamine acts as an inhibitory neurotransmitter to the putamen through D1 dopamine receptors resulting in an excitatory output to the GPi indirectly via the *Globus Pallidus externus* and the subthalamic nucleus. The direct and indirect pathways work in synergy to fine tune movement (reviewed by Dauer and Przedborski, 2003; Lewis *et al.*, 2003; Eriksen *et al.*, 2005a).

In PD, 60% of the SNpc neurons are lost which leads to 80% depletion of striatal dopamine (Fearnly and Lees, 1991). The deficiency of dopaminergic input to the putamen results in attenuated inhibition of GPi by the direct pathway with a concomitant abnormal increase in excitatory output on GPi by the indirect pathway; the combined action triggering an impaired movement observed in Parkinson's disease (Figure 1; Lewis *et al.*, 2003).

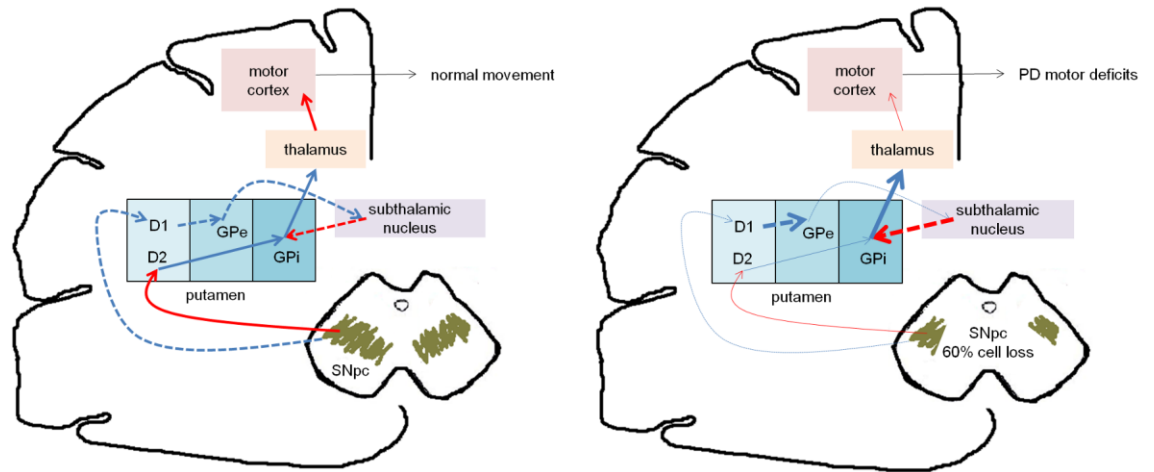


Figure 1. Nigrostriatal pathway. Left panel: SNpc neurons provide dopaminergic input to the putamen through direct (solid arrows) and indirect (broken arrows) pathways. Red and blue arrows indicate excitatory and inhibitory outputs, respectively. Right panel: Nigrostriatal pathway affected with Parkinson's disease. Arrow widths are altered to reflect decrease and increase in signal output.

Neuronal loss observed in PD extends well beyond the dopaminergic neurons of SNpc. Lesions are found in the cerebral cortex, cholinergic (dorsal motor nucleus of vagus, nucleus *basalis* of Meynert), serotonergic (raphe), and noradrenergic (*locus coeruleus*) systems which account for the non-motor symptoms that are associated with PD (Jellinger, 1991; Jellinger, 2001).

Aside from the loss of nigrostriatal dopaminergic neurons, another hallmark of PD is the presence of neuronal proteinacious inclusions called Lewy bodies (LB). These are spherical cytoplasmic deposits rich in a protein called α -synuclein and are usually found in affected brain regions (Gibbs and Lees, 1988). The role of LB in PD pathogenesis is not clear and it remains unresolved whether the post-mortem identification of LB is necessary for a definitive diagnosis of PD since some patients lack LB yet are still considered to have PD.

1.1.3 Pathways associated with PD pathogenesis

1.1.3.1 Oxidative stress

Oxidative stress occurs when an imbalance exists between the levels of reactive oxygen species (ROS) and the antioxidant capacity of the cell, whereby the former overwhelms the latter, leading to a deleterious damage to cells. ROS are endogenously produced as byproducts of normal metabolism, however, pathological processes such as mitochondrial dysfunction (Lin and Beal, 2006), reactive metal mishandling (Halliwell, 2006), and inflammation (Johnstone *et al.*, 1999) can significantly contribute to deleterious levels. A list of biologically relevant ROS is shown in Table 1.

Table 1. Reactive oxygen species

Radicals	Nonradicals
Superoxide, $O_2^{\cdot-}$	Hydrogen peroxide, H_2O_2
Hydroxyl, HO^{\cdot}	Organic peroxides, ROOH
Peroxyl, RO_2^{\cdot}	
Alkoxy, RO^{\cdot}	
Hydroperoxyl, HO_2^{\cdot}	

R = organic moiety

Oxidative stress has been intimately linked to the development of Parkinson's disease (Jenner and Olanow, 1996). Post-mortem histopathological examinations of PD patients' brains have provided evidence of the wide-spread effects of oxidative stress in the affected brain regions including decreased levels of the antioxidant glutathione, lipid peroxidation, increased neuromelanin production, DNA damage and protein oxidation (Dexter *et al.* 1989; Jenner and Olanow, 1996; Faucheux *et al.* 2003).

Animal studies using 1-methyl-4-phenyl-1,2,3,6-tetrahydropyridine (MPTP) and 6-hydroxydopamine (OHDA), neurotoxins that selectively kill dopaminergic neurons, support a role for an oxidative stress pathway to pathogenesis. MPTP is converted to a neurotoxic form MPP⁺ that can be absorbed selectively by dopaminergic neurons (Javitch and Snyder, 1984; Langston *et al.*, 1984). Superoxide radicals are produced by

MPP⁺ by inhibiting the mitochondrial electron transport chain complex I (Cleeter *et al.*, 1992). MPP⁺ can also contribute to an increase in free radical formation by inducing the inflammatory cascade (Wu *et al.*, 2003). The neurotoxicity of OHDA is also attributed to its ability to produce ROS such as superoxide radical, hydrogen peroxide, and hydroxyl radicals when it undergoes auto-oxidation (Cohen and Heikkila, 1974; Saito *et al.*, 2007). OHDA specificity for SNpc neurons is conferred by its affinity for dopamine (catecholamine) transporters (Marek *et al.*, 1990). Dopamine, a structural analogue of OHDA, can also auto-oxidise to form quiniones and semiquinones with the concomitant production of superoxide radicals, hydrogen peroxide and hydroxyl radicals (Smythies and Galzigna, 1998).

1.1.3.2 Mitochondrial dysfunction

The role of mitochondrial dysfunction in PD pathogenesis gained attention when the Parkinsonian neurotoxin MPP⁺ was discovered to block the mitochondrial electron transport chain I (Cleeter *et al.*, 1992). Subsequent studies have shown defective mitochondrial complex I function in some PD patients (Schapira *et al.*, 1990; Parker *et al.*, 2008). Inhibition of complex I results in a release of superoxide radicals (Kusssmaul and Hirst, 2006). Persistent complex I inhibition can also lead to energy deficiency that may trigger neuronal cell death (Fonk and Baudry, 2001; Schapira, 2003).

1.1.3.3 Proteotoxic stress

Protein quality control is tightly linked to cellular longevity (Morimoto *et al.*, 2011). The cell develops a network of interactions that maintain proper folding of proteins and the clearance of misfolded and damaged proteins. Proteotoxic stress occurs when cells abnormally build up misfolded proteins due to impairment of molecular chaperone systems or inhibition of protein turnover systems *e.g.* proteasome and autophagy (Morimoto, 2008). Accumulation of misfolded proteins has been associated with numerous neurodegenerative diseases (Ross and Poirier, 2004; Morimoto, 2008). In PD,

brain tissues that undergo progressive degeneration contain LB, protein deposits composed of alpha-synuclein fibrils, various ubiquitinated proteins, and neurofilaments (Gibbs and Lees, 1988). Aggregated proteins can interfere with numerous cellular processes including intracellular trafficking and proteasomal degradation (Bence *et al.*, 2001; Soper *et al.*, 2011). Protein deposits can also adsorb many other proteins that are required for cell survival (Pasinelli *et al.*, 2004). These deleterious effects contribute to the cytotoxic properties of protein aggregates (Bence *et al.*, 2001; Pasinelli *et al.*, 2004; Soper *et al.*, 2011).

1.1.4 Causative agents and risks factors

1.1.4.1 Exposure to agricultural chemicals

Recent meta-analyses of data from cohort and case-control studies concluded that occupational exposure to pesticides paraquat and maneb increases the risk of developing PD by about 2-fold (Pezolli and Cerada, 2013).

Paraquat is a herbicide with a chemical structure analogous to MPP⁺ (Dauer and Przedborski, 2003). Although paraquat does not easily cross the blood brain barrier, its systemic administration in mice leads to degeneration of SNpc dopaminergic neurons and formation of α -synuclein positive inclusions (Shimizi *et al.*, 2001; Manning-Bog *et al.*, 2002; McCormack *et al.*, 2002;). The neurotoxicity of paraquat may be attributed to its ability to generate superoxide radicals via its redox cycling with NADPH or NADH (Bus and Gibson, 1984; Hirai *et al.*, 1992). Due to its similarity with MPP⁺, paraquat has been hypothesised to inhibit mitochondrial complex I (Fukushima *et al.*, 1993; Tawara *et al.*, 1996).

Maneb or manganese ethylenebisdithiocarbamate is a fungicide used on agricultural crops. Maneb has been shown to potentiate the neurotoxicity of MPTP and paraquat (Takahasi *et al.*, 1989; Thiruchelvam, 2000) and, by itself, can induce parkinsonism

(Meco *et al.*, 1994). The metal and organic components of maneb contribute to its neurotoxicity, mainly due to mitochondrial dysfunction (Dominico *et al.*, 2006). Oxidative stress has also been implicated in maneb's toxicity because overexpression of SOD1 in mice protects against development of a parkinsonian phenotype induced by maneb (Thiruchelvam *et al.*, 2005).

1.1.4.2 Exposure to metals

Epidemiological studies suggest that chronic exposure to heavy metals such as manganese, copper, lead, iron, mercury, and aluminium is a risk factor for developing PD (Gorell *et al.*, 1997; Willis *et al.*, 2010). In 1997, Gorell *et al.* conducted a population-based case-control study to assess the role of occupational exposure to heavy metals in developing PD. Their study found that people with more than 20 years of exposure to copper or manganese have greater association with PD. Moreover, individuals exposed to combinations of metals such as lead-copper, lead-iron, or iron-copper have increased risk over those exposed to a single metal. A more recent study by Willis *et al.* (2010) supports a role for environmental exposure to copper and manganese in developing PD. The authors analysed the incidence of PD in US urban areas with various levels of industrial release of metals. They found that counties with high cumulative release of manganese or copper have greater incidence of PD.

Heavy metals could be neurotoxic through various mechanisms. Copper and iron can catalyse redox reactions that can generate deleterious levels of reactive oxygen species (Kohen and Chevion, 1985). Heavy metals *e.g.* copper and mercury can also trigger protein aggregation and misfolding (Paik *et al.*, 1999; Yang *et al.*, 2010). Aluminum, copper, iron and manganese have been shown to accelerate the aggregation of alpha-synuclein, with aluminium being the most effective metal species (Uversky *et al.*, 2001).

1.1.4.3 Genetics

Although the majority of PD cases are idiopathic in nature, monogenic PD forms with Mendelian inheritance account for 5-10% of the cases (Lesage and Brice, 2006). Familial PD shares common features with idiopathic PD including degeneration of SNpc dopaminergic neurons leading to motor deficits (Hardy *et al.*, 2006). Thus far, at least 16 loci have been associated with familial PD (reviewed by Corti *et al.*, 2011).

Autosomal dominant forms of PD are caused by mutations in the genes encoding α -synuclein and the leucine-rich repeat kinase 2 (LRRK2) (Polymeropoulos *et al.*, 1997; Zimprich *et al.*, 2004). In the case of α -synuclein, duplication or triplication of the gene is more common than missense mutations, accounting for 2% of all monogenic forms of PD (Eriksen *et al.*, 2005; Corti *et al.*, 2011). α -Synuclein represents a direct link between genetic and sporadic forms of PD as it is found as the major component of LB (Spillantini *et al.*, 1997). Consistently, mutations in α -synuclein or its augmented expression accelerate its tendency to form LB-associated aggregates (Conway *et al.*, 1998; Eriksen *et al.*, 2005). The biological function of α -synuclein remains largely unknown. Recent evidence suggests a role for α -synuclein in synaptic plasticity and neurotransmitter release, processes important for neuronal function (Burre *et al.*, 2010; Bendor *et al.*, 2013). Amongst the causative genes, *LRRK2* (*PARK8*) mutations are the most prevalent (Lesage and Brice, 2006). *LRRK2* encodes a 286-kDa multidomain protein with kinase, GTPase, and protein scaffolding activities (Mata *et al.*, 2006). Mutation hotspots include the Ras of complex protein (Roc) GTPase domain and the tyrosine-link kinase (TKL) domain (Corti *et al.*, 2011). *LRRK2*'s cellular function is associated with protein translation control, apoptosis, mitogen-activated protein kinase pathways, and cytoskeleton dynamics (reviewed by Webber and West, 2009).

Four genetic loci for autosomal recessive forms of PD have also been mapped. Three loci are found on chromosome 1, namely *PINK1* (*PARK6*) (Valente *et al.*, 2003), *DJ-1*

(*PARK7*) (Bonifati *et al.*, 2003), and *ATP13A2* (*PARK9*) (Ramirez *et al.*, 2006) while chromosome 6 contains *PARKIN* (*PARK2*) (Lucking *et al.*, 2000). Mutations in these genes lead to early-onset parkinsonism. Parkin, an E3 ubiquitin ligase, targets a set of protein substrates for degradation (Haas and Kahle, 2001). Parkin is also involved in the removal of damaged mitochondria via a process called mitophagy (Narendra *et al.*, 2009). PINK1 (PTEN-induced kinase 1) is a Ser/Thr kinase targeted to the mitochondria (Valente *et al.*, 2003). Recently, PINK1 has been shown to phosphorylate the Ubl domain of Parkin which in turn activates Parkin's E3 ubiquitin ligase activity, demonstrating an interplay between genes involved in familial PD (Vives-Bauza *et al.*, 2010; Kondapalli *et al.*, 2012; Iguchi *et al.*, 2013). *ATP13A2* is a cation-transporting ATPase that localises to endosomal and lysosomal membranes (Ramirez *et al.*, 2006). Deregulation of cation homeostasis and lysosomal dysfunction have been associated with *ATP13A2* mutational inactivation (Schneider *et al.*, 2010; Ramonet *et al.*, 2012; Rochet, 2012).

In 2003, Bonifati *et al.* identified mutations in *DJ-1* that are linked to autosomal recessive juvenile PD. Subsequent studies identified more sequence variants of *DJ-1* that are associated with PD development (Abou-Sleiman *et al.*, 2003; Hague *et al.*, 2003; Clark *et al.*, 2004; Djarmati *et al.*, 2004; Hering *et al.*, 2004; Anessi *et al.*, 2005; Tang *et al.*, 2006). *DJ-1* is a pleiotropic gene associated with numerous biological processes. A comprehensive introduction to *DJ-1* will be presented in the next section.

1.2 Introduction to DJ-1

1.2.1 The *DJ-1* gene and its product

The *DJ-1* gene has been mapped to chromosome 1p36.2-p36.3 (Figure 2; Taira *et al.*, 2001; Bonifati *et al.*, 2003). It is composed of 8 exons spanning 24 kbp, with exons 1A and 1B being non-coding and alternatively spliced (Bonifati *et al.*, 2003). *DJ-1* expression is controlled by an *Sp1* promoter (Taira *et al.*, 2001). The brain expresses *DJ-1*, with greater distribution in the subcortical regions *e.g.* hippocampus, thalamus, caudate nucleus and *substantia nigra*, the region affected in PD (Olzmann *et al.*, 2007).

DJ-1 encodes an ~19 kDa polypeptide that resides in the cytoplasm and the nucleus (Bonifati *et al.*, 2003); mitochondrial localisation may be triggered by oxidative stress (Canet-Aviles *et al.*, 2004). The structure of DJ-1 adopts a flavodoxin-like α/β fold composed of a 6-stranded β -sheet core sandwiched by 8 α -helices (Figure 3; Honbou *et al.*, 2003; Huai *et al.*, 2003; Lee *et al.*, 2003; Tao and Tong, 2003; Wilson *et al.*, 2003). Two protomers interact to form a homodimer (Figure 4). Mutations that disrupt homodimerization abrogate the antioxidant activity of DJ-1, hence highlighting the physiological role of the homodimeric state in the cellular function of DJ-1 (Taira *et al.*, 2004). The protein shares homology with the *Pyrococcus horikoshii* cysteine protease PfpI (30% identity), the *Escherichia coli* thiamine biosynthetic enzyme ThiJ (41% identity) and the *E. coli* molecular chaperone YajL (41% identity).

One of the structural features of DJ-1 is the nucleophile elbow identified by the consensus sequence Sm-X-Nu-X-Sm where Sm = a small residue (*i.e.* a residue with a side chain that spans less 5 Å such as Ala or Gly), Nu = nucleophile, and X = any residue (Nardini and Dijkstra, 1999). This motif uniquely positions the nucleophilic residue (Cys-106 in case of human DJ-1) in a tight turn of a strand-helix transition, specifically β 7-loop- α 5. This motif is important for a number of reported DJ-1

biochemical activities including its glyoxalase activity (Lee *et al.*, 2012) and weak proteolytic activity (Olzmann *et al.*, 2004).

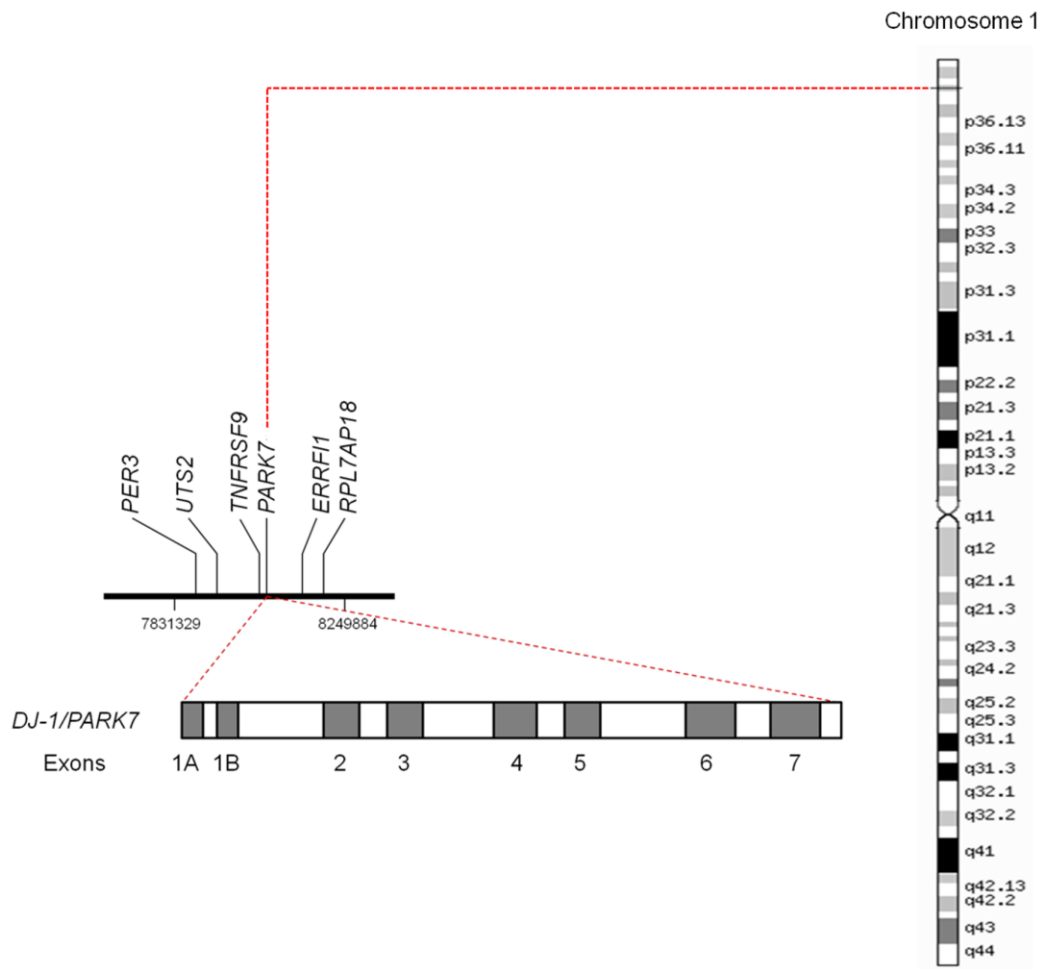


Figure 2. Chromosome location and gene structure of *DJ-1*. The *DJ-1/PARK7* locus is mapped to chromosome 1p36.2-p36.3. The 24-kbp gene is composed of 8 exons with exons 1A and 1B being non-coding and alternatively spliced. Chromosome 1 map was derived from www.genecards.com.

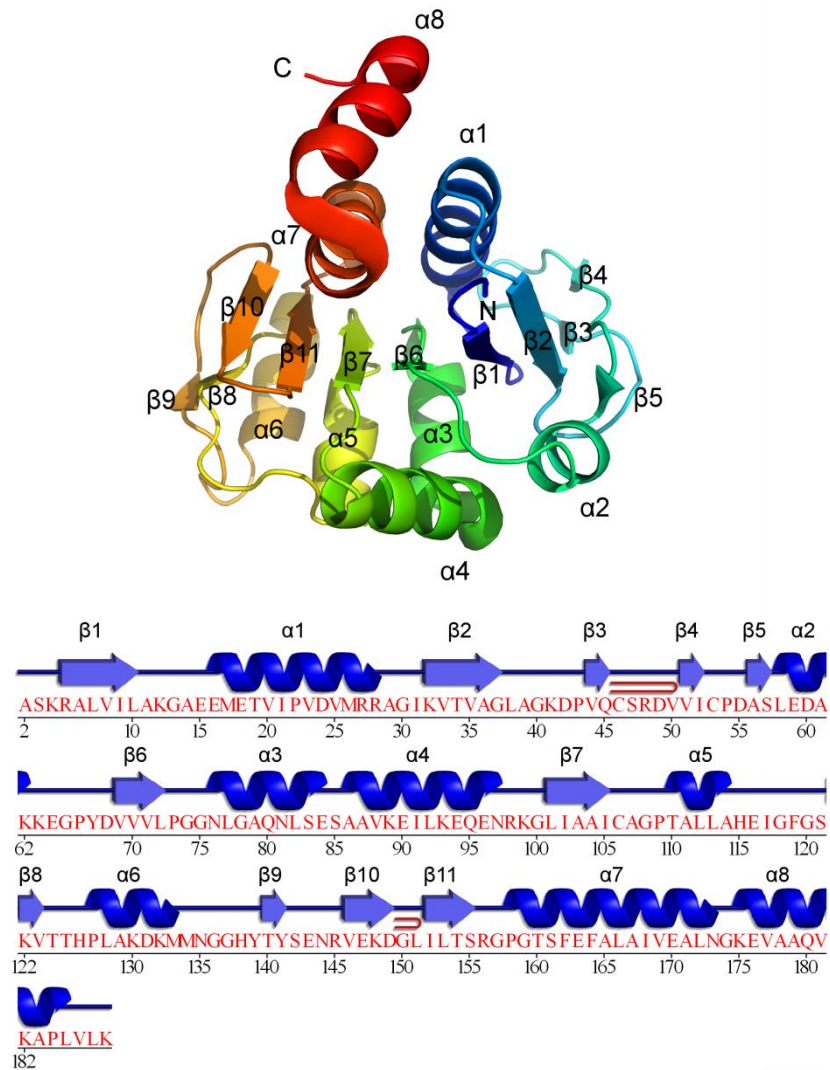


Figure 3. Protein sequence and structure of DJ-1. DJ-1 is a 189-amino acid polypeptide that adopts a flavodoxin-like fold composed of a six-stranded β -sheet core sandwiched by 8 α -helices. A cartoon representation of the DJ-1 structure (PDB ID code: 1PDV) rendered using PyMol (Delano, 2002) is depicted in the top panel with rainbow colouring to show the sequential arrangement of residues. The lower panel, obtained from PDBsum (www.ebi.ac.uk/pdbsum), shows the annotated amino acid sequence of DJ-1 with superimposition of the secondary structure.  represents an α -helix,  represents a β -strand, and  represents a β -turn.

1.2.2 DJ-1 and PD

DJ-1 or *PARK7* is the third locus to be discovered for autosomal recessive juvenile parkinsonism, after *PARKIN* (*PARK2*) and *PINK1* (*PARK6*) (Bonifati *et al.*, 2003). Similar to mutations in *PARKIN* and *PINK1*, the phenotype of patients with *DJ-1* mutations manifest the classical clinical symptoms *e.g.* postural tremor, bradykinesia with an asymmetric onset before the age of 40. Psychiatric symptoms including anxiety and psychotic episodes have also been documented in affected patients (Abou-Sleiman *et al.*, 2003; Bonifati *et al.*, 2003).

To date, there has been no pathology report on patients affected with a DJ-1 mutation. However, studies using transcranial ultrasound have demonstrated hyperechogenicity in the *substantia nigra*, a neuropathological feature of PD (Schweitzer *et al.*, 2007). Positron Emission Tomography (PET) neuroimaging also revealed significant depletion of dopamine in the patient's brain (Dekker *et al.*, 2004).

Structural and biochemical characterisations of disease-linked sequence variants of DJ-1 have provided insights into the molecular mechanisms by which mutations lead to loss of DJ-1 function. The positions of the mutations in the structure of DJ-1 are depicted in Figure 5. Most PD-linked mutations *e.g.* L166P, L10P, L158del in DJ-1 are found to destabilise the structure of DJ-1 leading to a rapid clearance of the protein inside the cell (Moore *et al.*, 2003; Gorner *et al.*, 2004; Olzmann *et al.*, 2004; Blackinton *et al.*, 2005; Ramsey and Giasson, 2010; Rannikko *et al.*, 2012). Some mutations (L166P, L10P, P158del, M26I, E163K, A104T, D149A) decreases the ability of DJ-1 form homodimers implicating the crucial role of the dimeric state in DJ-1 function (Moore *et al.*, 2003; Taira *et al.*, 2004; Takahashi-Niki *et al.*, 2004; Moore *et al.*, 2005; Hulleman *et al.*, 2007, Lakshminarasimhan *et al.*, 2007; Repici *et al.*, 2013). More subtle mutations (E64D, A179T) have also been linked to PD that do not show an apparent

change in the structural stability or dimerisation of the protein (Gorner *et al.*, 2004; Rannikko *et al.*, 2012; Repici *et al.*, 2013).

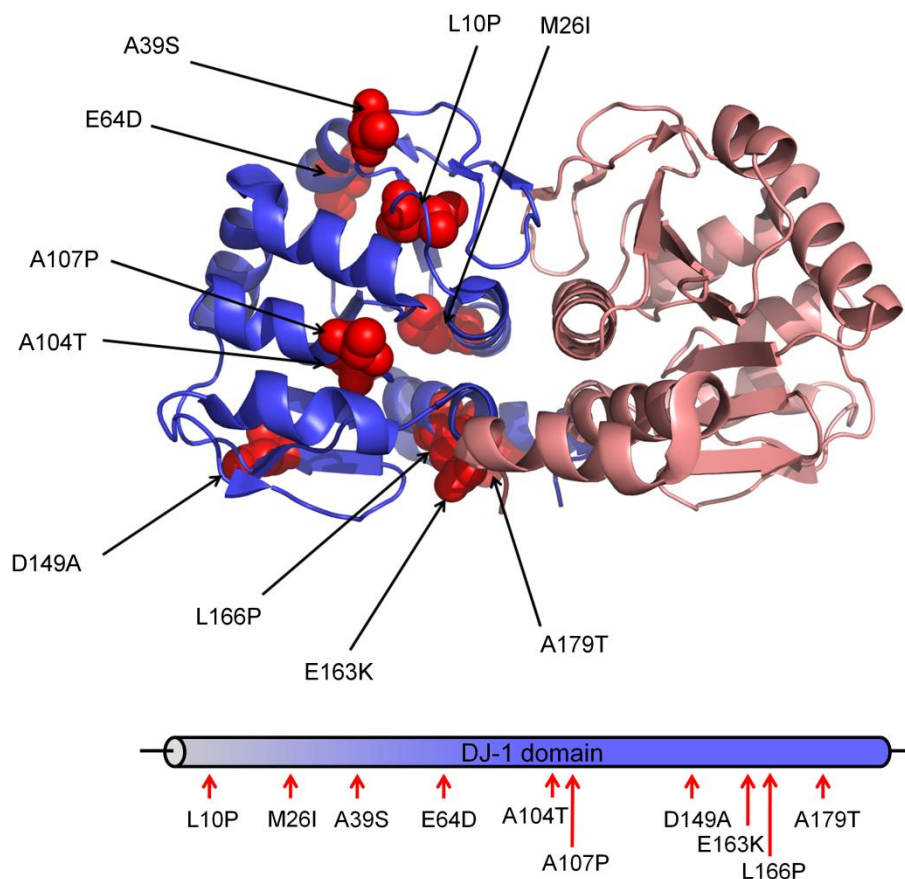


Figure 4. Structure of DJ-1 homodimer and the locations of PD-linked mutations. A cartoon representation of the DJ-1 homodimer (PDB ID code: 2OR3) with the side chains of residues individually mutated in PD shown as red spheres in one protomer. Structure was rendered using PyMol (Delano, 2002).

1.2.3 Biological activities of DJ-1

1.2.3.1 Peroxiredoxin-like peroxidase

The function of DJ-1 is closely associated with cellular protection against oxidative stress. Several groups have shown that DJ-1 knockdown sensitises cells to substances that induce oxidative stress such as H_2O_2 (Taira *et al.*, 2004), dopamine (Lev *et al.*, 2009) and PD toxins MPTP (Kim *et al.*, 2005; Aleyasin *et al.*, 2010), paraquat (Yang *et al.*, 2007) and OHDA (Sun *et al.*, 2012; Lev *et al.*, 2013).

The exact mechanism by which DJ-1 exerts its antioxidant effects remains elusive. Andres-Mateos *et al.* (2007) proposed that the antioxidant effect of DJ-1 is based on an atypical peroxiredoxin-like peroxidase activity whereby the highly conserved Cys-106 is critical for the detoxification reaction. Peroxiredoxins are enzymes that eliminate H₂O₂ and organic peroxides via redox cycling of cysteine residues (Wood *et al.*, 2003). Reaction of a peroxidatic cysteine with peroxides results in oxidation of the thiol moiety (-SH) into a sulphenic acid (-SOH) that is usually resolved to a disulphide linkage by another cysteine and/or reduced by an endogenous reducing agent (Figure 5A and 5B; Wood *et al.*, 2003). In contrast, the atypical peroxidatic cysteine in DJ-1, Cys-106, is converted to a sulphinic acid (-SOOH) that cannot be reduced by endogenous reductants or by sulfiredoxin, an ATP-dependent enzyme that catalyses the reduction of sulphinic acid (Figure 5C; Woo *et al.*, 2005). Therefore, the oxidation of Cys-106 to a cysteine sulphinic acid is irreversible and hence not capable of multiple turnover reactions challenging the notion that DJ-1 plays a major role in directly eliminating reactive peroxide species. Rather, the facile oxidation of DJ-1 Cys-106 has been considered to be a modification that influences its biological activities (Wilson, 2010).

1.2.3.2 Transcriptional regulation

Deficiency in DJ-1 has been shown to alter the mRNA expression levels of a number of proteins including the glutamate cysteine ligase (Zhou and Freed, 2005), superoxide dismutase 3 (Nishinaga *et al.*, 2005), bax (Breitaud *et al.*, 2007; Fan *et al.*, 2008), tyrosine hydroxylase (Ishikawa *et al.*, 2010), thioredoxin 1 (Im *et al.*, 2012), p21 and dual specificity phosphatase 1 or DUSP1 (Kato *et al.*, 2013).

One of the ways by which DJ-1 regulates transcription is through its inhibitory interaction with the negative regulators of transcription factors. The androgen receptor (AR) was the first transcription factor shown to be regulated by DJ-1 (Takahashi *et al.*, 2001). DJ-1 restores AR activity that is repressed by negative regulators protein

inhibitor of activated STAT x isoform alpha (PIASx α) and DJ-1 binding protein (DJBP) (Takahashi *et al.*, 2001; Niki *et al.*, 2003). DJ-1 is found to directly interact with the AR binding site of PIASx α thereby preventing its interaction with AR (Takahashi *et al.*, 2001). DJ-1 also interacts with DJBP, a scaffold protein that recruits the histone deacetylase complex (HDAC) to inhibit AR activity (Niki *et al.*, 2003). DJ-1 blocks the recruitment of HDAC to AR by binding the HDAC interaction site of DJBP (Niki *et al.*, 2003).

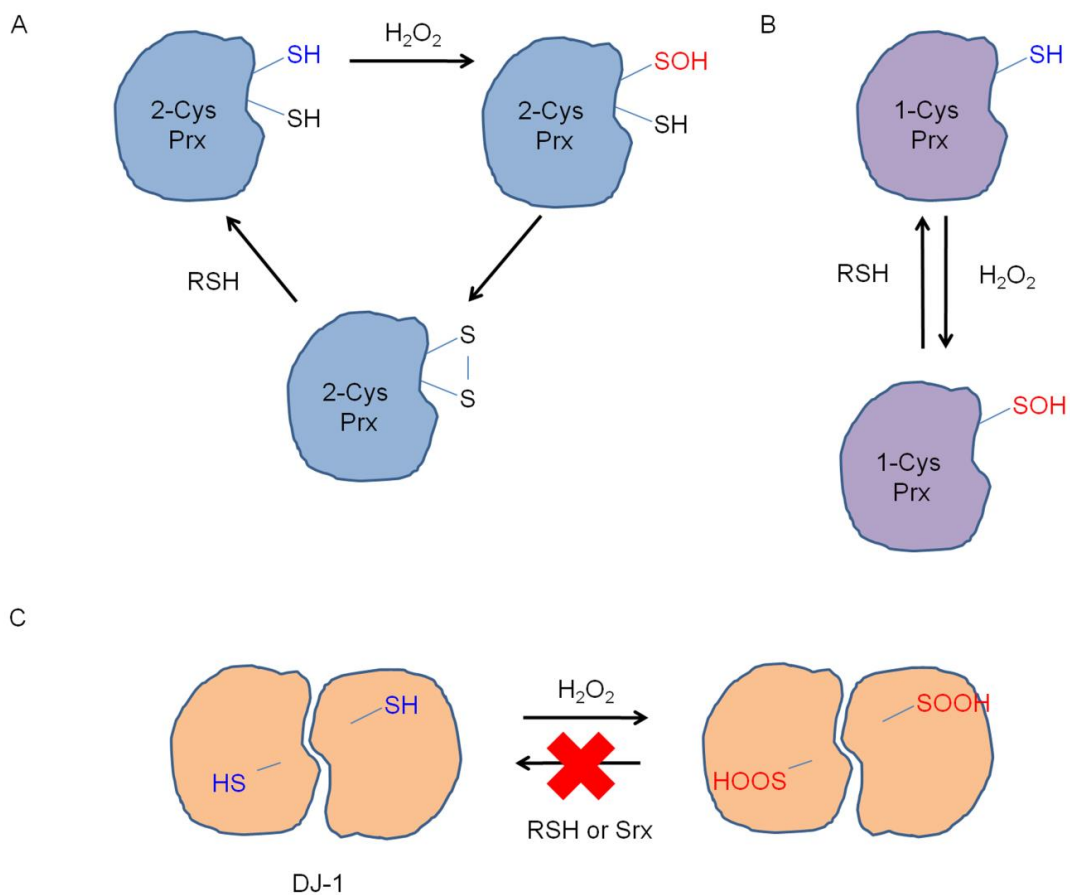


Figure 5. Enzymatic mechanism of peroxiredoxins. (A) 2-Cys peroxiredoxins detoxify hydrogen peroxide by oxidising the thiol moiety of the peroxidatic cysteine to a sulphenic acid. An adjacent cysteinyl residue resolves the sulphenic acid moiety by forming a disulphide bond with the peroxidatic cysteine. Finally, a thiol-based reductant (RSH) restores the thiol moieties. (B) In 1-Cys peroxiredoxins, the sulphenic acid is directly reduced by an endogenous RSH. (C) Oxidation of DJ-1 Cys-106 results in the irreversible formation of a cysteine sulphenic acid that cannot be reduced by a sulfiredoxin (Srx) or RSH.

DJ-1 can also directly interact with transcription factors such as p53 (Fan *et al.*, 2008; Kato *et al.*, 2013). The p53-dependent upregulation of bax expression observed after DJ-1 knockdown in zebrafish suggested a functional interaction between DJ-1 and p53 (Breitaud *et al.*, 2007). Later *in vitro* studies have shown a physical interaction between DJ-1 and the DNA-binding and C-terminal domains of p53 (Fan *et al.*, 2008; Kato *et al.*, 2013). Binding of DJ-1 to p53 selectively inhibits p53 transactivation based on promoter affinity (Kato *et al.*, 2013).

Tyrosine hydroxylase (TH) is required for dopamine synthesis and thus is highly expressed in dopaminergic neurons of the *substantia nigra* (Nagatsu *et al.*, 1964). TH expression is also regulated by DJ-1 in a species specific manner (Ishikawa *et al.*, 2010). DJ-1 controls TH expression by inhibiting the conjugation of small ubiquitin-like modifier 1 (SUMO-1) to Pyrimidine tract-binding protein-associated splicing factor or PSF (Zhong *et al.*, 2006). SUMOylated PSF recruits HDAC to repress the transcription of the TH promoter. Interestingly, DJ-1 also suppresses PSF SUMOylation to activate the peroxisome proliferator-activated receptor γ coactivator 1 alpha (PGC-1 α), a master regulator of mitochondrial biogenesis and stress response (Zhong and Xu, 2008).

1.2.3.3 Molecular chaperone

Molecular chaperones assist polypeptides to fold correctly and maintain their structural stability. DJ-1 has been reported to act as a molecular chaperone that is capable of preventing heat-induced aggregation of classic chaperone substrates citrate synthase and luciferase (Lee *et al.*, 2003; Shendelman *et al.*, 2004). Interestingly, two groups have shown that DJ-1 prevents the formation of α -synuclein aggregates *in vitro* and *in vivo* (Shendelman *et al.*, 2004; Zhou *et al.*, 2006). Both groups reported a redox state dependent chaperone activity whereby oxidation of a cysteine residue during oxidative stress activates the chaperone activity. Shendelman *et al.* (2004) have implicated Cys-53 as the critical residue for the chaperone activity however Zhou *et al.* (2006) have shown

that Cys-106 is the highly oxidisable residue that senses oxidative stress and is required for the chaperone activity.

1.2.3.4 RNA binding

In 2008, van der Brug *et al.* used four different methods to show that DJ-1 directly binds mRNA of genes associated with the mitochondria, glutathione metabolism, and effectors of PTEN/PI3K pathway. DJ-1 interacts with the GG/CC rich sequences of 5' and 3' untranslated regions of the mRNA. Binding of DJ-1 to an mRNA partially suppresses translation. During oxidative stress, mRNAs dissociate from DJ-1 thereby relieving translational inhibition. mRNA dissociation is determined by the oxidation state of DJ-1 albeit no information on which residues sense oxidative stress was reported.

1.2.3.5 Weak protease activity

The structural homology between DJ-1 and the prokaryotic protease PfpI suggested the possibility of DJ-1 acting as a protease. A putative catalytic triad involving Glu-18, Cys-106, and His-126 is suggested by the crystal structures of DJ-1 (Honbou *et al.*, 2003; Huai *et al.*, 2003; Lee *et al.*, 2003; Tao and Tong, 2003; Wilson *et al.*, 2003). Lee *et al.* (2003) noted the presence of a C-terminal $\alpha 9$ that blocks the catalytic site hence the lack of an apparent proteolytic activity of DJ-1. However, Olzmann *et al.* (2004) detected an intrinsic protease activity for casein using a highly sensitive fluorescence-based assay although about 6000-fold less efficient than trypsin. Subsequently, Chen *et al.* (2010) reported that mild oxidative stress results in the cleavage of the occluding C-terminal helix thereby exposing a protease catalytic dyad involving His-126 and the nucleophile Cys-106. Recently, the protease activity of DJ-1 was found to target the consensus sequences Val-Lys-Val-Ala (VK↓VA) (Mitsugi *et al.*, 2013).

1.2.3.6 Copper binding and activation of SOD1

The Cu-Zn superoxide dismutase (SOD1) is a homodimeric metalloenzyme essential for antioxidant defence against highly reactive superoxide radicals (Figure 6A). A copper cofactor in the active site, held by His-46, His-48, His-63, and His-120, is required for catalysis while a zinc ion plays a structural role (Figure 6B). SOD1 exploits the redox properties of copper to facilitate the conversion of superoxide radicals into hydrogen peroxide and oxygen.

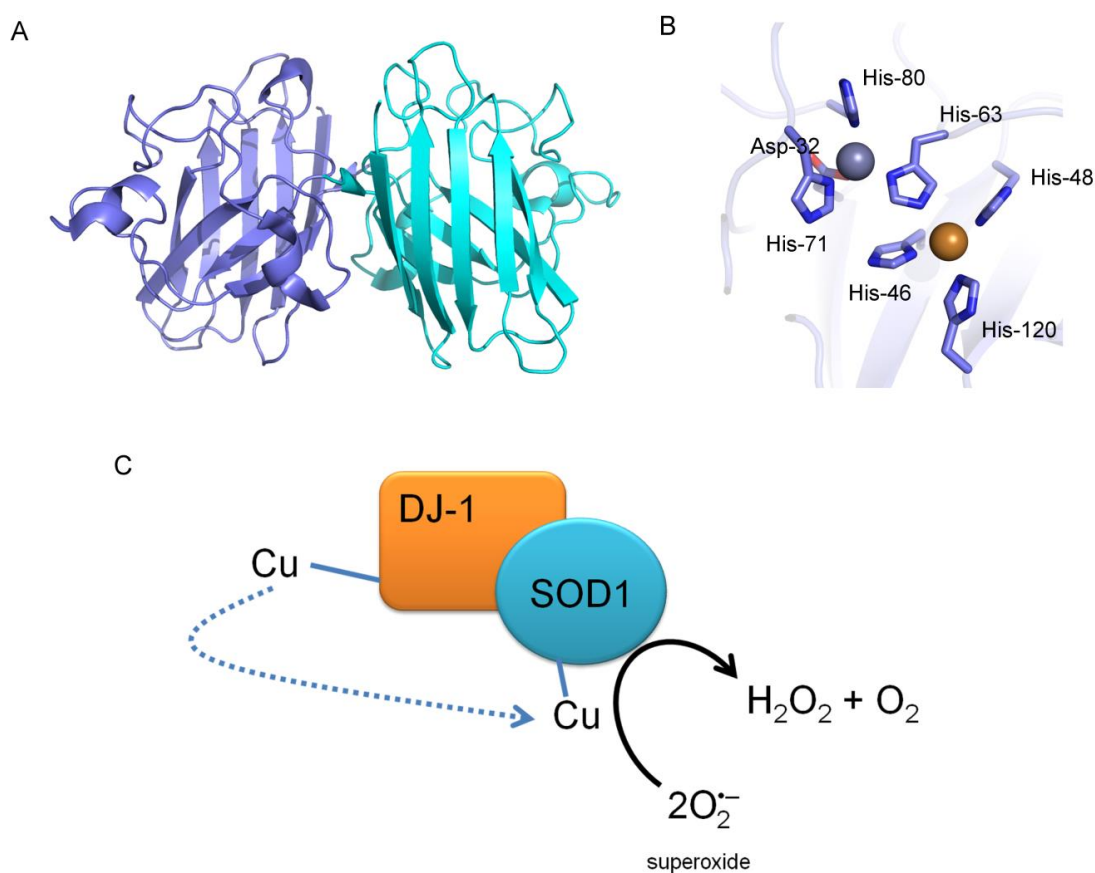


Figure 6. Cu-Zn superoxide dismutase. (A) Cartoon representation of the structure of the holo-SOD1 dimer (PDB ID code: 2C9V). Structure was rendered using PyMol (Delano, 2002). (B) The SOD1 active site with the copper ion (orange sphere) coordinated by His-46, His-48, His-63, and His-120. The zinc ion (grey sphere) is held by His-71, His-80, and Asp-82. (C) SOD1 catalyses the disproportionation of superoxide using a copper cofactor. DJ-1 has been proposed to provide the copper cofactor to SOD1 (Xu *et al.*, 2010).

An interaction between DJ-1 and SOD1 has been demonstrated (Xu *et al.*, 2010; Yamashita *et al.*, 2010; Knobbe *et al.*, 2012). Xu *et al.* (2010) have shown that DJ-1 not only interacts with SOD1 but also binds copper (as CuSO₄). They have further shown that DJ-1, when expressed recombinantly in the presence of copper, is capable of stimulating the activity of SOD1, suggesting a role for DJ-1 in providing the copper cofactor of SOD1 (Figure 6C). The activation of SOD1 by DJ-1 reveals a mechanism by which DJ-1 could potentially protect cells against oxidative stress. However, the molecular basis for this copper chaperone activity is lacking.

Recently, Bjorkblom *et al.* (2013) confirmed the ability of DJ-1 to sequester copper and mercury, a structural surrogate for copper. They have further shown that DJ-1 overexpression in dopaminergic neuroblastoma cells conferred protection from copper- and mercury-induced cytotoxicity. This protection was lost in PD-linked sequence variants (A104T, D149A) of DJ-1 that reduces DJ-1 homodimerisation. How DJ-1 sequesters free copper ions to prevent their nonspecific damaging reactions in the cell remains uncharacterised.

1.2.3.7 Cofactor-independent glyoxalase

α -Oxoaldehydes *e.g.* methylglyoxal (MGO) and glyoxal (GO) are ubiquitous products of cellular metabolism. MGO and GO are highly reactive dicarbonyl species generated by spontaneous breakdown of triose phosphates (Phillips and Thornalley, 1993), nonenzymatic protein glycation (Thornalley *et al.*, 1999), glucose oxidative degradation (Wells-Knecht *et al.*, 1995), and enzymatic oxidation of aminoacetone and ketone bodies (Cazassa *et al.*, 1984; Aleksandrovskii, 1992; Lyles and Chalmers, 1992). MGO and GO are strong electrophiles that can react with lysine, arginine, and histidine residues of proteins, producing adducts belonging to a class of irreversible modifications called advanced glycation end products (AGEs; Thornalley *et al.*, 1999). For instance, lysines react with GO and MGO to produce carboxymethyllysine (CML)

and carboxyethyllysine (CEL), respectively (Figure 7). MGO- and GO-induced modifications can lead to aggregation and functional inactivation of proteins (Assero *et al.*, 2001; Morgan *et al.*, 2002; Shaikh and Nicholson, 2008). MGO and GO can also target DNA resulting in strand breakage and interstrand crosslinking (Rahman *et al.*, 1990). Whilst oxidation can generate α -oxoaldehydes, MGO and GO are also capable of producing ROS (Ramasamy *et al.*, 2005; Ramasamy *et al.*, 2006; Kuntz *et al.*, 2010), feeding a vicious cycle of ROS- α -oxoaldehyde production.

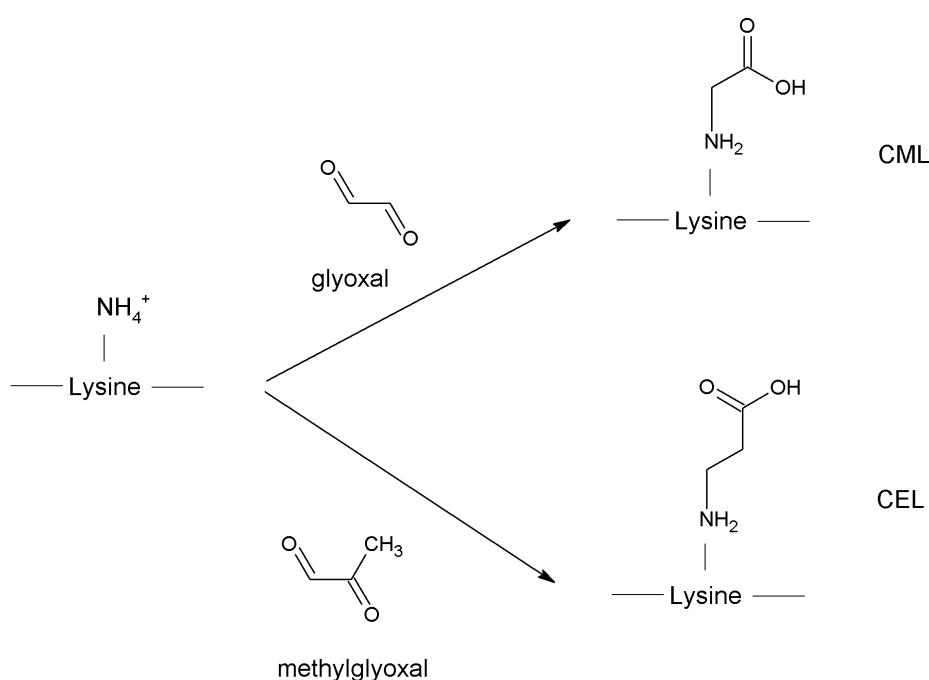


Figure 7. GO and MGO modifications of lysine residues lead to formation of AGEs. Endogenously produced GO and MGO can directly react with the free amine group of lysine to form CML and CEL, respectively.

To prevent the accumulation of cytotoxic levels of MGO and GO, cells employ a glutathione-dependent glyoxalase enzyme system composed of two distinct enzymes glyoxalase I (GLO1) and glyoxalase II (GLO2) that act together to inactivate α -oxoaldehydes (Thornalley, 1990). The substrate for GLO1 is a hemithioacetal formed by the reaction of glutathione with the α -oxoaldehydes (Thornalley, 2003). GLO1 converts the hemithioacetal substrate into S-(D)-lactosylglutathione that feeds into GLO2 for the hydrolytic removal of glutathione and the release of D-lactate (Thornalley,

1990; Cameron *et al.*, 1999; Thornalley, 2003). Figure 8A summarises the enzymatic breakdown of methylglyoxal by GLO1 and GLO2.

A glutathione-independent glyoxalase system was first identified in prokaryotes (Misra *et al.*, 1995). In *E. coli*, Hsp31 has been identified as a glyoxalase capable of catalysing the conversion of methylglyoxal into D-lactate in the absence of any cofactor (Figure 8B; Subedi *et al.*, 2011). Hsp31 is homologous to human DJ-1. Lee *et al.* (2012) demonstrated a glyoxalase activity for DJ-1 that does not require a glutathione cofactor, hence, insofar represents the only eukaryal cofactor-independent glyoxalase. DJ-1 converts GO and MGO into glycolic acid and lactic acid, respectively (Figure 8C). By acting as a glyoxalase, DJ-1 can protect cells from cellular degeneration induced by toxic accumulation of GO and MGO.

A reaction mechanism for the DJ-1 glyoxalase activity using methylglyoxal as a substrate was proposed based on the catalytic mechanisms of GLO1 and GLO2 (Figure 9; Kwon *et al.*, 2013). The initial step involves the nucleophilic attack on the aldehydic carbonyl carbon (C1) of methylglyoxal by the S-thiolate of Cys-106, forming a hemithioacetal intermediate. The next step involves a general acid-base catalysis whereby Glu-18 abstracts a proton from C1, forming an enediol intermediate, followed the ketonisation of C1 to form an S-lactoylcysteine. Finally, the lactic acid product is produced through hydrolysis of the thioester.

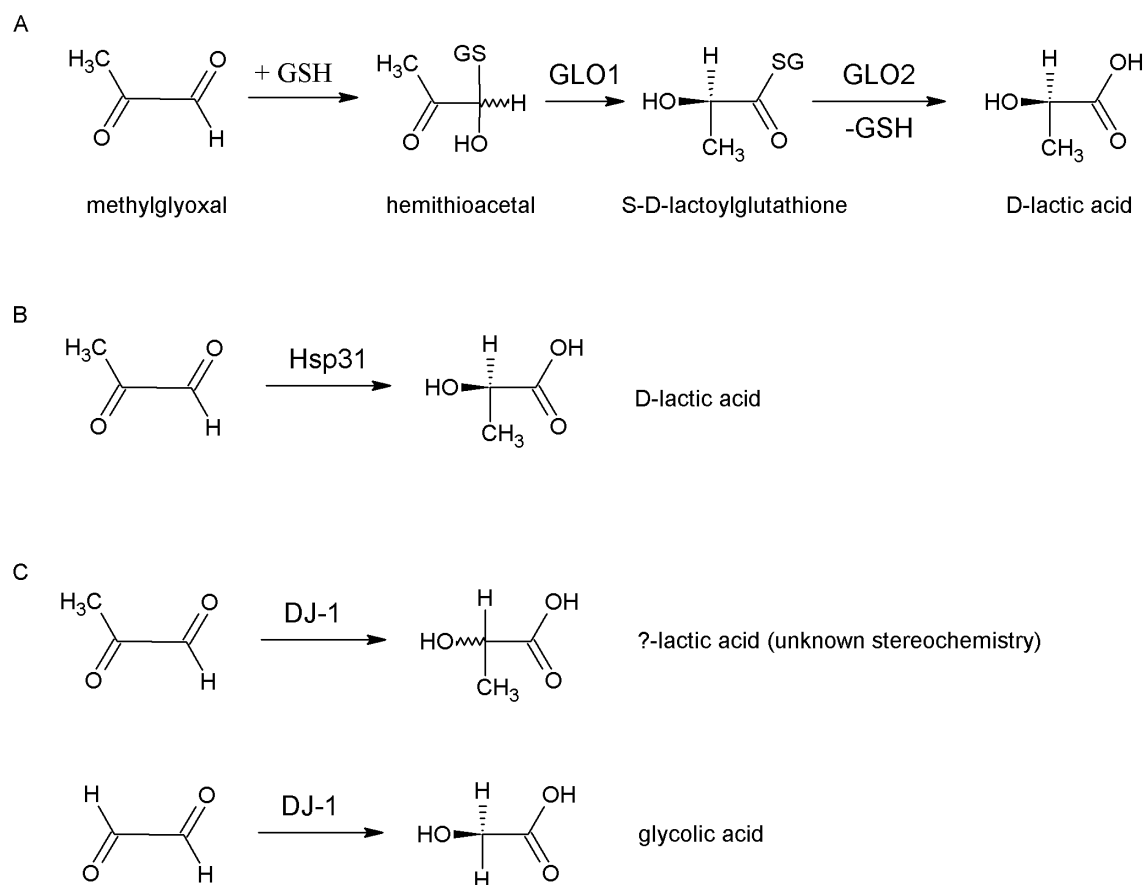


Figure 8. Glyoxalase reactions of GLO1/GLO2, Hsp31, and DJ-1. (A) The GLO1/GLO2 system catalyses the conversion of a glutathione (GSH) adduct of methylglyoxal into D-lactic acid. (B) In contrast, the *E. coli* Hsp31 is capable of converting methylglyoxal into D-lactic acid in the absence of any cofactor. (C) Likewise, DJ-1 possesses a cofactor-independent glyoxalase activity that detoxifies MGO and GO into lactic acid and glycolic acid, respectively.

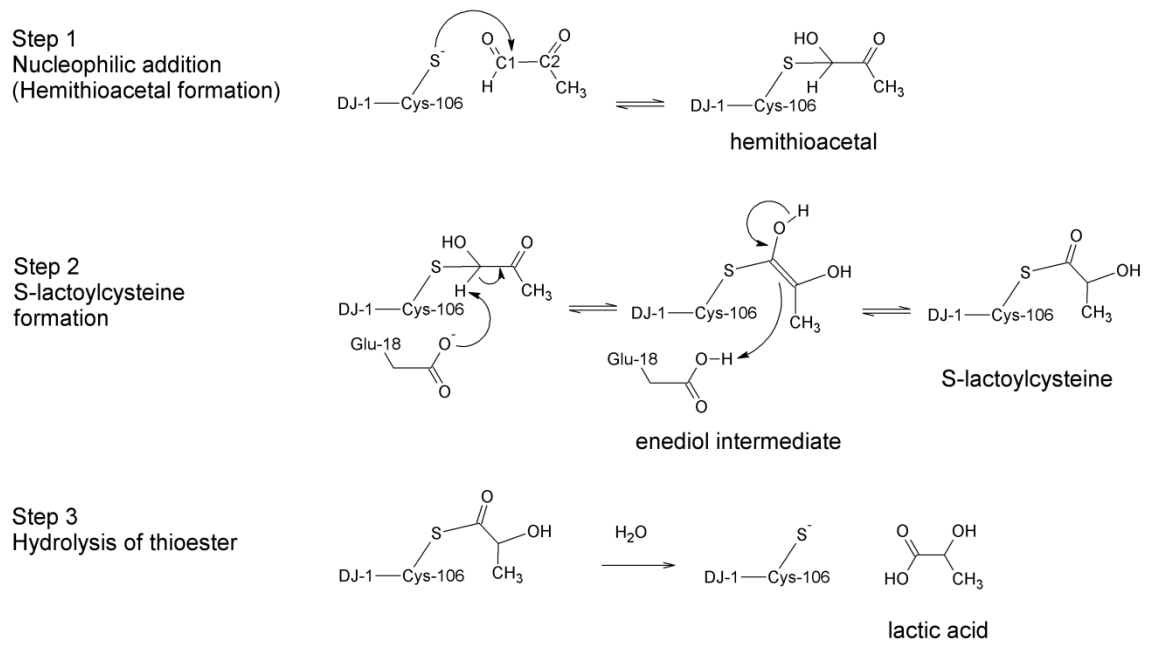


Figure 9. Proposed reaction mechanism for DJ-1 glyoxalase activity (adapted from Kwon *et al.*, 2013).

1.3 Aims

Although the ability of DJ-1 to sequester copper has been reported, the molecular means through which DJ-1 carries out this function is unknown. The first part of this dissertation aims to determine the structural and biochemical bases of the interaction of DJ-1 with copper, in order to provide insights into how PD-linked mutations would perturb this function. Specifically, the project attempted to achieve the following:

1. Define the chemical features and stoichiometry of the protein-metal complex using solution spectroscopy and mass spectrometry
2. Map the copper binding site using X-ray crystallography.
3. Determine the affinity of DJ-1 for copper to confirm the physiological formation of the complex.
4. Test the ability of DJ-1 to provide copper for SOD1.

The second part of this dissertation aims to characterise the structural and functional consequences of DJ-1 A107P mutation associated with early-onset Parkinson's disease. The mutation occurs in the nucleophile elbow motif of DJ-1, adjacent to a conserved cysteinyl residue that is critical for a number of DJ-1 cellular functions. This project aimed to achieve the following:

1. Produce a recombinant form of DJ-1 with the A107P mutation.
2. Determine the ability of the A107P variant to detoxify glyoxal.
3. Define the role of Ala-107 in the catalytic mechanism of DJ-1 glyoxalase activity using *in silico* and crystallographic analyses.
4. Determine the intracellular steady-state level of the A107P variant.
5. Characterise the structural changes caused by the A107P mutation using CD and NMR spectroscopy.

Chapter 2

Structural basis for the interaction of DJ-1 with Cu(I)

2.1 Introduction

Copper is an essential cofactor in several biological processes, however paradoxically, its mishandling may result in reactions that can lead to cellular damage. To prevent this deleterious effect, the eukaryotic cell limits the intracellular level of free copper ions down to a negligible concentration (Rae *et al.*, 1999). This poses a challenge for copper-binding proteins and a clear requirement for copper chaperones that can acquire and ferry copper ions to a target protein. SOD1 is a copper-requiring enzyme that converts the superoxide radical into less active products, hydrogen peroxide and oxygen (McCord and Fridovich, 1969). The 27-kDa protein CCS (Copper Chaperone for Superoxide dismutase) is mainly responsible for the copper acquisition and activation of SOD1 (Culotta, 1997). CCS has three domains; domains I and III are responsible for copper binding and transfer while domain II is required for interaction with SOD1 (Figure 11; Schmidt *et al.*, 1999; Rae *et al.*, 2001). The copper ions are held through metal binding sites identified by the consensus sequence CXXC or CXC where C is a cysteinyl residue and X is any residue (Figure 10; Schmidt *et al.*, 1999; Rae *et al.*, 2001).

An alternative pathway for copper acquisition by SOD1 is known to exist as a mouse CCS knockout retained ~15% of brain SOD1 activity (Wong *et al.*, 2000). The factors contributing to this alternative pathway remain elusive. In 2010, Xu *et al.* demonstrated the ability of DJ-1 to bind copper and stimulate the activity of SOD1. Their results suggest a copper chaperone function for DJ-1 that potentially plays a role in the alternative pathway.

More recently, Bjorkblom *et al.* (2013) also demonstrated the ability of DJ-1 to sequester metals such as copper and mercury and protect cells from metal-induced cytotoxicity. DJ-1 has neither a metal binding sequence motif (CXXC or CXC) nor a CCS SOD-like domain that can interact with SOD1. Hence, the structural and chemical means by which DJ-1 carries out either a copper chaperone activity or metal

sequestration is not understood. In this chapter, the molecular basis of the interaction of DJ-1 with copper was characterised using spectroscopic analysis, mass spectrometry and X-ray crystallography coupled with structure-guided mutational analysis.

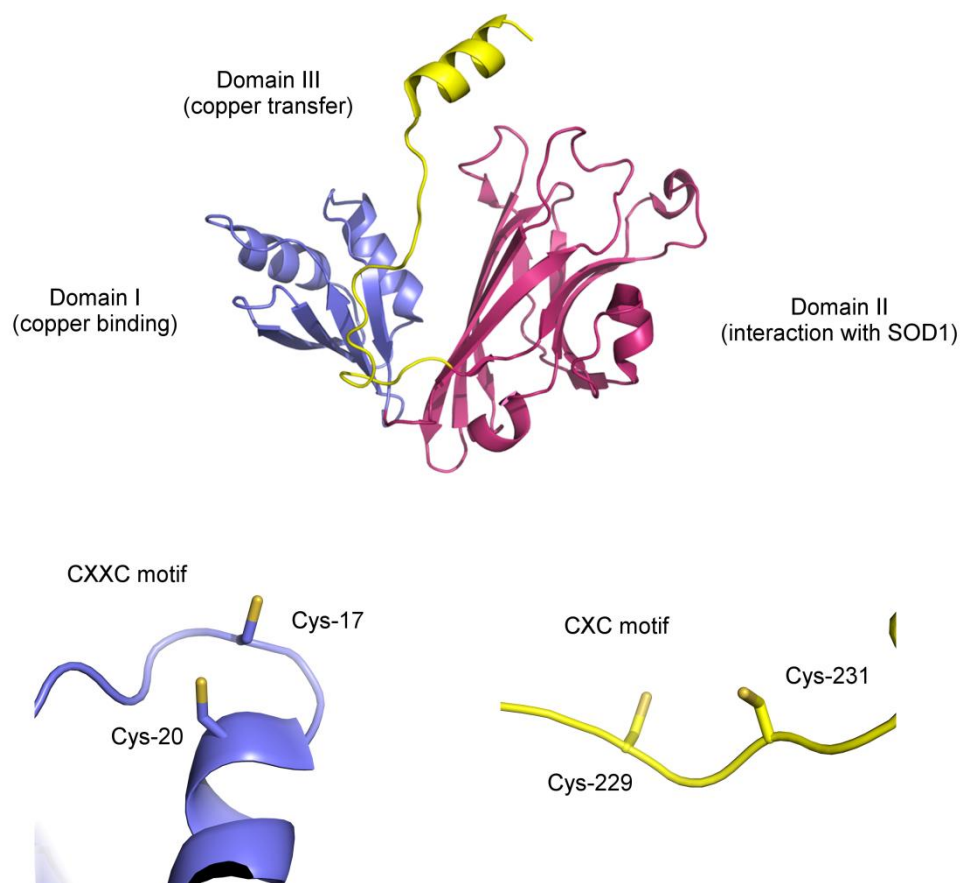


Figure 10. Crystal structure of the yeast CCS. Cartoon representation of the yeast copper chaperone for SOD1 (PDB ID code: IQUP). Domains I, II and III are coloured blue, magenta and yellow, respectively. The lower panel depicts the metal binding sequence motifs CXXC and CXC in domains I and III, respectively. Structures were rendered using PyMol (Delano, 2002).

2.2 Results

2.2.1 Recombinant protein expression and purification of human DJ-1

To produce proteins for structural and biochemical analysis, DJ-1 was cloned in a bacterial expression vector pET-28a. A DJ-1 construct with a C-terminal hexahistidine (His₆) tag was prepared to allow high-yield expression of DJ-1 that could be easily purified by Ni²⁺/Co²⁺-affinity chromatography. This construct is identical to the one used by Liang and Tong (2003) to produce diffracting crystals of DJ-1 and hence was used to set up crystal screens. An untagged DJ-1 construct was also prepared for biochemical assays to prevent fortuitous interaction of copper with the His₆ tag.

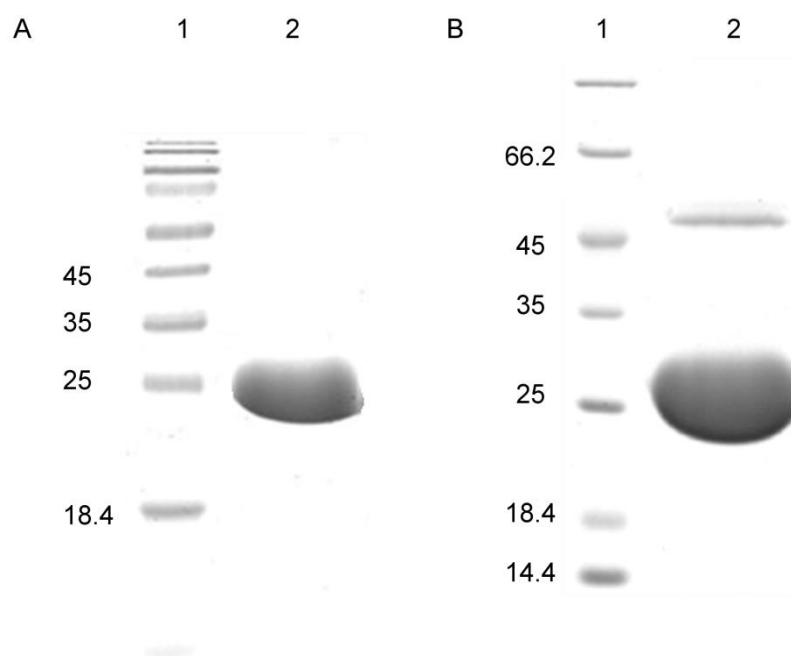


Figure 11. SDS-PAGE analysis of purified DJ-1. Proteins were expressed in *E. coli* BL21(DE3) cells, transformed with the appropriate pET-28a DJ-1 construct. A protein extract was prepared from the cells and was fractionated using Co²⁺-affinity resin (Pierce) for His₆ tagged protein or phenyl sepharose for untagged DJ-1 protein and finally passed through Q-sepharose resin. An aliquot of the final eluate was analysed by SDS-PAGE using a 12% w/v acrylamide gel stained with Coomassie R-250. (A) His₆ tagged DJ-1. Lane 1: Pierce PageRuler prestained molecular weight marker, indicated sizes in kDa; lane 2: Purified His₆ tagged DJ-1. (B) Untagged DJ-1. Lane 1: Pierce unstained molecular weight marker, indicated sizes in kDa; lane 2: Purified untagged DJ-1.

The recombinant His₆-tagged DJ-1 protein was expressed as a soluble protein with good yield, about 15 mg of purified protein was obtained per litre of culture, using *E. coli* BL21 (DE3). The protein was purified as a single band after Co²⁺-affinity and Q-sepharose chromatography with an apparent molecular weight of 25 kDa (Figure 11A). The theoretical molecular weight is 20956 Da for the His-tagged DJ-1 monomer.

Untagged DJ-1 was expressed in *E. coli* BL21 (DE3) following the same conditions used for His₆-tagged DJ-1. The initial ammonium sulphate (60% saturation) cut precipitated the majority of *E. coli* proteins while keeping DJ-1 soluble. Phenyl-sepharose chromatography successfully isolated pure DJ-1 which was eluted using 40% ammonium sulphate saturated buffer. Wild-type DJ-1 did not bind the Q-sepharose resin and eluted as a 25-kDa band (Figure 11B). The theoretical molecular weight of untagged DJ-1 is 19891 Da. The band at 50 kDa corresponds to a DJ-1 homodimer which is occasionally observed when the purified protein has not been thoroughly denatured. Fifteen milligrams of untagged protein was obtained per litre of culture

2.2.2 Electronic absorption spectroscopy indicates that Cu(I) is coordinated through thiolate S_γ.

Using isothermal calorimetry, Xu *et al.* (2010) have shown that DJ-1 can bind Cu(II). But inside the cell, Cu(I) is the predominant oxidation state of copper and the form delivered by metallochaperones (Davis and O'Halloran, 2008). Therefore I chose to characterise the interaction of untagged DJ-1 with Cu(I). Since Cu(I) is easily oxidised in the presence of oxygen, the experiments were performed in an anaerobic box under a N₂ atmosphere. A solution of [Cu(CH₃CN)₄]PF₆ was chosen as a Cu(I) source.

Interaction of metals with proteins can be monitored by electronic absorption spectroscopy (Boal and Resenzweig, 2009). The charge transfer transition between the metal and the ligating residues results in the absorption of a quantum of energy that is indicative of a specific metal coordinating complex (Que, 2000). The electronic

absorption spectrum of the Cu(I)-titrated DJ-1 displayed an absorption band centered at 254 nm (Figure 12), a common spectral feature of metallochaperones that bind Cu(I) via thiolate moieties of cysteinyl residues (Cobine *et al.*, 2000). This absorbance peak specifically results from a charge transfer transition between an S_{γ} atom of a thiolate group and a Cu(I) ion (Cobine *et al.*, 2000). There were no peaks observed around 500-600 nm which corresponds to the interaction of copper ions with histidine residues (Cobine *et al.*, 2000). This indicates that the copper ion is specifically coordinated by cysteinyl residues. The spectrum of as-isolated DJ-1 did not show the absorption band at 254 nm suggesting that the recombinant DJ-1 might have lost the copper during the purification procedure.

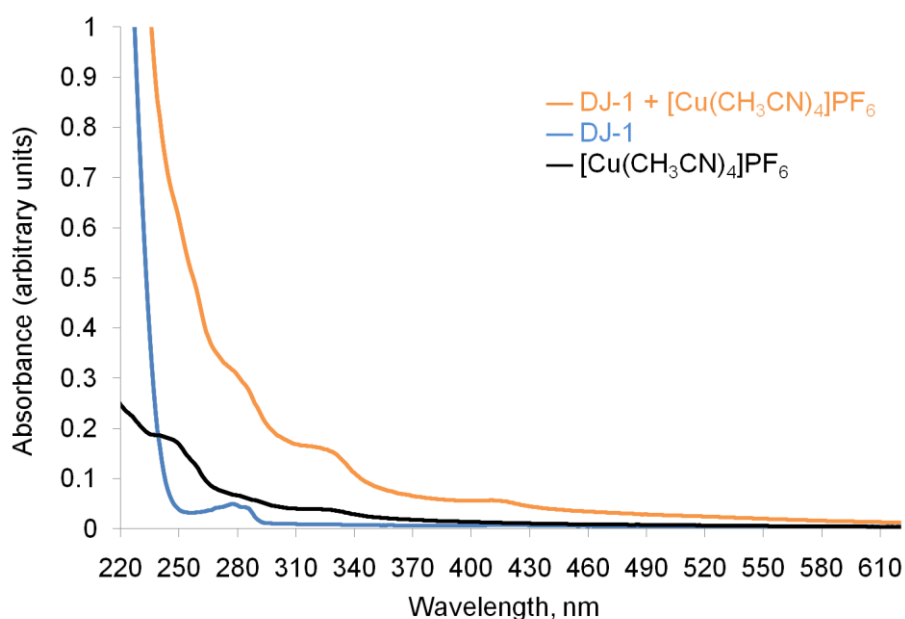


Figure 12. Absorption spectrum of Cu(I)-titrated DJ-1. Addition of a stoichiometric amount of Cu(I) to untagged DJ-1 solution (10 μ M dimer, orange line) under anaerobic conditions resulted in the development of an absorption band around 254 nm indicating the formation of a complex between a thiol sulphur and Cu(I). Copper-free (as-isolated) DJ-1 (blue line) did not show the characteristic absorption band. The spectrum of the Cu(I) titrant (10 μ M) is shown as a black line.

2.2.3 DJ-1 interacts with Cu(I) as a Cu^I(DJ-1)₂ complex

To determine the stoichiometry of the complex, DJ-1 was incubated with molar excess of Cu(I) stabilised with reduced glutathione (Ciriolo *et al.*, 1990), hereafter referred to as Cu(I)-GSH, and subjected to matrix-assisted laser desorption ionisation time-of-flight (MALDI-TOF) and nanoflow electrospray ionisation mass spectrometry (nESI-MS). MALDI-TOF has been used to determine metal adducts of proteins, however, samples are more prone to denaturation and fragmentation (Hartinger, *et al.*, 2008). nESI-MS has superior sensitivity with the advantage of analysing protein-protein, protein-ligand, and protein-metal interactions in a native state (Benesch *et al.*, 2007).

The mass spectrum derived from the MALDI-TOF analysis of the apo form of the untagged DJ-1 showed a predominant monomeric species with a centroid mass of 19753 Da, consistent with the notion that MALDI-TOF denatures most of the protein. However, the molecular ion peak at m/z 39513.1 indicated the presence of a DJ-1 homodimer (Figure 13A). When a 4-fold molar excess of fresh Cu(I)-GSH was incubated with DJ-1 solution prior to analysis, the molecular ion peak increased by ~67 Da, demonstrating the formation of a copper monoadduct of the DJ-1 homodimer (Figure 13B).

Subsequently, nESI-MS was used to analyse the complex in a more native state. Various charge states that match the molecular mass of untagged recombinant DJ-1 were detected in the mass spectrum of the metal-free protein (Figure 14A). In contrast to MALDI-TOF, a dimeric species dominated the spectrum consistent with the ability of nESI-MS to analyse native complexes. When Cu(I)-GSH was added in 4-fold excess over dimeric DJ-1, a mass increase of 374 m/z was observed for the peak corresponding to the dimeric species, suggesting an interaction between a DJ-1 homodimer, a single Cu(I) ion (63 Da), and a further glutathione species (305 Da) (Figure 14B). A small fraction of the DJ-1 monomer showed a mass increase of 302 Da, indicating a covalent

glutathione adduct. However, a greater proportion of monomeric species were not covalently linked to glutathione suggesting the possibility of glutathione participating as a third ligand for Cu(I) with the dimeric species. Glutathione has been previously shown to act as an exogenous ligand for coordinating Cu(I) to copper chaperones with a biscysteinate metal binding site (Ralle *et al.*, 2003). Such a tri-coordinate complex has been proposed to represent a metal-transfer mechanism involving the exchange of ligands between the copper chaperone and the target protein (Ralle *et al.*, 2003).

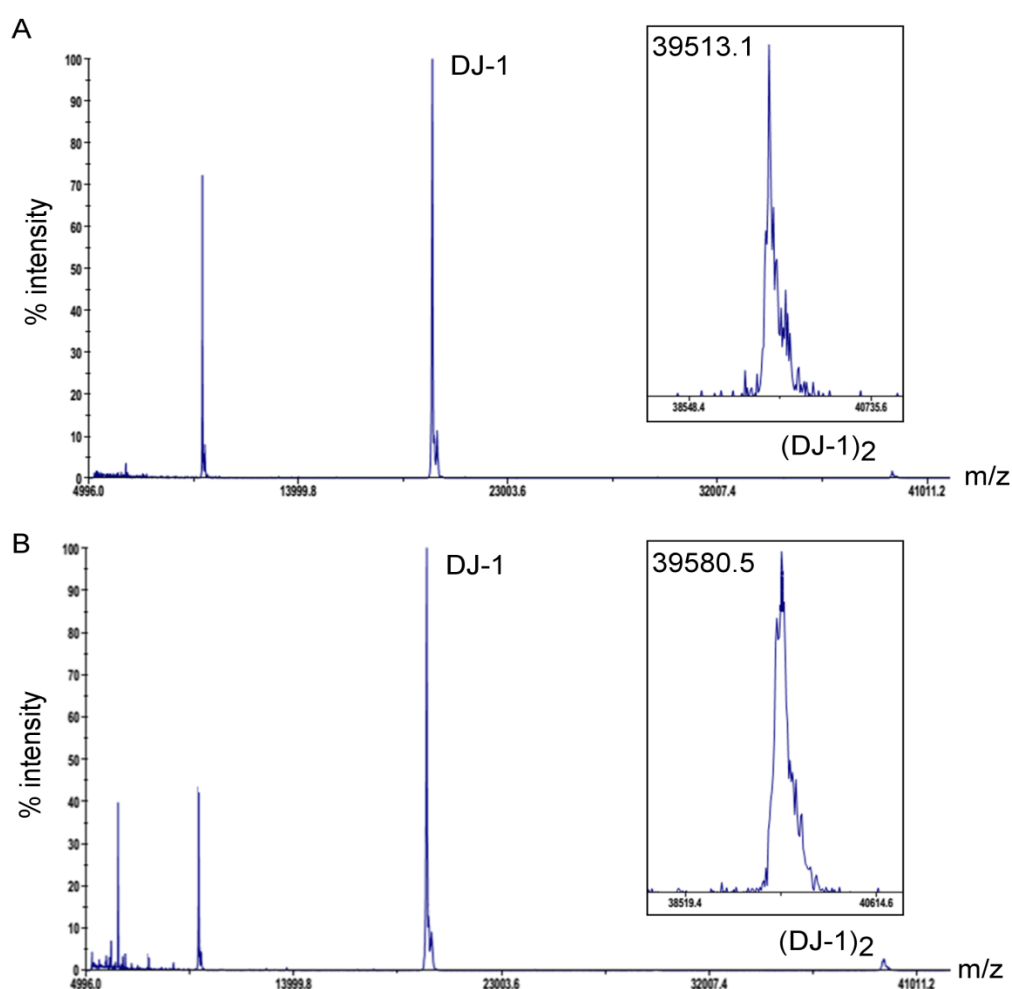


Figure 13. Cu(I) interaction of DJ-1 probed by MALDI-TOF. Panel A shows the mass spectrum of the apo-DJ-1. Inset shows the mass (39513.1 Da) of the molecular ion peak which represents DJ-1 homodimer (DJ-1)₂. Panel B shows the mass spectrum of the apo-DJ-1 treated with 4-fold molar excess of Cu(I)-GSH prior to sampling into the matrix. Inset shows the centroid mass (39580.5 Da) of the molecular ion peak which represents the Cu(I)-bound DJ-1 homodimer.

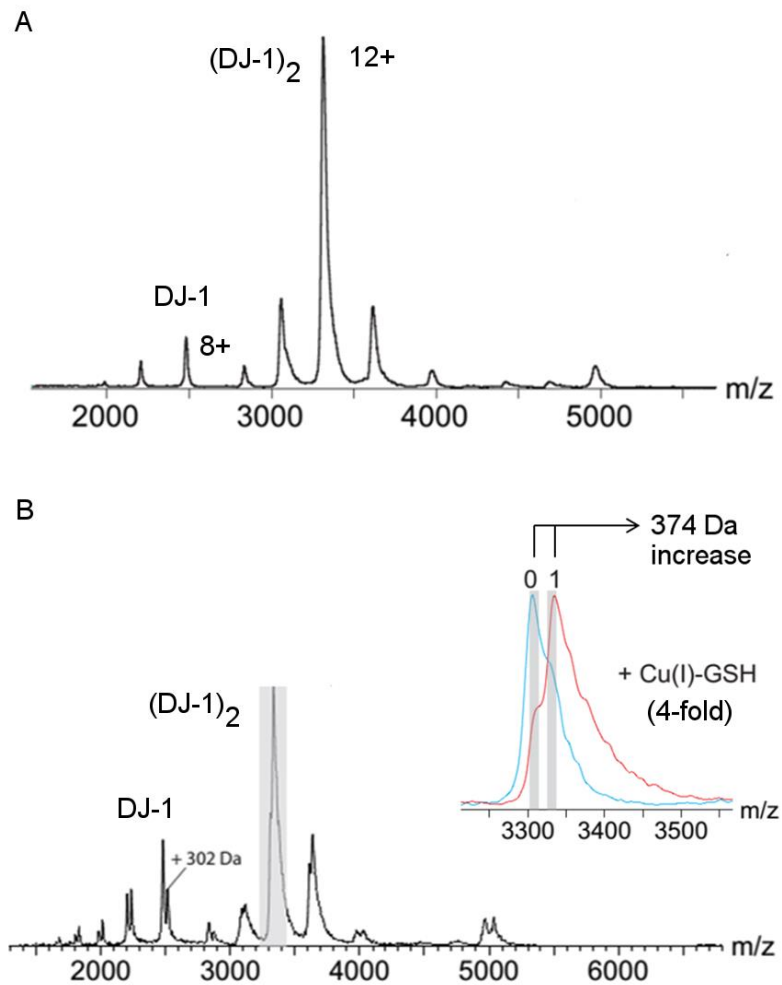


Figure 14. Cu(I) interaction of DJ-1 probed by nESI-MS. Panel A shows the mass spectrum of apo-DJ-1; calculated masses 19865 ± 1 Da (monomer/DJ-1; 8+ charge state) and 39842 ± 10 Da (homodimer/(DJ-1)₂; 12+ charge state). Panel B shows the mass spectrum of DJ-1 incubated with Cu(I)-GSH. Inset shows the mass increase of 374 Da of the DJ-1 homodimer ((DJ-1)₂; 12+ charge state) when incubated with 4-fold molar excess of Cu(I)-GSH (red peak).

2.3.4 Crystal structure of Cu(I)-bound DJ-1 reveals a new copper binding motif

X-ray crystallography was used to map the copper binding site. Crystals of His₆-tagged DJ-1 were grown according to conditions described by Tao and Tong (2003). Hexagonal bipyramidal crystals grew overnight (Figure 15A). Crystals were soaked in the mother liquor containing molar excess of Cu(I)-GSH. The soaked crystals diffracted to 1.4 Å and were isomorphous to the apoprotein crystal with a space group P3₁21. An initial model was obtained by molecular replacement and after several cycles of refinement, the final structure achieved an R_{work}/R_{free} of 0.1184/0.1498 (see Table 2 for data collection and refinement statistics).

The omit difference density map derived from the Cu(I)-soaked crystal showed that the Cu(I) is coordinated by the S_γ atoms of the thiolate side chains of cysteine 53 from each monomer forming a biscysteinate copper centre (Figure 15B and 15C). The coordinate-covalent bond between Cu(I) and S_γ exhibits a distance of 1.9 Å. The complex has almost a linear molecular geometry with S-Cu-S bond angle of 163.2°. Contrary to the nESI-MS results, glutathione was not found to be ligated to Cu(I) in the crystal structure. Crystal packing may have occluded the formation of a glutathione adduct. Copper binding did not induce a gross change in the conformation of DJ-1 (backbone RMSD to the apoprotein form was within 0.2 Å, see Figure 16 for the superimposed structures). The copper centre is expected to have a -1 charge as a result of +1 from the metal ion and -1 charge from each thiolate group. Unlike other copper centres, the site is not neutralised by a nearby positively-charged residue *e.g.* lysine such as in Atox1 (Rodriguez-Granillo and Wittung-Stafshede, 2009). The copper binding cysteine is succeeded by a proline residue. Such a Cys-Pro motif has been shown to maximise the charge neutralisation effect conferred by an α-helix macrodipole to a metal binding site (Changela *et al.*, 2003). However, the Cys-Pro motif in DJ-1 is not found at the N-

terminus of a α -helix therefore an α -helix macrodipole does not contribute to the neutralisation of the negative charge at the copper centre.

To determine the oxidation state of the bound copper ion *in crystallo*, single crystal electronic absorption spectroscopy was performed in collaboration with beamline scientists at the Diamond Light Source, Oxford. The absorption spectrum (Figure 17A) recorded from the crystal derivatised with Cu(I) showed the same absorption peak at 254 nm of the protein solution titrated with Cu(I) (Figure 12). In addition, X-ray fluorescence spectroscopy confirmed the incorporation of Cu(I) with a K-edge at 8995 eV and a distinct shoulder at 8983 eV corresponding to the characteristic $1s \rightarrow 4p$ transition observed on excitation of Cu(I) (Figure 17B; Ferraroni *et al.*, 1999).

To confirm the role of Cys-53 in binding copper, the Cys-53 was mutated to an alanine using PCR mutagenesis and the untagged mutant construct was expressed and purified using the same protocol as with the wild-type protein (Figure 18A). DJ-1 C53A protein (DJ-1^{C53A}) was incubated with molar excess of Cu(I) anaerobically and the electronic absorbance spectrum was recorded. Unlike the wild-type protein, DJ-1^{C53A} did not show a Cu(I)-S _{γ} specific absorbance at 254 nm, confirming the structural role of Cys-53 in copper binding (Figure 18B).

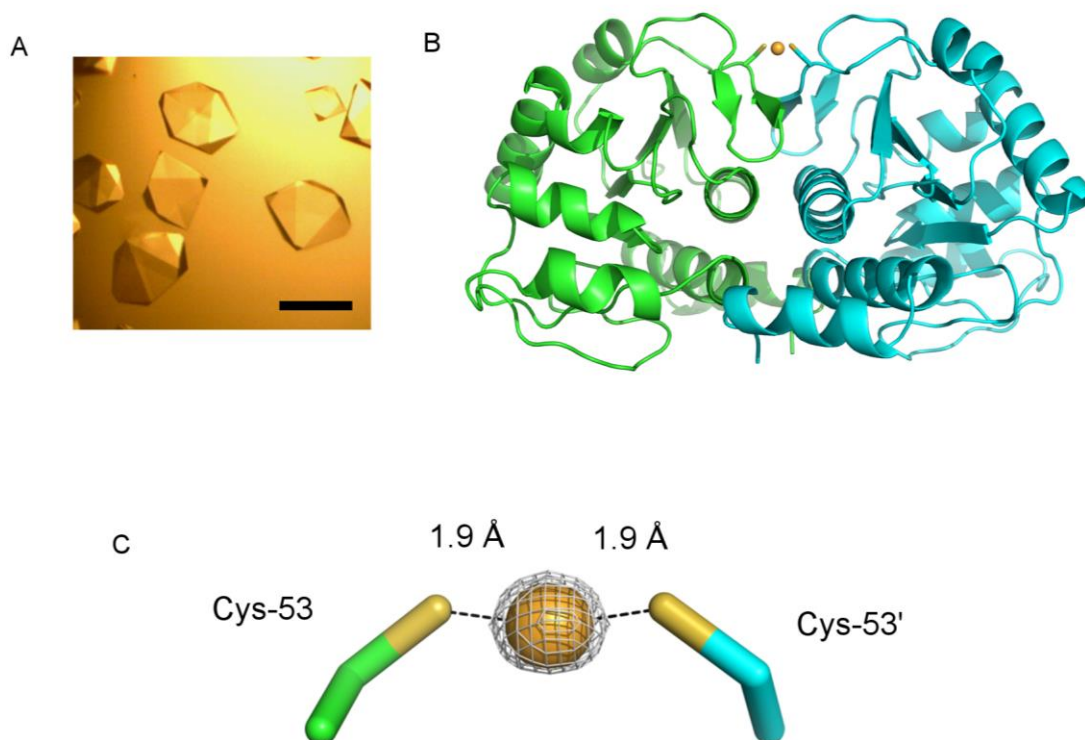


Figure 15. Crystal structure of the metal-bound DJ-1. (A) The hexagonal bipyramidal crystals of DJ-1 used for the metal soaking experiments are shown. Scale bar = 0.5 mm. (B) Cartoon representation of the crystal structure of DJ-1 with the Cu(I) (orange sphere) bound at the homodimer interface. One protomer is green and the other is cyan in the DJ-1 homodimer. The atomic coordinates and structure factors have been deposited in the Protein Data Bank (PDB ID: 4BTE). Panel C shows the anomalous difference map (grey, contoured at 10.0σ) of the Cu(I) binding site with the cysteinyl S γ distances to the metal centre in Å. Structures were rendered using PyMol (Delano, 2002).



Figure 16. Structural alignment of apo- and Cu(I)-bound DJ-1. Superposition of the backbone traces of the apo-DJ-1 (black trace; PDB ID code:1PDV) and the Cu(I)-DJ-1 complex (magenta trace; PDB ID code: 4BTE) indicated no gross conformation changes upon binding of Cu(I) to DJ-1. The backbone RMSD of the Cu(I) bound structure to the apoprotein form was within 0.2 Å. The copper ion is shown as an orange sphere. Structures were rendered using Pymol (Delano, 2002).

Table 2. Data collection and refinement statistics for Cu(I)-bound DJ-1.

Cu(I)-bound DJ-1	
<i>Data collection</i>	
Space group	P3 ₁ 21
Cell dimensions	
<i>a, b, c</i> (Å)	75.26, 75.26, 75.35
<i>α, β, γ</i> (°)	90, 90, 120
Resolution (Å)	26.2 (1.34 – 1.38)*
R_{merge}	0.077 (0.438)
I / σI	34.8 (3.1)
Completeness (%)	89.5 (15.2)
Redundancy	28.9 (3.8)
<i>Refinement</i>	
d_{min} (Å)	1.38
No. reflections	43643
R_{work}/ R_{free}	0.1184/ 0.1498
<i>No. atoms</i>	
Protein	1391
Cu(I)	1
Water	218
<i>B-factors</i> (Å ²)	
Protein	15.9
Ligand/ion	66.6
Water	42.4
RMSD	
Bond lengths (Å)	0.0249
Bond angles (°)	2.183

* Values in parentheses are for the highest resolution bin.

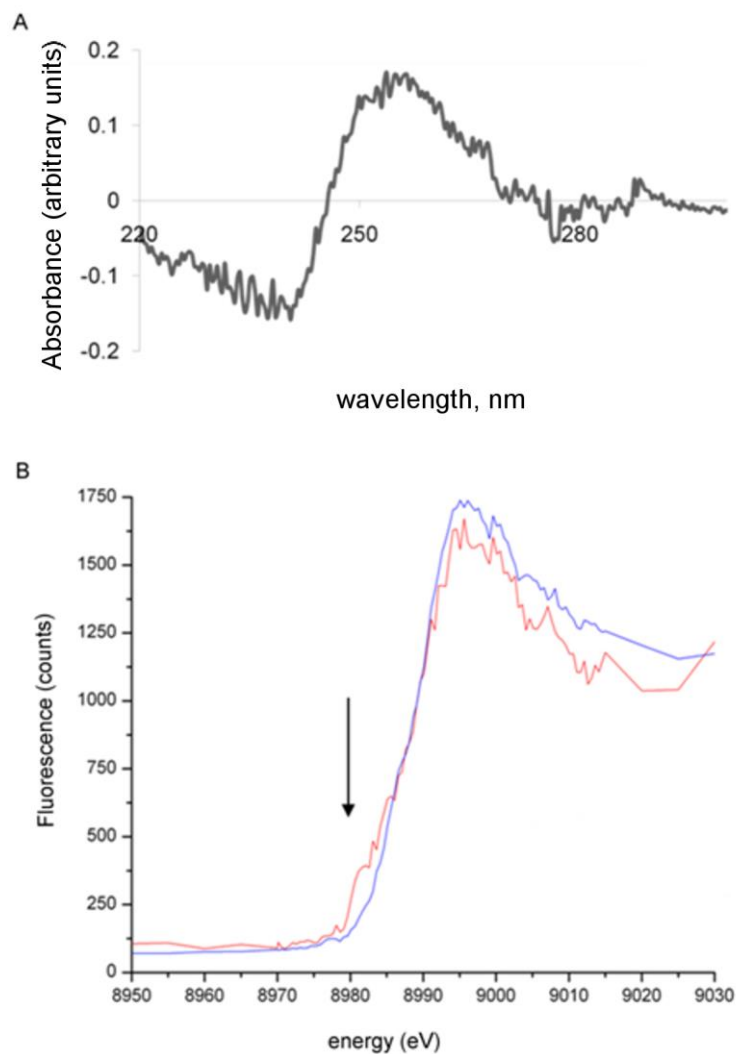


Figure 17. Spectroscopic analysis of Cu(I)-bound DJ-1 *in crystallo*. (A) Difference electronic absorption spectrum of the crystal soaked in Cu(I)-GSH indicating the interaction of Cu(I) with thiolate moieties. Spectrum was obtained by normalisation of the protein content followed by the subtraction of the spectrum of the non-derivatised DJ-1 crystal from the spectrum of the soaked crystal. (B) Fluorescence spectra of DJ-1 derivatised with either Cu(I) (red) or Cu(II) (blue). The shoulder (indicated by the arrow) before the Cu K-edge confirms the presence of Cu(I).

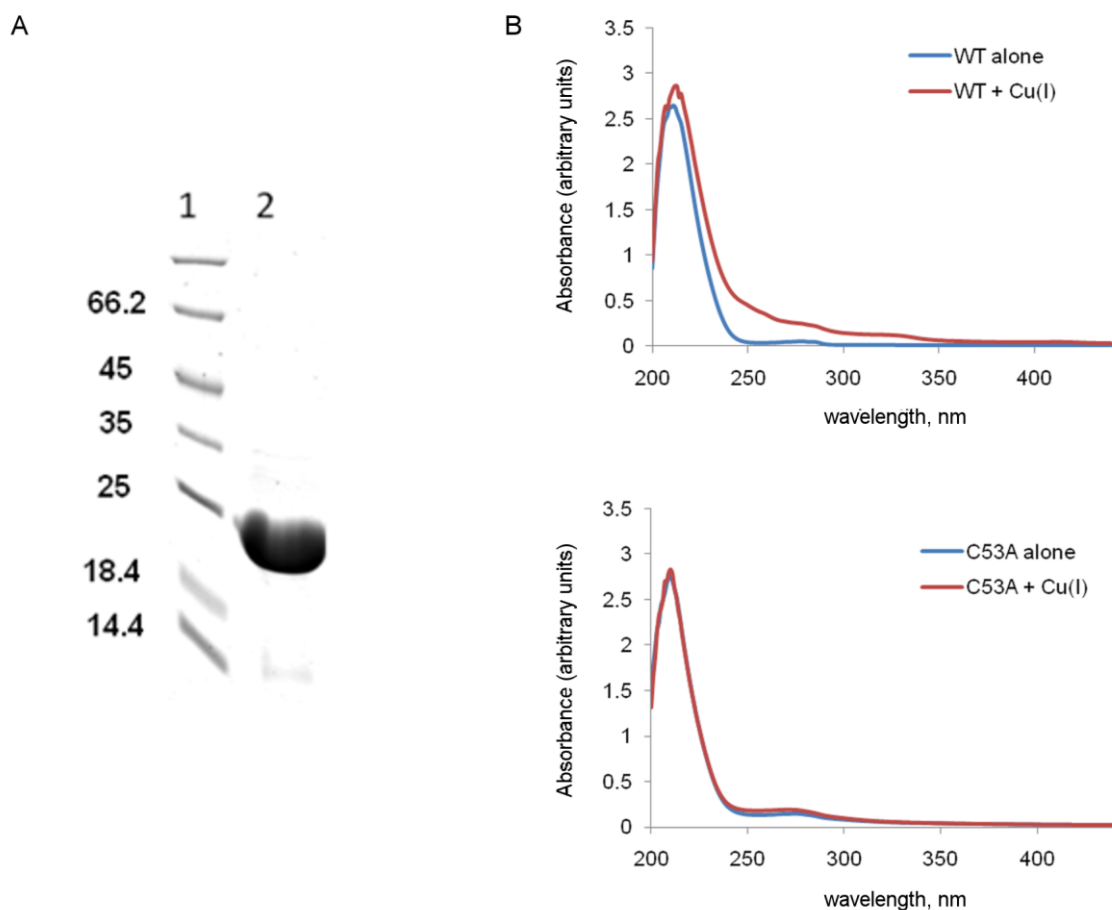


Figure 18. Cu(I) binding analysis of recombinant DJ-1^{C53A}. (A) Protein was produced in *E. coli* BL21(DE3) cells, transformed with the appropriate pET-28a construct of DJ-1 with a C53A mutation. Purification was performed using phenyl sepharose and Q-sepharose chromatography. An aliquot of the final eluate was analysed by SDS-PAGE using a 12% w/v acrylamide gel stained with Coomassie R-250. Lane 1: Pierce PageRuler unstained molecular weight marker with indicated sizes in kDa, lane 2: Purified untagged DJ-1^{C53A}. (B) Proteins were prepared in N₂-purged buffer containing 25 mM Tris pH 7.5, 100 mM NaCl. Two-fold molar excess of Cu(I) was added to apo-proteins anaerobically and the electronic absorbance spectra were recorded. [Cu(CH₃CN)₄]PF₆ was used as Cu(I) source. Spectra from Cu(I)-incubated proteins were normalised against the spectrum of the Cu(I) titrant.

2.2.5 DJ-1 binds Cu(I) with subfemtomolar affinity

Copper chaperones possess a high affinity for their cognate metal ion because of the controlled supply of copper ions in the intracellular milieu (Rae *et al.*, 1999; Xiao *et al.*, 2011). The majority of the copper chaperones have subfemtomolar affinity in order to retain the metal ion inside the cell (Xiao *et al.*, 2011).

To accurately measure the copper affinity of DJ-1, the Cu(I) exchange between DJ-1 and bicinchoninic acid (Bca), shown in the equation below, was carried out in both directions.



Bca is a Cu(I)-specific chelator that forms a chromophoric complex with an accurately measured formation constant (β) equal to $10^{17.2} \text{ M}^{-2}$ (Zhou *et al.*, 2008; Xiao *et al.*, 2011). To ensure that all Cu(I) ions are bound, the $\text{Cu}^{\text{I}}(\text{DJ-1})_2$ and $\text{Cu}^{\text{I}}(\text{Bca})_2^{3-}$ complexes were prepared by preincubating a molar excess of either DJ-1 dimer or Bca, respectively, relative to Cu(I). When equilibrium was reached, the concentration of each component was quantified which then enabled the calculation of the dissociation constant using the equation described in the section 5.5.4. An average dissociation constant of $6.41 \times 10^{-16} \text{ M}$ was estimated for the $\text{Cu}^{\text{I}}(\text{DJ-1})_2$ complex (data shown in Table 3). This is in the same range as other human copper binding proteins such as Atox1 ($10^{-17.4} \text{ M}$, Xiao and Wedd, 2010) and WLN5-6 ($10^{-17.6} \text{ M}$, Xiao *et al.*, 2011), highlighting the ability of a $\text{Cu}^{\text{I}}(\text{DJ-1})_2$ complex to form under physiological conditions.

Table 3. Dissociation constant for Cu^I(DJ-1)₂ complex based on competition with bicinchoninic acid (Bca).

[(DJ-1) ₂] _{total} (μM)	25 ^a	25 ^a	25 ^a	25 ^b	25 ^b	25 ^b
[Bca] _{total} (μM)	280	560	650	750	1000	1250
[Cu(I)] _{total} (μM)	10	10	10	10	10	10
[Cu(Bca) ₂ ³⁻] _{eq} (μM)	3.43	5.37	3.93	7.15	8.51	8.92
[Cu ^I (DJ-1) ₂] _{eq} (μM)	6.57	4.63	6.07	2.85	1.49	1.08
<i>K_d</i> (x 10 ⁻¹⁶ M)	8.14	4.94	1.88	6.48	8.78	8.21
Average <i>K_d</i> (x 10⁻¹⁶ M) = 6.41 ± 1.07^c						

Assay was performed in copper-free phosphate-buffered saline. ^aData from addition of Bca into Cu(I)-bound DJ-1. ^bData from addition of DJ-1 into Cu(Bca)₂³⁻. ^cError shown as ± SEM.

2.2.6 DJ-1 does not stimulate the activity of SOD1 *in vitro*

To test the role of the copper binding site in the DJ-1 dependent activation of SOD1, recombinant wild-type DJ-1 and DJ-1^{C53A} were assayed for stimulation of SOD1 activity *in vitro* using a method established by Rae *et al.* (2001). The recombinant form of SOD1 was expressed and purified to homogeneity (Figure 19). A demetallation step was carried out to remove the copper ion in the active site of as-isolated SOD1. The percentage of SOD1 activity after demetallation was less than 5%.

Copper-dependent activation of apo-SOD1 was performed in anaerobic conditions. Since the activation of SOD1 requires oxygen, reaction mixtures were assayed aerobically. Cu(I)-GSH, which has been shown to be capable of activating apo-SOD1 *in vitro* (Ciriolo *et al.*, 1990), was used as a positive control. Consistently, the Cu(I)-GSH complex was capable of stimulating SOD1 activity. However, neither wild-type DJ-1 nor DJ-1^{C53A} showed substantial stimulation of SOD1 activity (Figure 20). The lack of *in vitro* activation suggests that an unknown cellular factor may be required to facilitate the interaction and/or activation of SOD1 by DJ-1. An alternative protocol was performed by our collaborators in Stavanger University Hospital (Norway) whereby DJ-1 proteins were immunoprecipitated from MEF *DJ-1*^{-/-} back-transfected with wild-type

or the C53A variant to capture factors that may mediate the copper transfer. The immunoprecipitated proteins were then incubated with apo-SOD1. However, neither wild-type DJ-1 nor the C53A variant exhibited an ability to activate apo-SOD1 (Appendix 1). Thus far, our results fail to show the DJ-1 dependent stimulation of SOD1 activity reported by Xu *et al.* (2010).

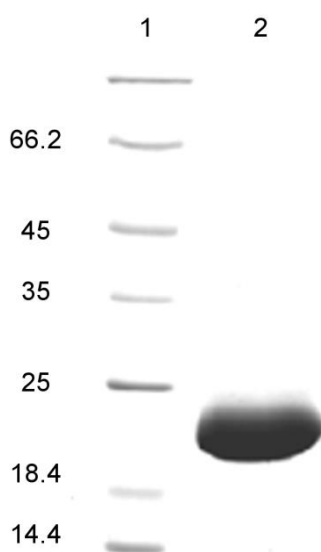


Figure 19. SDS-PAGE analysis of purified human SOD1. Protein was produced from *E. coli* BL21 (DE3) pLysS transformed with the pLEICS-03 SOD1 plasmid. A protein extract was prepared from the cells and was fractionated using Ni²⁺-affinity resin (Qiagen). An aliquot of the final eluate was analysed by SDS-PAGE using a 12% w/v acrylamide gel stained with Coomassie R-250. Lane 1: Pierce PageRuler unstained molecular weight marker with sizes indicated in kDa, lane 2: Purified recombinant SOD1.

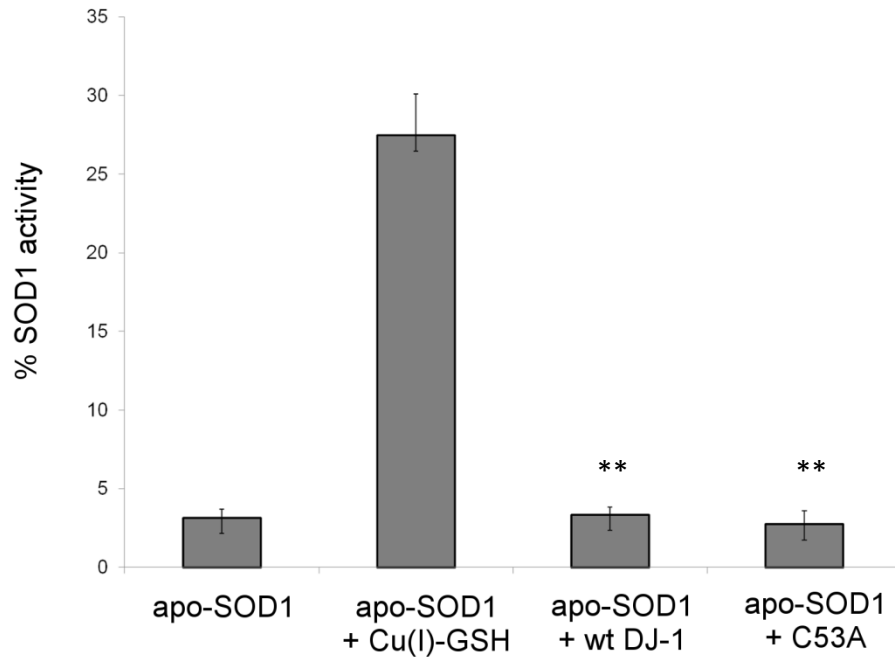


Figure 20. SOD1 activity assays *in vitro*. Untagged wild-type DJ-1 and its C53A variant were loaded with 30 μ M of Cu(I)-GSH complex and desalted to remove unbound metal ions. The DJ-1 proteins were then incubated with 15 μ M apo-SOD1 and 15 μ M zinc acetate at 37°C for 1 hour and assayed using a Sigma SOD assay kit. Holo-SOD1 was prepared by incubating apo-SOD1 with 30 μ M Cu(I)-GSH complex. SOD1 activity was measured as percent inhibition rate of WST-1 conversion to WST-1 formazan by the substrate superoxide. Error bars represent standard deviation. Data (n = 3) were collected in three independent experiments. **Unpaired t-test indicates that the difference is not statistically significant relative to the activity of apo-SOD1.

2.2.7 DJ-1 does not interact with SOD1

To determine if the recombinant forms of DJ-1 and SOD1 are capable of direct interaction, protein mixtures of DJ-1 and SOD1 variants were subjected to nESI-MS. We first determined whether the apo-DJ-1 and the copper-free, zinc-loaded SOD1 (Zn-SOD1) could form a complex. The mass spectrum of an equimolar mixture of apo-DJ-1 and Zn-SOD1 showed various charge states corresponding to dimers and tetramers of DJ-1 and SOD1 but no peaks for a binary complex were observed (Figure 21A). Interaction between DJ-1 and Zn-SOD1 perhaps requires a copper ion, thus, we recorded the mass spectrum of copper-loaded DJ-1 incubated with Zn-SOD1. However,

none of the resulting m/z states indicated the formation of a DJ-1-SOD1-Cu ternary complex (Figure 21B). The rate of copper transfer could be extremely fast thus making it difficult to capture the complex. Interaction between SOD1 and CCS was successfully trapped through phenylalanine substitution of an SOD1 copper binding residue His-48 and serine substitution of Cys-146 involved in the internalisation of the delivered copper ion to the active site (Lamb *et al.*, 2001). To capture the potential protein complex between DJ-1 and SOD1, an analogous SOD1 H46F/C146S variant (HCV) expressed and purified from *E. coli* (Figure 22), was incubated with copper-loaded DJ-1 and the mass spectrum of the mixture was recorded (Figure 22C). No peaks corresponding to a binary complex were formed suggesting that the interaction of the recombinant forms of DJ-1 and SOD1 does not exist under the conditions we have tested (Figure 21C). This provides a molecular explanation for the lack of SOD1 activation by DJ-1.

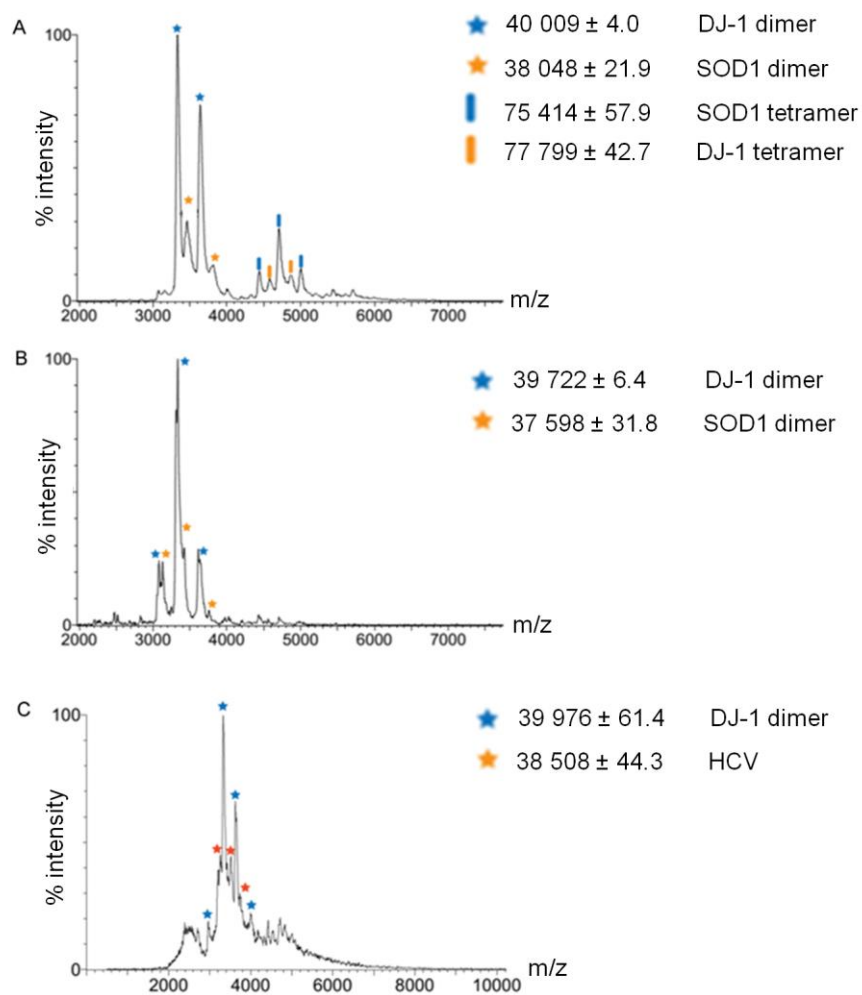


Figure 21. nESI analysis of interaction between DJ-1 and SOD1. (A) Mass spectrum of apo-DJ-1 incubated with Zn-SOD1. (B) Mass spectrum of copper-loaded DJ-1 mixed with Zn-SOD1. (C) Mass spectrum of the mixture of copper-loaded DJ-1 and the SOD1 H46F/C146S double mutant, HCV.

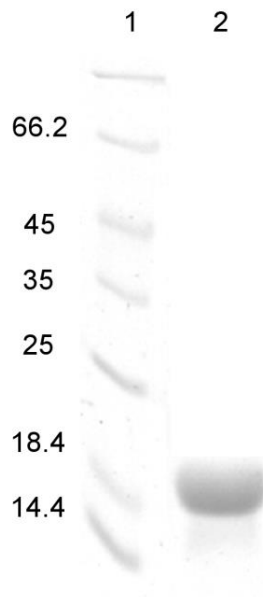


Figure 22. SDS-PAGE analysis of purified HCV. Protein was produced in *E. coli* BL21 (DE3) pLysS transformed with the pLEICS-03 SOD1 H46F/C146S (HCV) plasmid. A protein extract was prepared from the cells and was fractionated using Ni²⁺-affinity resin (Qiagen). An aliquot of the final eluate was analysed by SDS-PAGE using a 12% w/v acrylamide gel stained with Coomassie R-250. Lane 1: Pierce PageRuler unstained molecular weight marker with sizes indicated in kDa, lane 2: Purified HCV.

2.3 Discussion

The redox activity of copper ions is exploited by several proteins to carry out vital cellular processes. However, the same chemical reactivity can lead to deleterious effects in the cell, hence, the tight regulation of copper's intracellular availability (Rae *et al.*, 1997). To facilitate the proper distribution and homeostatic control of copper, the cell employs copper binding proteins to handle the storage and delivery of the metal ion. DJ-1 is a protein that has been suggested to be capable of delivering the copper cofactor of SOD1 and/or sequester free copper ions to prevent toxic accumulation in the intracellular milieu (Xu *et al.*, 2010; Bjorkblom *et al.*, 2013). In this chapter, we defined the molecular determinants that allow DJ-1 to function as a copper carrier.

Cuprous and cupric ions are the two oxidation states of copper that are relevant to biological processes (Davis and O'Halloran, 2008). Previous work by Xu *et al.* (2010) has shown that DJ-1 binds Cu(II), however, because of the reducing nature of the cytosol, Cu(I) is more likely the physiological form bound by DJ-1. Indeed, Cu(II) incubation of DJ-1 results in the formation of aggregates interlinked via disulphide bridges (Figure 23). Using electronic absorption spectroscopy, we have demonstrated the interaction of DJ-1 with Cu(I) and obtained information about the nature of ligation *i.e.* metal interaction through thiolate moieties. Mass spectrometric techniques consistently showed that one Cu(I) is held by each DJ-1 homodimer. Furthermore, nESI-MS results suggested that glutathione may also coordinate the copper ion, as has been observed in other copper binding proteins (Ralle *et al.*, 2003; Ralle *et al.*, 2004). However, glutathione was not observed in the crystal structure of Cu(I)-bound DJ-1. Crystal packing might have occluded the incorporation of the glutathione species.

Our crystallographic analysis of copper-bound DJ-1 reveals the first high resolution structure of a copper trafficking protein that forms a Cu(I)-biscysteinate complex whereby the thiolate

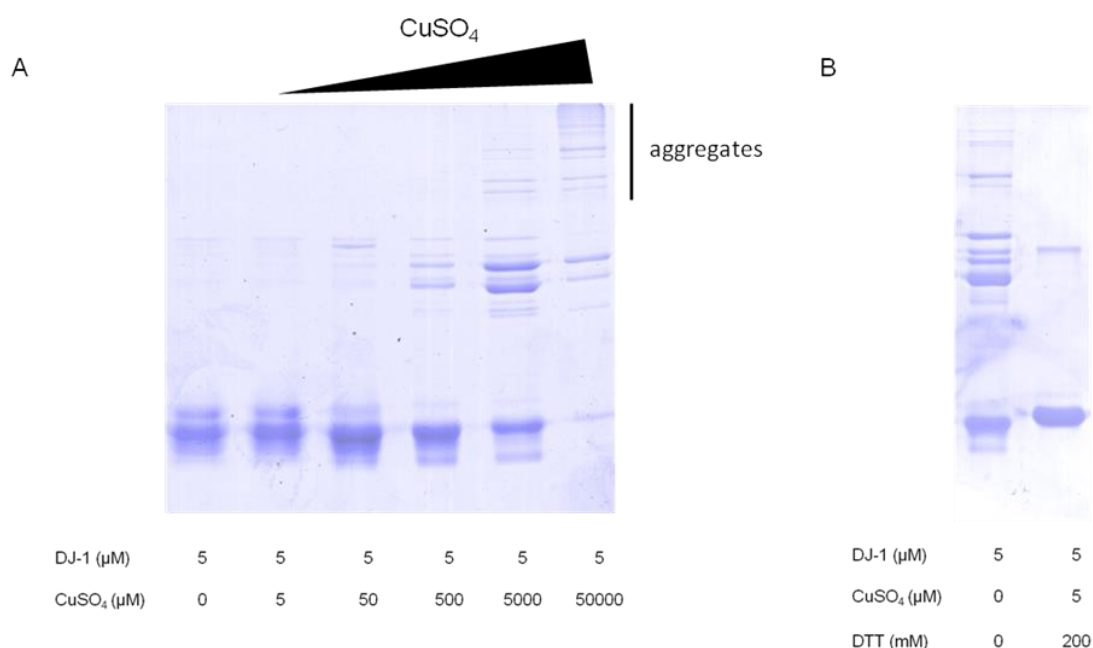


Figure 23. Cu(II)-induced aggregation of DJ-1. (A) Untagged DJ-1 (5 μM) was incubated with various concentration of CuSO₄ for 5 minutes. The reaction mixtures were quenched with SDS-PAGE sample buffer and heated for 5 minutes. Protein samples were analysed using SDS-PAGE. (B) DTT treatment of DJ-1 aggregates induced by CuSO₄ reverses protein aggregation.

ligands are coming from two separate subunits of the protein rather than from the canonical sequence motifs CXXC or CXC (Pufahl *et al.*, 1997; Davis and O’Halloran, 2008). Biscysteinate metal binding sites fulfill the requirements of a good metal ion donor. Firstly, they possess high metal affinity to acquire copper ions from a strictly limited intracellular pool. We have measured a subfemtomolar dissociation constant ($K_d = 6.4 \times 10^{-16}$ M) for the Cu^I(DJ-1)₂ complex, consistent with other human copper chaperones with similar biscysteinate sites such as Atox1 (3.9×10^{-18} M) and the N-terminal metal-binding domains 5 and 6 of the Wilson disease protein WLN5-6 (2.5×10^{-18} M) (Xiao *et al.*, 2011). Such high affinity supports the physiological retention of Cu(I) by DJ-1 inside the cell. Secondly, the low coordination number of biscysteinate sites is also favourable for ligand-exchange and metal transfer mechanisms. Biscysteinate sites form high-order complexes with residues (usually cysteines) of the cognate protein to facilitate metal transfer (Davis and O’Halloran, 2008).

SOD1 acquires its copper cofactor mainly through CCS (Culotta *et al.*, 1997; Wong *et al.*, 2000). But a CCS-independent pathway of copper acquisition has also been reported (Leitch *et al.*, 2009). Factors directly mediating this alternative pathway remain largely unknown. The report by Xu *et al.* (2010) of a copper-dependent stimulation of SOD1 activity by DJ-1 prompted us to determine whether DJ-1 contributes to the CCS-independent pathway. Thus, to show direct copper chaperone activity of DJ-1, the protocol developed by Rae *et al.* (2001) was used whereby copper loading to DJ-1 and copper transfer to SOD1 was performed in an anaerobic environment followed by measurement of SOD1 activity under aerobic conditions. In contrast to the previous report of Xu *et al.* (2010), no significant stimulation of SOD1 activity by DJ-1 was demonstrated under the conditions tested. Similarly, our collaborators failed to show activation of SOD1 by DJ-1 purified from mammalian cells. The absence of DJ-1-dependent SOD1 activation led us to determine whether the two proteins interact using nESI-MS. However, neither the absence nor the presence of copper in the mixture of recombinant DJ-1 and SOD1 showed the formation of a binary complex between the two proteins. Hence, our results are not consistent with the ability of DJ-1 to activate SOD1 *in vitro*. Initial data from our cell-based assays suggest that DJ-1 copper binding site does not considerably influence the intracellular SOD1 activity and the steady-state levels of superoxide radicals (Figure 24). Thus, the role of the copper binding site is not likely involved in the activation of SOD1.

Using X-ray fluorescence, Bjorkblom *et al.* (2013) reported the ability of DJ-1 to selectively sequester copper and mercury albeit no information on the residues involved in metal binding. Additionally, they have shown that DJ-1 was able to protect cells against the cytotoxicity induced by these metal ions (Bjorkblom *et al.*, 2013). Environmental exposure to copper and mercury has been associated with an increased risk of developing PD (Gorell *et al.*, 1997; Willis *et al.*, 2010). Heavy metals e.g. copper

and mercury are potent neurotoxins, capable of inducing oxidative stress and damaging cellular macromolecules (Paik *et al.*, 1999; Olivieri *et al.*, 2000; Arciello *et al.*, 2005; Yang *et al.*, 2010). The ability of DJ-1 to sequester copper and mercury is therefore important in the context of metal-induced neurodegeneration. Consistently, parkinsonism-linked mutations *e.g.* A104T and D149A abolished the cytoprotection conferred by DJ-1 against metal-induced cell death (Bjorkblom *et al.*, 2013).

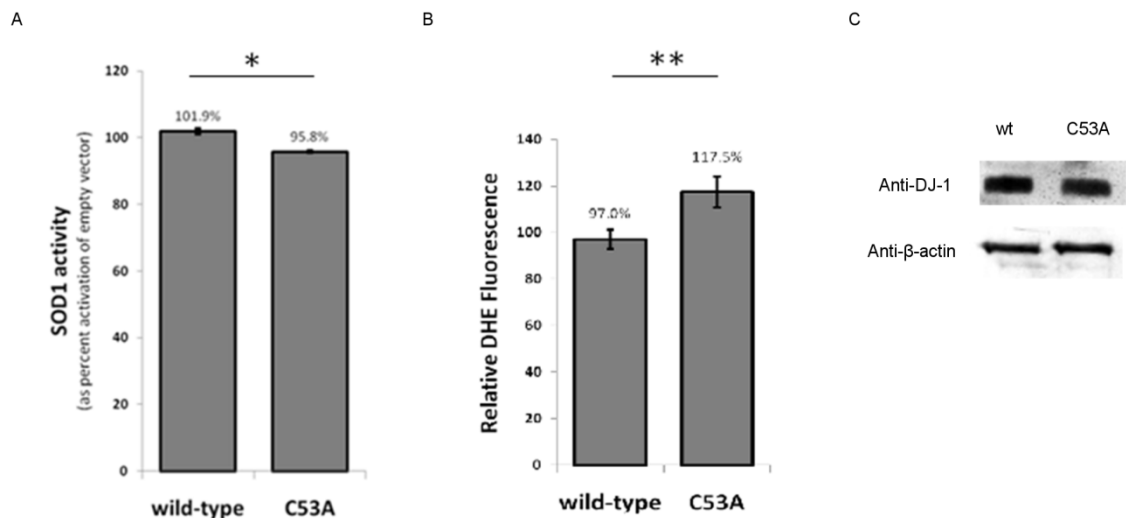


Figure 24. Cys-53 role in superoxide level modulation and SOD1 activation *in vivo*. (A) shows the relative intracellular SOD1 activity in SH-SY5Y cells stably transfected with wild-type DJ-1 or the C53A variant. Cells were treated with 20 μ M menadione to induce production of superoxide. Error bars represent standard deviation. Data (n = 3) were collected in three independent experiments.*Unpaired t-test indicates that the difference is statistically significant with a two-tailed $p < 0.001$. (B) Intracellular superoxide levels were measured using FACS analysis of DHE-stained SH-SY5Y cells stably transfected with a pCDNA 4 myc/His A vector expressing wild-type DJ-1, a C53A variant, or the empty vector. Superoxide production was induced by treating the cells with 20 μ M menadione for 30 minutes prior to staining. The bar graph shows the average relative DHE fluorescence from three independent experiments (n = 3). Each experiment counts 10 000 cells. Relative fluorescence of the empty vector was set to 100%. Error bars represent \pm SEM.** Unpaired t-test indicates that the difference is not statistically significant. (C) Western blot analysis of ectopically expressed DJ-1 in SH-SY5Y stable-transfected cell lines.

Our work elucidates the critical role of Cys-53 in metal sequestration, providing a structural basis by which DJ-1 overexpression could prevent the damaging reactions of free copper ions in the intracellular milieu. Mercury, a structural analogue of copper, has been found to bind biscysteinate sites of copper binding proteins (Larin *et al.*, 1999; Wernimont *et al.*, 2000). Thus, mercury would likely be held by Cys-53, allowing DJ-1 to modulate its cytotoxic effects. Sequence alignment of DJ-1 homologues across different species shows that Cys-53 is only conserved among vertebrates (Figure 25). This suggests that the ability of DJ-1 to bind copper is an emergent function that perhaps has been developed by vertebrates to tightly regulate copper homeostasis.

Because the copper binding site requires a DJ-1 homodimer, PD-linked mutations e.g. L10P, L158del, L166P, M26I, and E163K that disrupt homodimerisation would impair the ability of DJ-1 to sequester copper. The loss of cytoprotection against metal toxicity observed for the PD-linked A104T and D149A, are likely due to the fact that these mutations decrease DJ-1 homodimerisation (Moore *et al.*, 2005), potentially reducing the ability of these variants to form a copper binding site. Bjorkbolm *et al.* (2013) have also demonstrated that dopamine augmented the toxicity of the metals and significantly reduced the cytoprotection conferred by DJ-1. Cytosolic accumulation of dopamine has been shown to induce the covalent modification of Cys-53 by dopamine-derived quinones (Giroto *et al.*, 2012). This modification would render DJ-1 incapable of metal binding, thus explaining the reduced cytoprotective effect of DJ-1 when cells were co-treated with dopamine and metals (Bjorkbolm *et al.*, 2013). Cys-53 can also be modified through S-nitrosylation (Ito *et al.*, 2006) and oxidation (Choi *et al.*, 2006). These chemical alterations of Cys-53 would impair the ability of DJ-1 to sequester copper/mercury and as a result could increase the vulnerability of dopaminergic neurons to abnormal levels of copper/mercury.

```

Q99497|PARK7_Human/1-189      1  . . . . . MASKRALVILA-KGAEEMETVIPVDVMRRAG30
Q99LX0|PARK7_Mouse/1-189     1  . . . . . MASKRALVILA-KGAEEMETVIPVDVMRRAG30
QB8W59|PARK7_Chicken/1-189   1  . . . . . MASKRALVILA-KGAEEMETVIPDVMRRAG30
Q5XJ36|PARK7_Zebrafish/1-189 1  . . . . . MAGKRALVILA-KGAEEMETVIPVDVMRRAG30
P90994|DJ-11.1_C.elegans/1-187 1  . . . . . MAQKSALIIIAAEGAEEMEVIIITGDVLRARGE31
Q9VA37|DJ-1beta_Fruitfly/1-205 1  MVFFGFPPQISRHF SKFTKMSKSALVILA-PGAEEMEFIIAADVLRRAAG47
Q46948|YAJL_E.coli/1-196     1  . . . . . MSASALVCLA-PGSEETEA VTTIDLLVRGG29

Q99497|PARK7_Human/1-189     31  IKVTVAGLA--GKDPVQC SRD VVI  CPDASLEDAKKEGPDVVVLPGGN78
Q99LX0|PARK7_Mouse/1-189     31  IKVTVAGLA--GKDPVQC SRD VMI  CPDTSLEDAKTQGPYDVVVLPGGN78
QB8W59|PARK7_Chicken/1-189   31  IKVTVAGLT--GKEPVQC SRD VLI  CPDASLEDAKKEGPDVIVLPGGN78
Q5XJ36|PARK7_Zebrafish/1-189 31  IAVTVAGLA--GKEPVQC SRD EVM  CPDSSLEDAHKQGPYDVVLPGG78
P90994|DJ-11.1_C.elegans/1-187 32  IRVYYAGLD--GAEPVQC ARG AHIV  PDVKLEDVETEKFDIVLPGGQ78
Q9VA37|DJ-1beta_Fruitfly/1-205 48  IKVTVAGLN--GGEAVKCSR D VQIL  P D TSLA QV A S D K - F D V V V L P G G L 92
Q46948|YAJL_E.coli/1-196     30  IKVTTASV A S D G N L A I T C S R G V K L L A D A P L V E V A D G E - Y D V I V L P G G I 78

Q99497|PARK7_Human/1-189     77  LGAQNLSESAAVKEILKEQENR KGL I A A I C A G P - T A L L A H E I G F G S K V 123
Q99LX0|PARK7_Mouse/1-189     77  LGAQNLSESPMVKEILKEQESR KGL I A A I C A G P - T A L L A H E V G F G C K V 123
QB8W59|PARK7_Chicken/1-189   77  LGAQNLSESAAVKDI L K D Q E S R K G L I A A I C A G P - T A L L A H G I G F G S K V 123
Q5XJ36|PARK7_Zebrafish/1-189 77  LGAQNLSESPAVKEV L K D Q E G R K G L I A A I C A G P - T A L L A H G I A Y G S T V 123
P90994|DJ-11.1_C.elegans/1-187 77  PGNSTLAESLLVRDVLK SQVESGGL I G A I C A A P - I A L L S H G V K A - E L V 122
Q9VA37|DJ-1beta_Fruitfly/1-205 93  GGSNAMGESSLVGDLLRSQESGGGL I A A I C A A P - T V L A K H G V A S G K S L 139
Q46948|YAJL_E.coli/1-196     77  KGAECFRDS TLLVETV K Q F H R S G R I V A A I C A A P A T V L V P H D I F P I G N M 124

Q99497|PARK7_Human/1-189     124  T T H P L A K D K M M N G G H Y T Y S E N R V E K D G L I L T S R G P G T S F E F A L A I V E A 171
Q99LX0|PARK7_Mouse/1-189     124  T T H P L A K D K M M N G S H Y S Y S E S R V E K D G L I L T S R G P G T S F E F A L A I V E A 171
QB8W59|PARK7_Chicken/1-189   124  I T H P L A K D K M M N G A H Y C Y S E S R V E K D G N I L T S R G P G T S F E F G L A I V E A 171
Q5XJ36|PARK7_Zebrafish/1-189 124  T T H P G A K D K M M A G D H Y K Y S E A R V Q K D G N V I T S R G P G T S F E F A L T I V E E 171
P90994|DJ-11.1_C.elegans/1-187 123  T S H P S V K E K L E K G G - Y K Y S E D R V V V S G K I I T S R G P G T A F E F A L K I V E L 169
Q9VA37|DJ-1beta_Fruitfly/1-205 140  T S Y P S M K P Q L V N N Y S Y V D D K T - V V K D G N L I T S R G P G T A Y E F A L K I A E E 186
Q46948|YAJL_E.coli/1-196     125  T G F P T L K D K I P A E Q - W L D K R V V W D A R V K L L T S Q G P G T A I D F G L K I I D L 171

Q99497|PARK7_Human/1-189     172  L N G K E V A A Q V K A P L V L K D - - - - - 189
Q99LX0|PARK7_Mouse/1-189     172  L V G K D M A N Q V K A P L V L K D - - - - - 189
QB8W59|PARK7_Chicken/1-189   172  L M G K E V A E Q V K A P L I L K D - - - - - 189
Q5XJ36|PARK7_Zebrafish/1-189 172  L M G A E V A A Q V K A P L I L K D - - - - - 189
P90994|DJ-11.1_C.elegans/1-187 170  L E G K D K A T S L I A P M L L K L - - - - - 187
Q9VA37|DJ-1beta_Fruitfly/1-205 187  L A G K E K V Q E V A K G L L V A Y N - - - - - 205
Q46948|YAJL_E.coli/1-196     172  L V G R E K A H E V A S Q L V M A A G I Y N Y Y E 196

```

Figure 25. Protein sequence alignment of DJ-1 homologues. The copper binding cysteine Cys-53, highlighted in red, is only conserved among vertebrates. Residues with high degree of conservation are highlighted in blue. The alignment was generated using CLUSTALW and visualised using Jalview 2.8.

Chapter 3

**Structural and functional characterisation of the
Parkinsonism-linked DJ-1 A107P mutant**

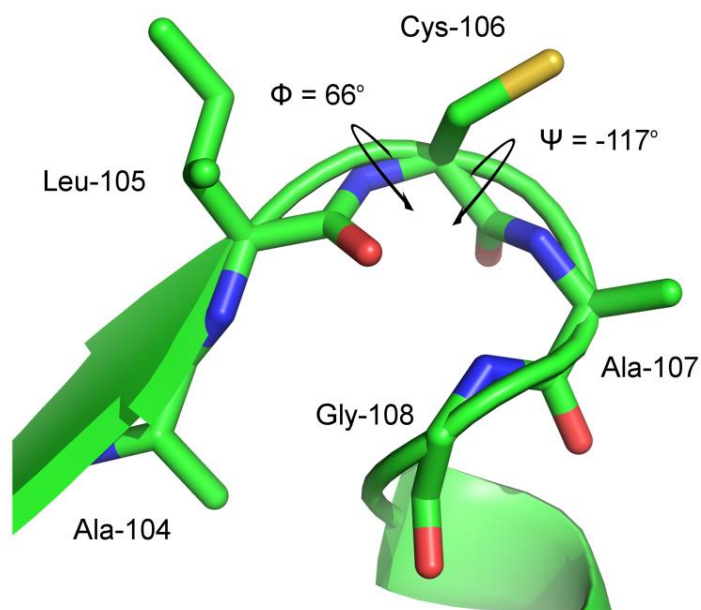
3.1 Introduction

A missense mutation in DJ-1 involving a proline substitution of Ala-107 was isolated in a patient diagnosed with early-onset familial PD (Ghazavi *et al.*, 2011). The mechanism by which this mutation disrupts DJ-1 function is unknown. Ala-107 is adjacent to the highly conserved Cys-106 residue that is essential for DJ-1 to carry out many of its cellular activities including glyoxalase (Lee *et al.*, 2012), weak protease (Chen *et al.*, 2010), molecular chaperone (Zhou *et al.*, 2006), and mRNA translational control (van der Brug *et al.*, 2008).

Ala-107 and Cys-106 are both found in a motif called the nucleophile elbow (Figure 24). This motif is a distinct structural element first described in the active sites of α/β hydrolases (Ollis *et al.*, 1992; Nardini and Dijkstra, 1999). It is identified by the consensus sequence Sm-X-Nu-X-Sm where Sm = a small residue e.g. Ala or Gly, Nu = nucleophile, and X = any residue. The sequence A-I-C-A-G/A is found in the nucleophile elbow motifs of prokaryotic and eukaryotic homologues of DJ-1. The motif positions the nucleophilic residue (Cys) in a tight turn of a strand-helix transition (Figure 26; Ollis *et al.*, 1992; Nardini and Dijkstra, 1999). The sharpness of the turn results from the energetically unfavourable backbone torsion angles ($\phi = 66^\circ$, $\psi = -117^\circ$ in human DJ-1) of the nucleophilic residue (Ollis *et al.*, 1992). Thus far, mutational analyses of the nucleophile elbow motif have focused on its role in catalysis. The role of nonenzymatic residues in the structural integrity of the active site and the protein fold as a whole has not been characterised.

This chapter presents the structural and functional consequences of the disease-linked A107P mutation in DJ-1. We produced recombinant forms of the A107P variant and tested its ability to act as a glyoxalase. Subcellular localisation, oligomeric state, and intracellular steady-state level of the A107P mutant were compared with the wild-type

protein to identify the aspects of DJ-1 function that may be perturbed by the mutation. Structural analysis using CD and NMR spectroscopy of the A107P variant was also carried out to determine the effects of the mutation on the structure of the active site and the DJ-1 fold. In essence we found that the A107P mutation not only impaired the ability of DJ-1 to act as a glyoxalase but remarkably disrupted the proper folding of the protein.



<i>H. sapiens</i> DJ-1	I LKEQENRKGL I A A I C A G P T A - L L A H E I G F G S K V T T H P L A
<i>M. musculus</i> DJ-1	I LKEQESRKGL I A A I C A G P T A - L L A H E V G F G C K V T T H P L A
<i>D. rerio</i> DJ-1	V L K D Q E G R K G L I A A I C A G P T A - L L A H G I A Y G S T V T T H P G A
<i>D. melanogaster</i> DJ-1β	L L R S Q E S G G G L I A A I C A A P T V - L A K H G V A S G K S L T S Y P S M
<i>D. melanogaster</i> DJ-1α	V L R C Q E S K G G L I A A I C A A P T A - L A K H G I G K G K S I T S H P D M
<i>C. elegans</i> DJ-1 1.1	V L K S Q V E S G G L I G A I C A A P I A - L L S H G V K A E - L V T S H P S V
<i>E. coli</i> YajL	T V K Q F H R S G R I V A A I C A A P A T V L V P H D I F P I G N M T G F P T L
<i>K. pneumoniae</i> ThiJ	T V R Q F H L S G R I V A A I C A A P A T V L V P H Q L F P I G N M T G F P A L
<i>S. typhimurium</i> YajL	T V K Q F H R S G R I V A A I C A A A A T V L V P H D I F P I G N M T G F P A L

Figure 26. The nucleophile elbow motif of human DJ-1. Cartoon representation depicts the nucleophile elbow found in β 7-loop- α 5 of DJ-1 (PDB ID code: 1PDV) whereby the backbone torsion angles of the nucleophilic residue Cys-106 adopt an unfavourable conformation (upper panel). Structure was rendered using Pymol (Delano, 2002). The nucleophile elbow motif is conserved in various prokaryotic and eukaryotic homologues of DJ-1. Cys-106 and Ala-107 residues (numbered as in human DJ-1) are marked with (*) and (#), respectively.

3.2 Results

3.2.1 Bacterial expression of DJ-1 A107P variant

Recombinant forms of DJ-1 have been useful *in vitro* models to compare the intrinsic structural properties and biochemical activities of the wild-type protein relative to the ones with disease-linked mutations (Lakshminarasimhan *et al.*, 2008; Malgieri and Eliezer, 2008). Hence, we expressed recombinant wild-type DJ-1, DJ-1 with the PD-linked A107P mutation (DJ-1^{A107P}) and DJ-1 with glyoxalase-inactivating alanine substitution of Cys-106 (DJ-1^{C106A}) in *Escherichia coli* and purified the proteins to homogeneity. The protein expression level of DJ-1^{A107P} is greatly diminished compared to the wild-type protein suggesting a negative effect of the mutation on the solubility or stability of the protein inside the cell (Figure 27). The estimated molecular size of DJ-1^{A107P} is 53 kDa (theoretical molecular size for monomer = 21 kDa) as determined by size exclusion chromatography (Figure 28). The molecular size of DJ-1^{A107P} is closest to a homodimeric species albeit a larger size than wild-type DJ-1 dimers. Results from our collaborators in Tuebingen, however, indicated the lack of homodimerisation exhibited by DJ-1^{A107P} ectopically expressed in human embryonic kidney (HEK) 293E cells (Appendix 2). Therefore, the apparently larger molecular size of DJ-1^{A107P} suggests an increase in the hydrodynamic volume of the monomeric protein that may be due to some degree of disordered structure caused by the mutation, as observed with some intrinsically disordered proteins such as α -synuclein which has a molecular size of 14 kDa but runs as a 65 kDa monomeric protein in SEC (Burre *et al.*, 2013).

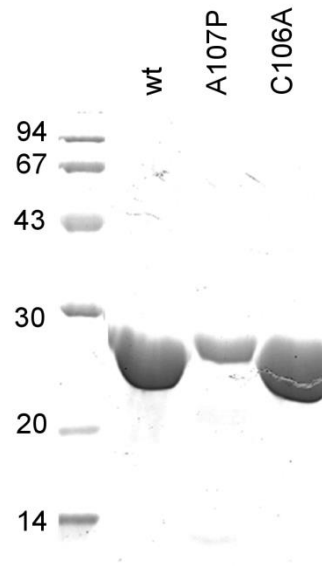


Figure 27. Purified recombinant DJ-1 proteins produced in bacteria. Proteins were expressed in *E. coli* BL21(DE3) cells, transformed with the appropriate pET-28a DJ-1 construct. Recombinant proteins were obtained using Ni-NTA affinity chromatography and analysed using a 12% w/v acrylamide SDS-PAGE. Proteins were purified from equal amounts of bacterial cell lysates to ascertain the effect of mutations on the protein expression levels. The leftmost lane shows the molecular weight marker in kDa (Pharmacia).

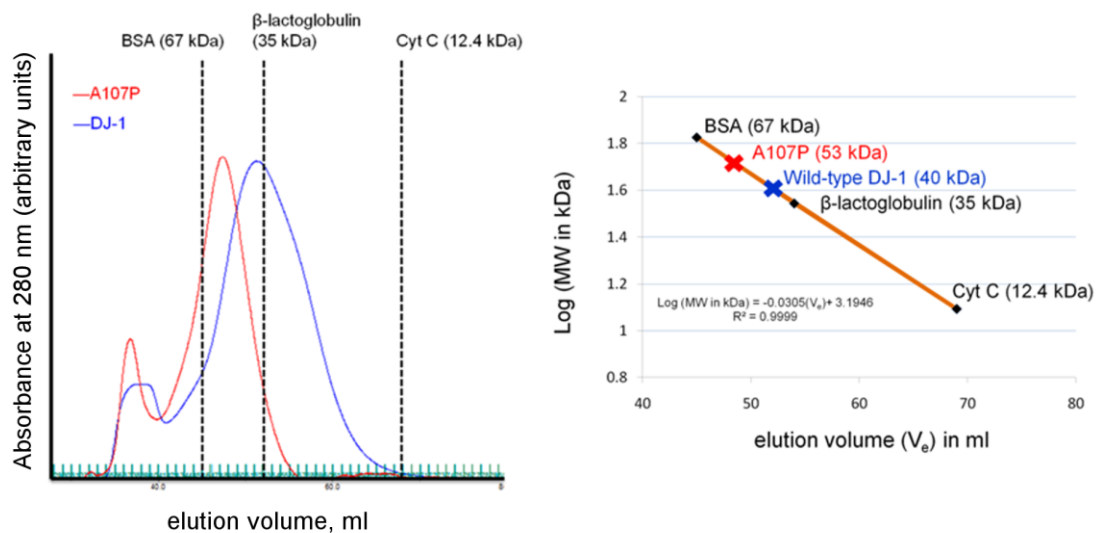


Figure 28. Comparative size exclusion chromatography analysis of wild-type DJ-1 and DJ-1^{A107P}. Proteins (1 mg/ml) were separated using Sephacryl S-100 with 20 mM Tris pH 7.15, 100 mM NaCl as mobile phase. Chromatograms of wild-type DJ-1 (blue curve) and DJ-1^{A107P} (red curve) were overlaid for comparison (left panel). A calibration curve was used to estimate the apparent molecular size of the proteins using bovine serum albumin (BSA), β -lactoglobulin, and cytochrome c (cyt c) as standards (right panel).

3.2.2 A107P mutation abolishes DJ-1 glyoxalase activity

The mutation A107P is located adjacent to the highly conserved Cys-106 that acts as the nucleophilic residue in the glyoxalase active site of DJ-1. To determine if the mutation affects the glyoxalase activity of DJ-1, we estimated the catalytic rate constant (k_{cat} , min^{-1}) using glyoxal as the substrate (Figure 29A). The unreacted substrate concentration was measured using a quantitative DNPH assay for aldehydes (Lee *et al.*, 2012). In accord with a previous report, the k_{cat} for wild-type DJ-1 was estimated to be 198 min^{-1} (Lee *et al.*, 2012). In contrast, DJ-1^{A107P} exhibited a negligible k_{cat} similar to the active site mutant DJ-1^{C106A} control. This infers that the mutation makes DJ-1 incapable of catalysing the detoxification of glyoxal perhaps resulting from disruption of the structural integrity of the active site.

We then correlated the *in vitro* glyoxalase activity assay results with the ability of the mutant protein to protect cells against glyoxal-induced cytotoxicity. Wild-type and mutant proteins were prepared with an N-terminal His₆ tag to allow purification and a tat transduction domain (RKKRRQRRR) that has been used previously to facilitate cell internalisation (Figure 30A; Batelli *et al.*, 2008). Tat-fused proteins were successfully transduced into a mouse embryonic fibroblast (MEF) *DJ-1*^{-/-} cell line and human neuroblastoma SH-SY5Y cell line (Figure 30B). We have used 2 mM glyoxal to induce cytotoxicity according to Lee *et al.* (2012) protocol. In both cell lines, transduction of wild-type DJ-1 protein conferred protection against reduction in cell viability induced by glyoxal (Figure 29B). In contrast, neither the A107P variant nor the C106A variant protected either cell lines from glyoxal cytotoxicity (Figure 29B). This is consistent with the abrogation of glyoxalase activity caused by the A107P mutation. Notably, SH-SY5Y cells were more vulnerable to glyoxal than MEF *DJ-1*^{-/-} cells. We posit that the embryonic knockout of *DJ-1* may induce a compensatory mechanism whereby other

glyoxalase scavenging mechanisms are upregulated in the absence of DJ-1, although this requires further investigation.

Glyoxal cytotoxicity is accompanied by the formation of advanced glycation end products such as N ϵ -carboxymethyllysine (CML) (Glomb and Monnier, 1995). CML modification of proteins can lead to protein aggregation and inactivation, contributing to glyoxal's deleterious effect on cell viability (Munch *et al.*, 2012). An antibody against CML allowed the detection of total cellular proteins modified with CML. Protein extracts from glyoxal-treated SH-SY5Y cells transduced with the active site mutant C106A showed remarkable immunoreactivity against the CML antibody, consistent with the accumulation of CML-modified proteins as a result of glyoxal treatment (Figure 29C). Conversely, transduction of wild-type protein into SH-SY5Y cells prevented the build up of CML-modified proteins after glyoxal treatment, demonstrating the ability of DJ-1 to detoxify glyoxal. Immunoblot analysis of cells with the DJ-1^{A107P} showed a concomitant accumulation of CML upon glyoxal treatment, confirming the lack of glyoxalase activity caused by the A107P mutation.

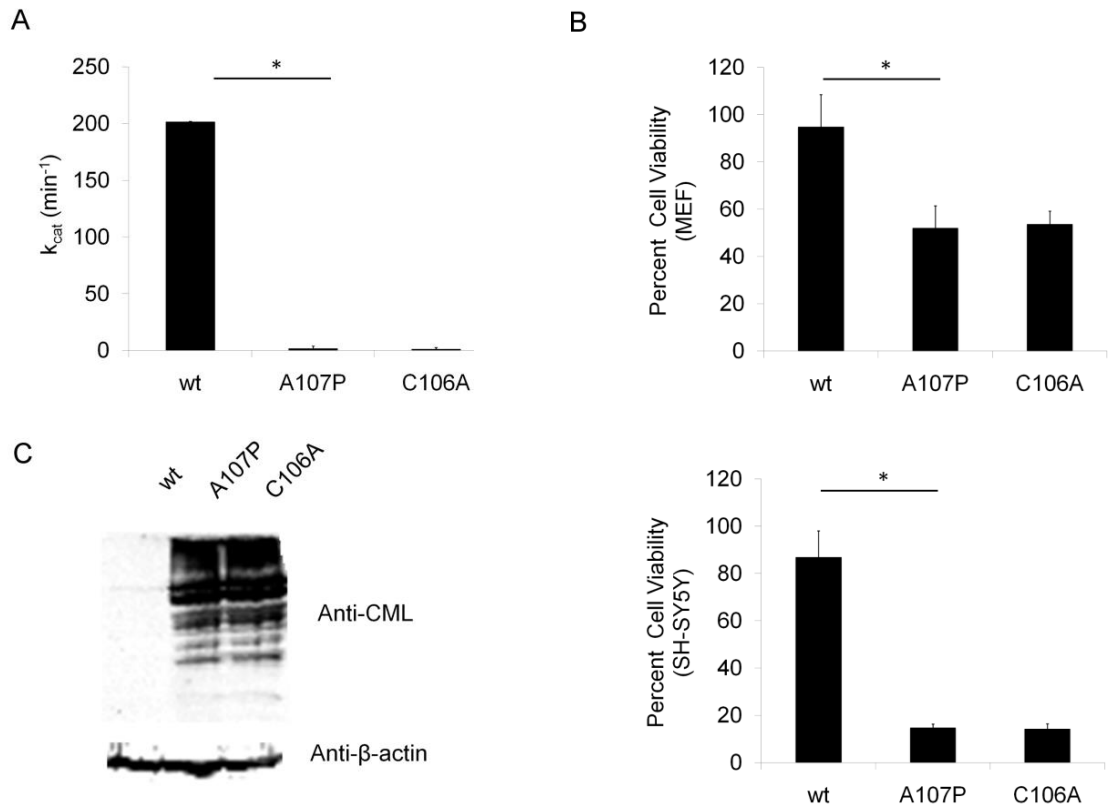


Figure 29. The A107P mutation abrogates the ability of DJ-1 to protect against glyoxal cytotoxicity and accumulation of CML. (A) Catalytic efficiencies of wild-type (wt) and mutant proteins were obtained using a DNPH-based quantitative assay. Error bars are ± 2 SD obtained from data ($n = 3$) in three independent repeats. (*) denotes $p < 0.0001$ in an unpaired t-test. (B) Bar graphs showing the percent cell viability after glyoxal treatment of MEF DJ-1^{-/-} (upper panel) and SH-SY5Y cells (lower panel) transduced with various DJ-1 variants. Cell viability was measured using the Prestoblu assay (Life Technologies). Data ($n = 25$ for MEF; $n=16$ for SH-SY5Y) were collected in three independent experiments. Error bars represent SD. (*) denotes $p < 0.0001$ in an unpaired t-test. (C) Western blot analysis of CML-modified proteins in glyoxal-treated SH-SY5Y cells transduced with either wild-type or mutant DJ-1 proteins. Levels of β -actin were probed to show equal loading for each sample.

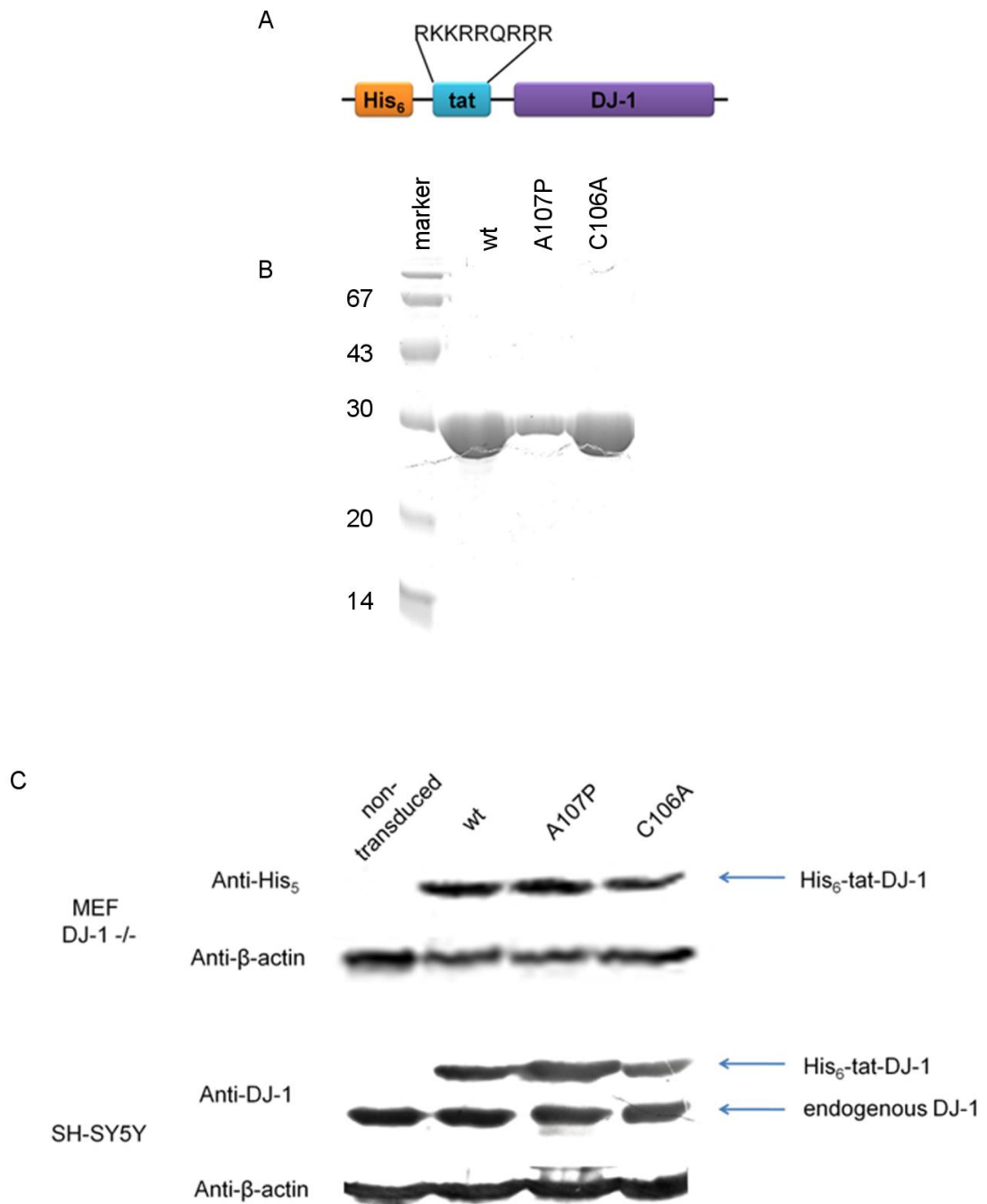


Figure 30. Immunoblot analysis of transduced DJ-1 proteins in MEF and SH-SY5Y cells. (A) Diagram of the tat-fused DJ-1 construct used in cells assays. (B) SDS-PAGE analysis of tat-fused DJ-1 proteins expressed in *E. coli* BL21 (DE3) and purified using Ni²⁺-affinity (Qiagen) and anion-exchange (Q-sepharose, GE Healthcare) chromatography. The leftmost lane shows the molecular weight marker with the indicated sizes in kDa (Pharmacia). (C) Recombinant tat-fused proteins were successfully transduced into MEF *DJ-1*^{-/-} and SH-SY5Y cells. Cells were grown for 24 hours prior to transduction. To allow internalisation, cells were incubated with 10 μ M tat-fused proteins in serum free media for at least 2 hours prior to assay. β -actin was used as a loading control.

3.2.3 Clues on the catalytic role of Ala-107 from *in silico* analysis and the crystal structure of DJ-1 bound to SO_4^{2-} and glycerol

To elucidate the effect of the A107P mutation on the molecular architecture of the glyoxalase active site of DJ-1, we have attempted to crystallise the DJ-1 with the A107P mutation. Previously determined conditions used to crystallise DJ-1 mutants did not yield crystals, thus we set up crystallisation screens to find new conditions that would crystallise the mutant. JCSG-plus HT Condition D3 (0.2 M sodium chloride, 0.1 M sodium dihydrogen phosphate, 0.1 M potassium dihydrogen phosphate, 50.0% v/v polyethylene glycol 200) gave a crystal but when diffracted, the crystal turned out to be salt.

Failing to get a crystal, the structural effects of the A107P mutation were analysed by *in silico* mutagenesis of the protein. Mutagenesis was carried out in Coot (Emsley and Cowtan, 2004). In the structure of the wild-type protein, the backbone torsion angles ($\phi = 66^\circ$, $\psi = -117^\circ$) of the nucleophilic residue Cys-106 lie in the unfavourable region of the Ramachandran plot, a diagram of allowed backbone conformations in proteins as indicated by ϕ , ψ dihedral angles. Such an unusual backbone strain on the nucleophilic residue is a distinct feature of the nucleophile elbow motif that likely contributes to the chemical reactivity and proper orientation of the nucleophile (Ollis *et al.*, 1992; Nardini and Dijkstra, 1999). The role of non-nucleophilic residues in the motif in dictating the unique conformation of the nucleophile has not been explored. Measurement of the torsion angles of Cys-106 in the *in silico* model suggests that proline substitution of the Ala-107 (of the human DJ-1 nucleophile elbow motif A₁₀₄-I₁₀₅-C₁₀₆-A₁₀₇-G₁₀₈) does not drastically change the backbone torsion angles ($\phi = 66^\circ$, $\psi = -114^\circ$) of Cys-106, with ψ only changing by 3 degrees (Figure 31A). The Ramachandran plot of the A107P mutant generated using Chimera (Pettersen *et al.*, 2004) indicated that the Cys-106 backbone conformation remained in the disallowed region, suggesting that the mutation

does not alter Cys-106 nucleophilicity via changes in Cys-106 backbone conformation (Figure 31B).

Site directed mutagenesis of the putative active site residues suggested a reaction mechanism for DJ-1 glyoxalase activity whereby Glu-18 not only contributes to the chemical reactivity of Cys-106 nucleophile but also acts as a general base (Lee *et al.*, 2012). However, the function of the nonenzymatic residues *e.g.* Ala-107 in the nucleophile elbow motif have not been characterised. To determine the potential role of Ala-107 in the catalytic mechanism of DJ-1 glyoxalase activity, the crystal structure of DJ-1 with a substrate (methylglyoxal) bound to the active site and/or engaged in catalysis was sought. Wild-type protein or a variant whereby the nucleophilic residue Cys-106 was substituted for a serine to prevent the catalytic turnover of the substrate were used to produce crystals. To introduce the substrate we either grew the crystals using protein pre-incubated with molar excess of methylglyoxal or soaked the crystals in mother liquor supplemented with 1.2 M methylglyoxal for various incubation times. However, none of the crystals contained methylglyoxal in the active site when their structure was solved.

Nonetheless, a crystal structure was determined with the C106S variant of the protein bound to a sulphate anion (carried over from purification procedure) and glycerol (a component of the crystallant) in the active site (Figure 32A-E; see Table 4 for data collection and refinement statistics). In this structure, the hydroxyl moiety of Ser-106 is displaced by 1.5 Å relative to the position of Cys-106 in the wild-type structure, perhaps to accommodate the sulphate anion. Glycerol, which we propose to mimic the substrate, is mainly bound by Arg-28' (of subunit B) at the homodimer interface (Figure 32D). Arg-28' is anchored to subunit A via guanidinium stacking with the side chain of Arg-

48 (of subunit A). This suggests that the recruitment of the substrate to the active site potentially requires the formation of a homodimer.

The sulphate anion is held through hydrogen bonding with the main-chain NH of Gly-75 and Ala-107 and the side chains of Glu-18 and Ser-106 (Figure 32E). We propose that the sulphate anion mimics the tetrahedral transition state intermediate during the nucleophilic attack on the methylglyoxal aldehyde carbon by the thiolate group of Cys-106 (Kwon *et al.*, 2013). The oxyanion formed during the transition state is potentially stabilised by an oxyanion hole formed by the amide NH's of Gly-75 and Ala-107. This is supported by a recent study by Buller and Townsend (2013). The authors analysed enzymes that use an acylation-based mechanism to look for geometric relationships within the active sites to predict the catalytic mechanism and stereochemistry of the reaction. They have found that the configuration of the reactive rotamer of the nucleophilic residue dictates which backbone NH moiety will stabilise the oxyanion in the transition state. In the active site of DJ-1 where the nucleophilic Cys-106 thiol ($-SH$) group adopts a trans rotamer relative to the residue's backbone NH group (Fig. 31C), the amide NH of the succeeding residue (Nu+1) is predicted to play a direct role in stabilising the oxyanion formed during nucleophilic attack (Buller and Townsend, 2013). Because the backbone nitrogen of a proline residue cannot donate a hydrogen bond, proline substitution of the residue Ala-107 (Nu+1) will not allow the formation of a stabilising oxyanion hole in the transition state.

In summary, proline substitution of Ala-107 does not change the backbone torsion angles of Cys-106 but potentially affects the ability of DJ-1 to catalyse glyoxal detoxification by impairing the formation of an oxyanion hole during the nucleophilic attack.

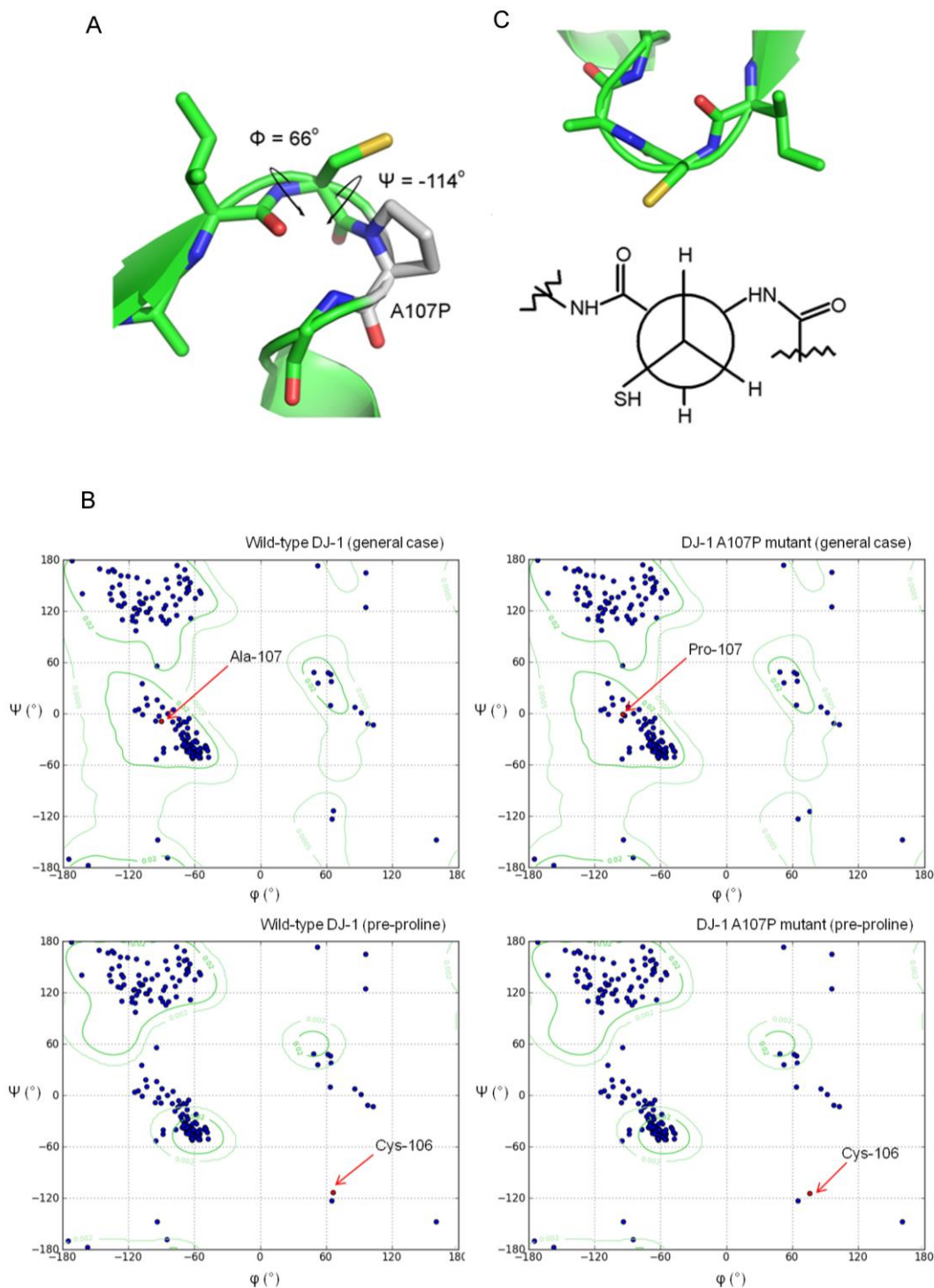


Figure 31. *In silico* structural analysis of the A107P mutation. (A) A107P mutation was generated *in silico* using Coot with DJ-1 PDB ID code: 1PDV as template. The *in silico* model suggests that the backbone torsion angles of Cys-106 in the A107P variant do not significantly deviate from the native conformation. (B) Ramachandran plot (general case and pre-proline) generated using Chimera (Pettersen *et al.*, 2004) of wild-type DJ-1 (PDB ID code: 1PDV) and the A107P mutant. (C) The thiol moiety of the cysteine residue adopts a *trans* configuration relative to the residue's backbone amide. Structures were rendered using PyMol (Delano, 2002).

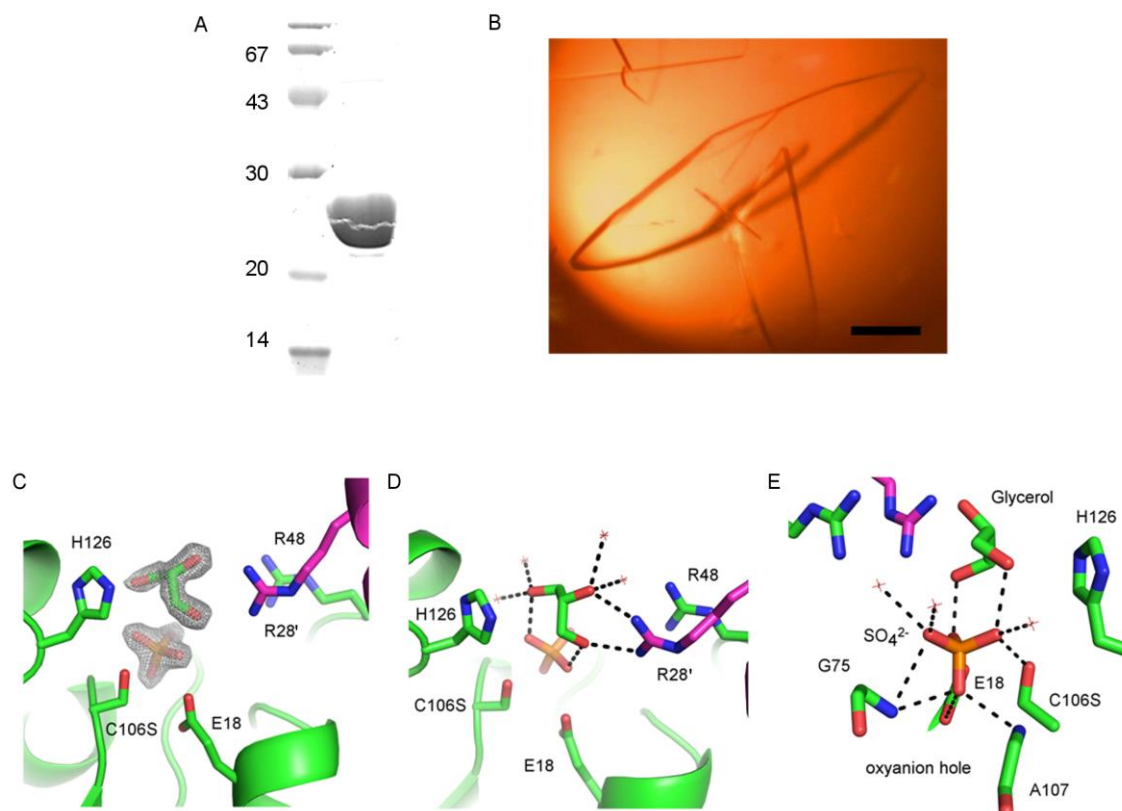


Figure 32. The glyoxalase active site of DJ-1 with sulphate anion and glycerol bound. (A) SDS-PAGE analysis of recombinant DJ-1 C106S mutant (right lane) expressed in *E. coli* BL21 (DE3). The left lane shows the molecular weight marker with the indicated sizes in kDa (Pharmacia). (B) Crystals of DJ-1 C106S mutant in a crystallant solution containing 20% v/v glycerol and 24% w/v PEG 1500. Scale bar = 0.5 mm. (C) $F_o - F_c$ electron density map (contoured at 2σ) of the sulphate anion and glycerol bound to the active site of DJ-1. (D) Noncovalent interaction of glycerol in the active site. Glycerol is held by Arg-28 of subunit B (in magenta). (E) Noncovalent interactions of the sulphate anion. Backbone amide NH moieties of Gly-75 and Ala-107 donate hydrogen bonds to the sulphate oxyanion. Water molecules are shown as red asterisks. Dashed lines indicate hydrogen bonds. Structures were rendered using PyMol (Delano, 2002).

Table 4. Data collection and refinement statistics for DJ-1 C106S with glycerol and sulphate bound.

C106S – Glycerol/SO₄²⁻	
<i>Data collection</i>	
Space group	P2 ₁ 2 ₁ 2
Cell dimensions	
<i>a, b, c</i> (Å)	43.86, 86.60, 49.52
<i>α, β, γ</i> (°)	90, 90, 90
Resolution (Å)	12.12 (1.85 - 1.81)*
R_{merge}	0.036 (0.052)
Mean I / σI	23.3 (12.8)
Completeness (%)	98.7 (96.4)
Redundancy	3.4 (2.2)
<i>Refinement</i>	
d_{min} (Å)	1.81
No. reflections	17549
Rwork/ Rfree	0.150/ 0.1894
<i>No. atoms</i>	
Protein	1386
Glycerol	6
Sulphate	5
Water	268
<i>B-factors</i> (Å ²)	
Protein	8.9
Glycerol	11.6
Sulphate	8.4
Water	22.2
<i>RMSD</i>	
Bond lengths (Å)	0.008
Bond angles (°)	1.17

* Values in parentheses are for the highest resolution bin.

3.2.4 Intracellular steady-state levels of DJ-1^{A107P}

A number of PD-linked mutations in DJ-1 reduce the intracellular steady state levels of the protein (Olzmann *et al.*, 2004; Ramsey and Giasson, 2010; Rannikko *et al.*, 2012). To determine the effects of the A107P mutation on the protein levels of DJ-1, SH-SY5Y cells were transiently transfected with plasmid constructs of DJ-1 with a C-terminal His₆ tag. Western blot analysis using antibodies against DJ-1 was used to compare the amount of the two proteins. As shown in Figure 33, the steady-state levels of the wild-type DJ-1 are comparable to that of DJ-1^{A107P}. This suggests that the A107P mutation does not lead to a rapid clearance of the protein in SH-SY5Y cells. RT-PCR was used to confirm equal mRNA expression levels of wild-type DJ-1 and DJ-1^{A107P} (Figure 33).

Our collaborators in Tuebingen performed similar experiments and found that the steady-state level of DJ-1 varies between cell types and is not influenced by the presence of endogenous DJ-1 (Appendix 3). In HEK 293E, the DJ-1^{A107P} steady-state level was only slightly reduced compared to wild-type DJ-1. In contrast, when DJ-1^{A107P} was ectopically expressed in MEF cells derived from either *DJ-1*^{-/-} mice or *DJ-1*^{+/+}, the protein level of DJ-1^{A107P} was significantly diminished compared to the wild-type protein (Appendix 3).

We have determined whether the A107P mutation alters the subcellular localisation of DJ-1. MEF *DJ-1*^{-/-} were back-transfected with DJ-1 plasmid constructs and the ectopically expressed proteins were detected using immunofluorescence. Wild-type DJ-1 and DJ-1^{A107P} were detected in the cytosol (Figure 34). However, unlike the wild-type protein, DJ-1^{A107P} was absent in the nucleus. Notably, DJ-1^{A107P} was found in foci compared to the uniform cellular distribution of the wild-type DJ-1.

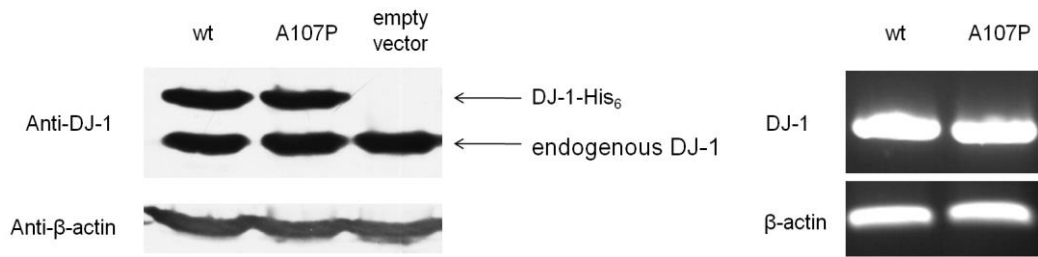


Figure 33. Steady-state levels of the DJ-1^{A107P} when expressed in SH-SY5Y cells. Left panel: SH-SY5Y cells were transiently transfected with DJ-1 pCDNA 4 constructs with the His₆ tag. Twenty four hours post-transfection, cells were lysed and DJ-1 detected using an anti-DJ-1 primary antibody (Enzo Life Sciences) and anti-mouse IgG secondary antibody conjugated with horseradish peroxidase (Sigma). β -actin was immunodetected as a loading control. Right panel: Equal mRNA expression of the constructs was determined using semi-quantitative RT-PCR using primers specific for human *DJ-1*, with β -actin probed as a loading control.

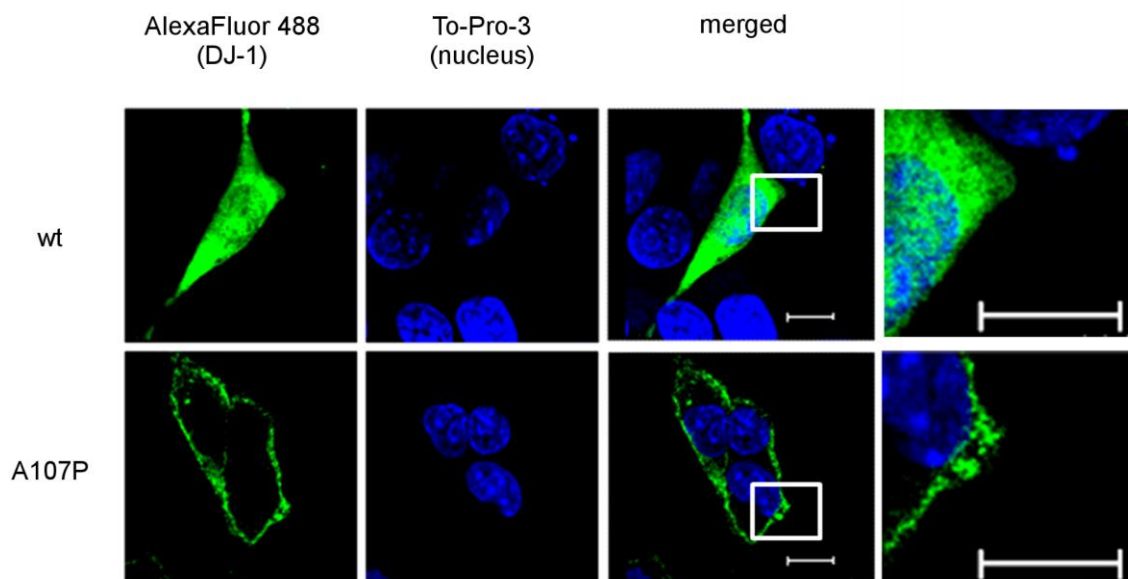


Figure 34. Subcellular localisation of DJ-1^{A107P}. MEF *DJ-1*^{-/-} cells were transfected with pCDNA 4 DJ-1 constructs with a C-terminal His₆ tag. After 24 hours, cells were immunodetected for DJ-1 using an anti-DJ-1 primary antibody (Enzo Life Sciences) and anti-mouse IgG secondary antibody conjugated with Alexa Fluor 488 (Life Technologies). The nuclei were counterstained with To-Pro-3 (Life Technologies). Magnified images of the boxed areas in the merged micrographs are shown at the rightmost panel. Micrographs were taken using the 60X objective of the Leica TCS SP2 confocal microscope. Scale bar = 11 μ m.

3.2.5 The A107P mutation leads to DJ-1 misfolding

The reduced steady-state levels and loss of homodimerisation of DJ-1^{A107P} observed by our Tuebingen collaborators prompted us to further investigate the structural changes caused by the mutation.

Changes in the secondary structure of the mutant protein were determined using circular dichroism (CD) spectroscopy. The far-UV region (200-260 nm) of the CD spectra of DJ-1^{wt} and DJ-1^{A107P} were recorded at room temperature (20°C). At physiological pH, the CD spectrum of the wild-type DJ-1 protein indicated a properly folded protein with maximum negative ellipticity between 208 nm to 220 nm that corresponds to well-structured α -helices (Figure 35). The secondary structure content obtained using the K2D3 program (Louis-Jeune, 2012) estimated 38% α -helix, 20% β -sheet, and 42% coil/turn/other from the CD spectrum of the wild-type DJ-1 protein. This is consistent with the calculated secondary structure content derived from the crystal structure of DJ-1 (38% α -helix, 20% β -sheet, 42% coil/turn/other) (Tao and Tong, 2003). In contrast, remarkable misfolding was evident in the far-UV CD spectrum of the A107P variant. The decrease in negative ellipticity was concomitant with the reduction in total alpha helical content (24.4% α -helix). However, the estimated β -sheet content (19.7% β -sheet) did not change. This suggests that DJ-1^{A107P} exhibits marked misfolding yet maintains some level of folded structures mainly comprising of β -sheets perhaps from the retention of a structured core.

To further characterise the changes in the structure of the A107P variant, the ¹H-¹⁵N HSQC spectra of the wild-type and mutant proteins were recorded (Figure 36). The spectrum of the wild-type DJ-1 protein displayed well-resolved resonance peaks typical for a well-folded protein. In contrast, the DJ-1^{A107P} spectrum showed poorly dispersed resonance peaks indicative of an ensemble of highly flexible protein conformational states caused by protein unfolding. These results do not support the presence of a well-

ordered core as indicated by the CD spectrum. Interestingly, similar spectroscopic features were described for the L166P mutation (Malgieri and Eliezer, 2008). However, unlike the L166P variant (Olzmann *et al.*, 2004), DJ-1^{A107P} is capable of heterodimerisation with the wild-type DJ-1 protein suggesting that a transient state exists that could potentially oligomerise with the wild-type DJ-1. The DJ-1^{A107P} spectrum also revealed the perturbation of the structural framework of the glyoxalase active site of DJ-1 as indicated by the loss of the resonance peak corresponding to the active site residue Cys-106 (Figure 37), illuminating the deleterious effect of the A107P mutation on the enzymatic activity of DJ-1.

Together, these results provide a molecular basis for the apparent decreased intracellular steady-state level of the DJ-1^{A107P} variant observed in HEK 293E and MEF cells. Furthermore, our results reveal a critical role for the nucleophile elbow motif residues not only in providing a structural integrity for the glyoxalase active site but also for the overall DJ-1 fold.

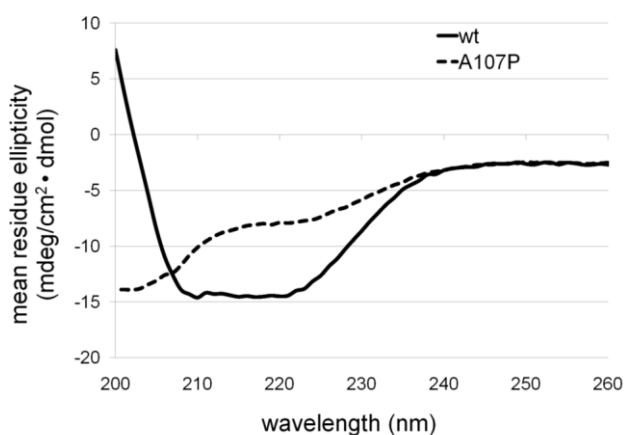


Figure 35. CD spectra of wild-type DJ-1 and DJ-1^{A107P}. CD spectra of proteins (7.5 μ M) in 20 mM HEPES pH 7.5, 50 mM NaCl were recorded at 20°C.

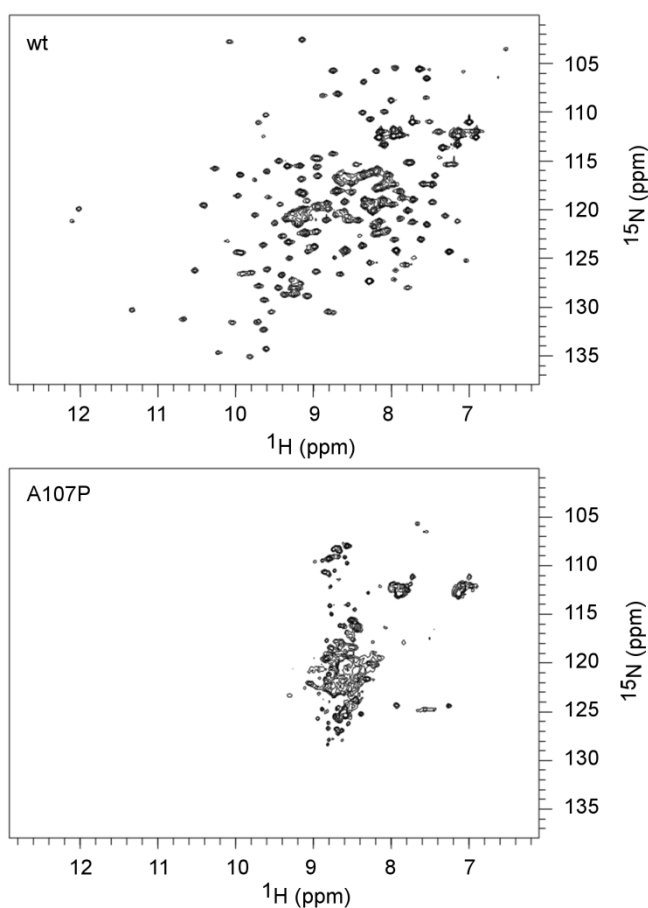


Figure 36. ^1H - ^{15}N HSQC of wild-type DJ-1 and DJ-1^{A107P}. The proton-nitrogen correlation NMR spectra of uniformly ^{15}N -labelled proteins, wild-type DJ-1 (top panel) and DJ-1^{A107P} (lower panel), in 20 mM sodium phosphate pH 6.5 were recorded at 25°C. The well-dispersed correlation peaks in the HSQC spectrum of DJ-1^{wt} indicates the well-folded structure of the protein. Conversely, the poor dispersion of peaks in the DJ-1^{A107P} is evidence for the misfolding caused by the mutation. The NMR data was collected by Altin Sula (Birkbeck/UCL) under the supervision of Dr. Mark Williams (Birkbeck/UCL).

3.3 Discussion

A mutation screening of DJ-1 in PD patients with an average age of onset <31 years identified two novel mutations (Ghazavi *et al.*, 2011). One of these is a point mutation that results in a proline substitution of Ala-107, a highly conserved residue located in the protein's nucleophile elbow motif. In this chapter, the effects of this mutation on the structure and function of DJ-1 were determined with the goal of providing insights into the molecular basis of its pathogenicity.

DJ-1 has been reported to act as a glyoxalase that catalyses the breakdown of reactive α -oxoaldehyde species *e.g.* glyoxal and methylglyoxal (Lee *et al.*, 2012). The adjacency of the A107P mutation to the active site residue Cys-106 prompted us to investigate the effects of this mutation on the ability of DJ-1 to act as a glyoxalase. We found that the introduction of the A107P mutation in DJ-1 abrogates glyoxalase activity. Additionally, the A107P variant was not capable of protecting cells against glyoxal cytotoxicity and the accumulation of CML, an advanced glycation end product.

A107P occurs in the nucleophile elbow motif, a structural element that lies within the glyoxalase active site of DJ-1. This motif positions the cysteine nucleophile, Cys-106, in a sharp turn induced by unfavourable backbone torsion angles (Ollis *et al.*, 1992; Nardini and Dijkstra, 1999). Our *in silico* analysis suggests that the A107P mutation does not affect significantly the backbone conformation of Cys-106 and hence cannot explain the lack of glyoxalase activity. The nucleophile elbow also contains residues that promote nucleophilic attack (Nardini and Dijkstra, 1999). Specifically, the motif participates in the stabilisation of an oxyanion transition state that forms during a nucleophilic attack. To determine the contribution of Ala-107 in the catalysis, we sought to capture a snapshot of DJ-1 engaged with a substrate and/or in a nucleophilic attack. Our attempts to introduce the substrate, methylglyoxal, into the active site of DJ-1 have failed. Nevertheless, we solved a crystal structure of the C106S variant bound to

glycerol and sulphate in the active site. The position of the sulphate ion makes it a good representation of the proposed tetrahedral intermediate that forms during the nucleophilic attack. Sulphate ions have been found to occupy oxyanion holes (Molgaard *et al.*, 2000; Wang *et al.*, 2002; Tanaka *et al.*, 2010). In our structure, the sulphate oxyanion is hydrogen bonded to the amide groups of Ala-107 and Gly-75 forming a putative oxyanion hole. The stabilisation of the oxyanion intermediate governs the catalytic efficiency of a number of enzymes. Mutations that abrogate the formation of oxyanion holes negatively affect catalysis (Bryan *et al.*, 1986; Ordentlich *et al.*, 1998). Proline substitution of Ala-107 removes a backbone amide hydrogen and renders the protein incapable of stabilising an oxyanion intermediate. For this reason, the A107P mutation may impair the glyoxalase activity of DJ-1. However, the effects of the A107P mutation extend beyond enzymatic catalysis.

Early indications of alterations in the structure and the stability of the A107P variant were observed during the preparation of the recombinant protein. The reduced amount of protein retrieved from the heterologous expression of DJ-1^{A107P} was indicative of a destabilising effect caused by the mutation. Moreover, the apparent increase in the molecular size of the A107P variant estimated using size exclusion chromatography is not consistent with homodimerisation but suggested an altered conformational state of DJ-1^{A107P} accompanied by an increase in effective hydrodynamic radius, a phenomenon observed for a number of unfolded and intrinsically disordered proteins (Batas *et al.*, 1997; Burre *et al.*, 2013).

The reduction in protein stability was not immediately apparent in eukaryotic cells. In the human cell line SH-SY5Y, the protein level of DJ-1^{A107P} was comparable to the wild-type protein. Yet our collaborators have shown a slightly reduced DJ-1^{A107P} level in HEK 293E cells. Intuitively, the presence of endogenous wild-type protein may

stabilise the mutant protein through heterodimerisation. Neither MEF *DJ-1*^{+/+} nor MEF *DJ-1*^{-/-} retained a significant amount of the mutant protein, explaining the weak immunofluorescent detection of ectopically expressed DJ-1^{A107P} in MEF *DJ-1*^{-/-}. These results suggest that the intracellular steady state level of DJ-1^{A107P} may be cell type-specific and is not determined by the presence of endogenous wild-type protein. Since the constructs used were not identical *i.e.* different location and type of tag we cannot rule out the possibility of the effects of the fused tags in terms of intracellular protein concentration and decay.

The reduced intracellular protein level of DJ-1^{A107P} in HEK 293E and MEF cell lines has led to us to investigate the structural effects of the A107P mutation. We first compared the secondary structure content of the wild-type protein and DJ-1^{A107P} using CD spectroscopy. Proteins, being optically active macromolecules, interact with circularly polarised light. Each type of secondary structure absorbs circularly polarised light to a different extent, which makes CD spectroscopy a useful tool in analysing gross changes in protein structure. The CD spectrum of wild-type DJ-1 represented a well-folded protein with calculated secondary structure content consistent with the crystal structure. In contrast, the CD spectrum of DJ-1^{A107P} showed an apparent loss of α -helical content, indicating global changes in protein structure. NMR spectroscopy was used to characterise further the structural defect caused by the A107P mutation. The HSQC spectrum of the DJ-1^{A107P} immediately indicated protein misfolding reminiscent of the L166P mutation (Malgieri *et al.*, 2008). The structural integrity of the active site was greatly compromised as shown by the overlay of the wild-type DJ-1 and DJ-1^{A107P} HSQC spectra (Figure 37). This provides a molecular explanation for the lack glyoxalase activity caused by the A107P mutation. Although we couldn't exactly map the location of the structural perturbations, both CD and NMR data suggested the retention of some structures in spite of the remarkable misfolding of the mutant protein.

The retained structures perhaps enable the heterodimerisation with wild-type DJ-1 but are not sufficient for self-association hence the lack of mutant homodimers observed by our Tuebingen collaborators. With reference to the crystal structure of DJ-1 (Tao and Tong, 2003), Ala-107 does not contribute directly to homodimer contacts. Hence, the loss of mutant homodimerisation suggests that the structural effects of the A107P mutation extend beyond local perturbations, disrupting critical points of contact between the mutant polypeptides.

The remarkable misfolding of DJ-1^{A107P} also explains its lack of nuclear translocation. DJ-1 translocation into the nucleus requires the SUMOylation of Lys-130. This residue is evidently perturbed in the HSQC spectrum of the mutant protein (Figure 37). The absence of properly-folded DJ-1 in the nucleus would render it incapable of controlling its associated transcription factors such as AR and p53.

In essence, the A107P mutation in DJ-1 devoids the cell of a multifunctional cytoprotective protein that can rescue neuronal cells from progressive degeneration.

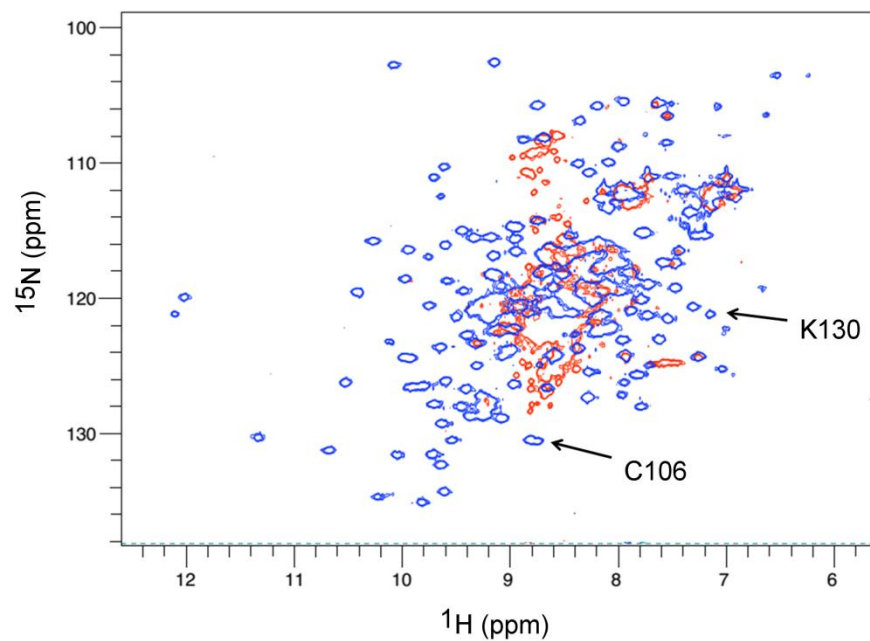


Figure 37. Overlay of the ^1H - ^{15}N HSQC spectra of wild-type DJ-1 and DJ-1^{A107P}. The proton-nitrogen correlation NMR spectra of wild-type DJ-1 and DJ-1^{A107P} are shown in blue and red, respectively. Positions of resonance peaks for Cys-106 and Lys-130 in the wild-type protein spectrum are indicated by arrows. The NMR data was collected by Altin Sula (Birkbeck/UCL) under the supervision of Dr. Mark Williams (Birkbeck/UCL).

Chapter 4

Discussion and Outlook

4.1 Biological role of the copper binding site

The nature of ligation provides clues on the biological function of a copper binding site in a protein (Roat-Malone, 2007; Davis and O'Halloran, 2008; Boal and Rosenzweig, 2009). Proteins involved in enzymatic catalysis, dioxygen transport, and electron transfer bind Cu(II) via O-carboxylates (aspartate, glutamate) and N-imidazoles (histidine). Proteins involved in copper transport and homeostasis commonly interact with Cu(I) using S-thiolates (cysteines) and S-thioethers (methionines).

The biscysteinate copper binding site of DJ-1 closely resembles that of many copper chaperones that possess the sequence motif CXXC or CXC (Davis and O'Halloran, 2008; Boal and Rosenzweig, 2009). Uniquely, the copper binding site of DJ-1 is formed through pseudo 2-fold symmetry related Cys-53, conserved across vertebrates. The solvent exposed, docking accessible location of the copper binding site makes DJ-1 a good copper donor and/or acceptor. Prompted by the previous work of Xu *et al.* (2010), we tested the ability of DJ-1 to transport copper to SOD1. In our hands, we found no stimulation of SOD1 activity by copper-loaded recombinant DJ-1 *in vitro*. Similarly, our collaborators tested the copper chaperone activity of DJ-1 for SOD1 using a different method and found no evidence of copper transport. The stimulation of SOD1 by DJ-1 described by Xu *et al.* (2010) may have resulted from a fortitious binding of copper to the His₆ tag, which was not used in the our assays, resulting in nonspecific copper acquisition by SOD1. The absence of interaction between DJ-1 and SOD1, perhaps due to a lack of a SOD1-interacting domain similar to CCS (Lamb *et al.*, 1999; Lamb *et al.*, 2001), may also explain the inability of DJ-1 to specifically deliver the copper to SOD1. Nonetheless, because of its chemical features, the copper binding site of DJ-1 remains competent for copper transfer to a target protein that is yet to be identified. With a coordination number of 2, the biscysteinate site of DJ-1 is capable of

engaging in higher-order complexes potentially a tri-coordinate complex that serves as a common mechanism for copper transfer used by copper chaperones (Banci *et al.*, 2006).

Alternatively, DJ-1 could be involved in the homeostatic control of copper by means of direct metal sequestration and/or trafficking of copper out of the cell. Chronic occupational exposure to copper has been linked to an increased risk of developing Parkinson's disease (Gorell *et al.*, 1997; Willis *et al.*, 2010). Free copper ions can promote neurodegeneration by damaging proteins, nucleic acids, and lipids (Halliwell and Gutteridge, 1990). Specifically, copper has been shown to accelerate the formation of cytotoxic oligomers of α -synuclein, a protein linked to autosomal dominant, familial Parkinson's disease (Wright *et al.*, 2009). The complex of copper with α -synuclein can also induce the generation of reactive oxygen species (Paik, *et al.*, 1999; Wang *et al.*, 2010). Therefore, DJ-1, through its ability to sequester copper, could prevent copper's deleterious interactions with cellular components. Additionally, DJ-1 can potentially aid in the removal of copper from the intracellular milieu via its secretion out of the cell (Tsuboi *et al.*, 2008). The proposed biological functions of the copper binding site are depicted in Figure 38.

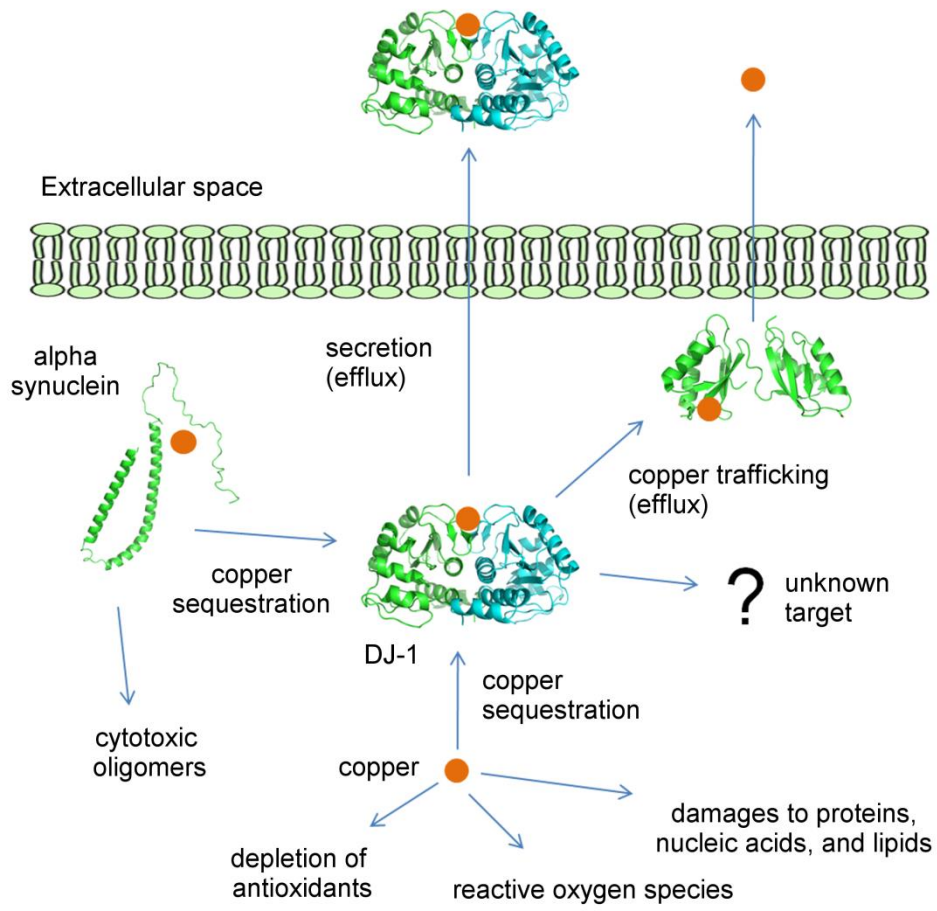


Figure 38. Proposed biological roles of the copper binding site of DJ-1.

4.2 Structure of Cu(I)-bound DJ-1 establishes the role for DJ-1 homodimerisation in copper sequestration: insights into mutational inactivation of DJ-1 in PD

The structure of DJ-1 complexed with a Cu(I) ion reveals the requirement for a stable homodimer in order to function as a copper carrier. This is supported by the fact that DJ-1 mutations A104T and D149A, which have been reported to reduce DJ-1 homodimerisation (Moore *et al.*, 2005), abrogated the ability of DJ-1 to confer cytoprotection against copper- and mercury- induced cell death (Bjokblom *et al.*, 2013). The structural basis on how these mutations affect DJ-1 homodimerisation awaits further investigation. Nonetheless, the A104T mutation has been shown to destabilise the DJ-1 fold by introducing a polar residue in the hydrophobic core (Lakshminarasimhan *et al.*, 2008) which can potentially lead to weakened interactions between the monomers.

Several other mutations in DJ-1 have been shown to decrease homodimerisation and/or reduce the intracellular levels of the protein (Figure 39; Moore *et al.*, 2003; Gorner *et al.*, 2007; Hulleman *et al.*, 2007; Lakshminarasimhan *et al.*, 2008). The mutation L166P completely impairs dimerisation and is rapidly degraded in mammalian cells (Moore *et al.*, 2003; Hulleman *et al.*, 2007). L166P disrupts helix G found in the C-terminal helix-kink-helix motif resulting in the destabilisation of the DJ-1 dimer (Gorner *et al.*, 2007). Another mutation M26I, which resides in helix A, causes a subtle change in the core of the dimer, forming a cavity that results in inefficient packing (Lakshminarasimhan *et al.*, 2008). M26I has been shown to reduce the extent of dimerisation *in vitro* (Hulleman *et al.*, 2007) and *in vivo* (Repici *et al.*, 2013). A charge reversal mutation E163K has been identified from a patient manifesting parkinsonism with dementia and amyotrophic lateral sclerosis (Annesi *et al.*, 2005). E163K abolishes a salt bridge between Glu-163 and Arg-145, which further participates in a hydrogen bond network that spans across the dimer interface, therefore weakening the homodimer interactions

(Lakshminarasimhan *et al.*, 2008). The L10P and L158del mutations have also been shown to impair DJ-1 homodimerisation albeit no details have been reported on how these mutations affect the oligomeric state of DJ-1 (Rannikko *et al.*, 2013; Repici *et al.*, 2013). These aforementioned mutations that lead to loss of homodimerisation and protein stability would potentially impair the ability of DJ-1 to protect against metal-induced cellular degeneration.

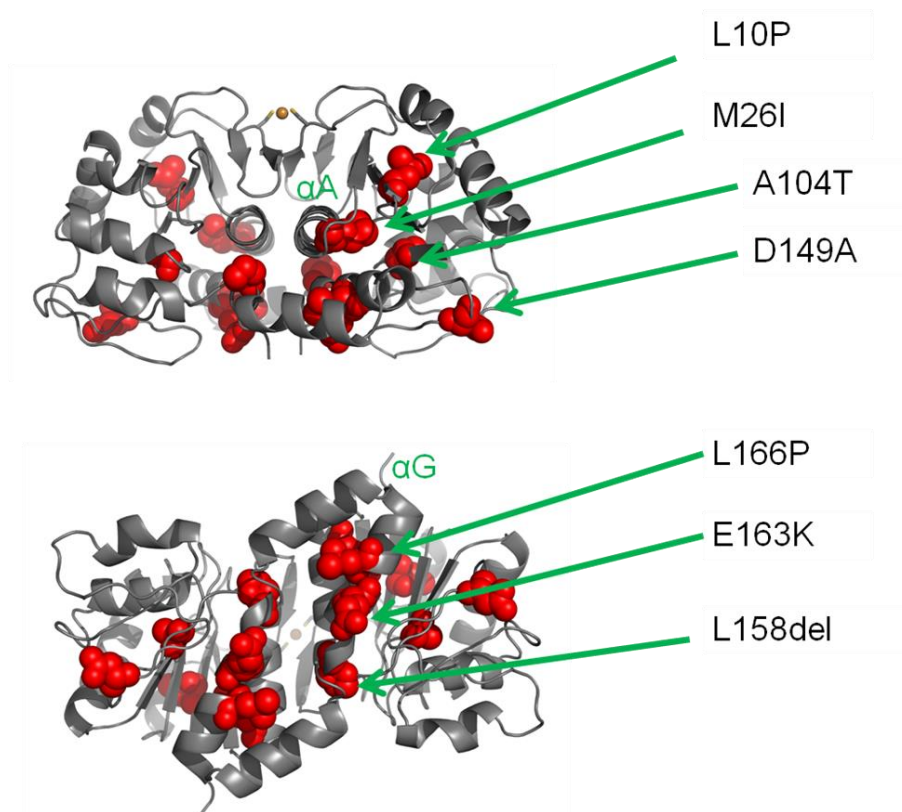


Figure 39. Location of Parkinsonism-linked mutations that reduce DJ-1 dimerisation. The mutation M26I, which lies in helix αA , results in a packing defect in the core of the dimer. Two mutations in helix αG , L166P and E163K, also result in weakening of dimer interactions. The positions of the L10P, A104T, D149A and L158del mutations are also shown. Structure of DJ-1 (PDB ID code: 4BTE) was rendered using PyMol (Delano, 2002).

4.3 Molecular basis for the pathogenicity of the DJ-1 A107P mutation

In Chapter 3, we have characterised the pathogenic effects of the A107P mutation on the structure and function of DJ-1. Firstly we have shown that DJ-1^{A107P} lacks glyoxalase activity *in vitro* which correlated with the loss of protection against glyoxal cytotoxicity and increased CML damage to cellular proteins. α -Oxoaldehydes are by-products of metabolism (Phillips and Thornalley, 1993). Their accumulation contributes to pathological processes associated with neurodegeneration including proteasomal inhibition (Bento *et al.*, 2010; Queisser *et al.*, 2010), mitochondrial dysfunction (Wang *et al.*, 2009), protein aggregation (Shaikh and Nicholson, 2008), and oxidative stress (Ramasamy *et al.*, 2005; Ramasamy *et al.*, 2006; Kuntz *et al.*, 2010). Hence the cell employs multiple systems to eliminate α -oxoaldehydes. Although the glutathione-dependent GLO1/GLO2 system plays a major role in protecting cells against α -oxoaldehyde-induced damage, DJ-1's ability to catalyze the detoxification of α -oxoaldehyde in the absence of a glutathione cofactor poses an advantage when cellular glutathione levels are depleted (Lee *et al.*, 2012). One of the pathological features of neurons affected in PD is the significant decrease in the cellular glutathione concentration (Perry *et al.*, 1982). Intuitively, in such pathological event, the absence of DJ-1 glyoxalase activity can lead to a deleterious accumulation of α -oxoaldehyde.

Secondly we and our collaborators have shown that the A107P mutation affects the intracellular steady state levels and the oligomeric state of the DJ-1 protein. In our hands, the protein levels of wild-type DJ-1 and DJ-1^{A107P} showed no apparent difference. But when our Tuebingen collaborators compared the intracellular steady-state levels of the wild-type protein and DJ-1^{A107P} they found a decrease in the levels of DJ-1^{A107P} relative to the wild-type protein albeit in different cell lines, HEK 293E and MEF. The difference may be due to the effects of the tags used in the experiments however Gorner *et al.*, (2007) have shown that the type and the position of the tag does not dictate the

intracellular concentration of the wild-type protein relative to variants with the same tag. Hence, it is possible that the effects of the mutation is cell-type specific. Nonetheless, the rate of protein turnover should also be investigated to ascertain the inherent stability of the various constructs in different cell lines. Similar effect on intracellular steady-state levels has been demonstrated for a number of PD-linked DJ-1 mutations e.g. L10P, L158del, and L166P (Moore *et al.*, 2003; Gorner *et al.*, 2004; Olzmann *et al.*, 2004; Blackinton *et al.*, 2005; Ramsey and Giasson, 2010; Rannikko *et al.*, 2012). Expression of the A107P variant does not affect the levels of endogenous wild-type DJ-1, consistent with the recessive nature of the mutation.

Using NMR and CD spectroscopy we have shown that the DJ-1^{A107P} exhibits remarkable degree of misfolding, providing a molecular basis for the lack of glyoxalase activity, the absence of nuclear translocation, and the decrease in intracellular protein levels. The structural and biochemical properties of DJ-1^{A107P} recapitulate those of the L166P mutant. However unlike the L166P mutant, DJ-1^{A107P} is capable of heterodimerisation with wild-type DJ-1 (Olzmann *et al.*, 2004). In addition, HEK 293E expressed DJ-1^{A107P} does not exhibit proteolytic breakdown products which are observed for ectopically expressed L166P mutant (Olzmann *et al.*, 2004). This suggests that the structural defect caused by the A107P mutation is distinct from the L166P mutant. Nevertheless, both mutations lead to a loss of a multifunctional protein that aids in cellular protection against cellular degeneration.

4.5 Role of the nucleophile elbow motif in the structural integrity of the DJ-1 fold

Our structural characterisation of the A107P mutation in human DJ-1 highlights the role for the nonenzymatic residues of the nucleophile elbow motif not only in the molecular architecture of the active site but also in the proper folding of the DJ-1 polypeptide.

The nucleophile elbow motif, first described in α/β -hydrolases, is a conserved structural feature among DJ-1 homologues. This motif uniquely positions the nucleophilic residue, Cys-106 in the case of human DJ-1, in a sharp turn imposed by constrained backbone torsion angles ($\phi = 66^\circ$, $\psi = -117^\circ$ in human DJ-1). The motif is identified by the consensus sequence Sm-X-Nu-X-Sm where Sm = small residue, Nu = nucleophile, and X = any residue. The requirement for residues with small side chains at positions Nu-2 and Nu+2 arises from the fact that these residues are very close to each other, thus in order to prevent steric clash, either of these positions are usually occupied by an alanine or a glycine residue (Ollis *et al.*, 1992). In human DJ-1, the C $_{\alpha}$ of Ala-105 and Gly-108 are separated by a distance of 5Å (Figure 40A). Moreover, the side chains of Nu-2 and Nu+2 are pointed towards the hydrophobic core of the protein (Figure 40B), hence, a nonpolar residue usually occupies these positions (Figure 26). Indeed, substitution of Ala-104 in human DJ-1 for a polar and relatively larger threonine residue causes local structural perturbation of the hydrophobic core (Lakshminarasimhan *et al.*, 2008). The A104T mutation also recruits a water molecule into the hydrophobic core, further destabilising the fold (Lakshminarasimhan *et al.*, 2008). Unsurprisingly, the A104T mutation was isolated from a patient with early-onset Parkinsonism (Hague *et al.*, 2003). It was previously thought that the position Nu+1 could be occupied by any amino acids. In this study, we have shown that proline substitution of Ala-107 (Nu+1 in human DJ-1) results in a remarkable misfolding of the DJ-1 protein. Hence, to maintain proper folding at least in DJ-1 homologues, the residue at position Nu+1 should be a nonproline residue. Close inspection of this residue in the structure of human DJ-1 does

not show any obvious steric hindrance or disruption of interactions when substituted by proline. Perhaps, the slight change in backbone torsion angles predicted *in silico* is translated into a more profound structural perturbation of the fold. Another possibility is the disruption of a quasi-helical conformation, conserved among DJ-1 homologues, succeeding the elbow turn (Figure 40C). Further investigation is necessary to ascertain the exact structural basis by which the A107P disrupts the DJ-1 fold.

We surmise that the nucleophile elbow motif is also involved in critical interactions that anchor the fold together. A sequence alignment of DJ-1 homologues reveals two highly conserved sequence motifs that interact with the nucleophile elbow (Figure 41A). The two motifs exhibit a strand-loop-helix topology (Figure 41B). Motif I interacts with the nucleophile elbow via main-chain hydrogen bonding between Leu-72 and Ile-105 while the Ser-155 main-chain amide donates a hydrogen bond to the main-chain amides of Ile-105 and Ala-104 (Figure 41C). Disruption of these interactions by disease-linked point mutations is predicted to cause a deleterious effect on the proper folding of DJ-1.

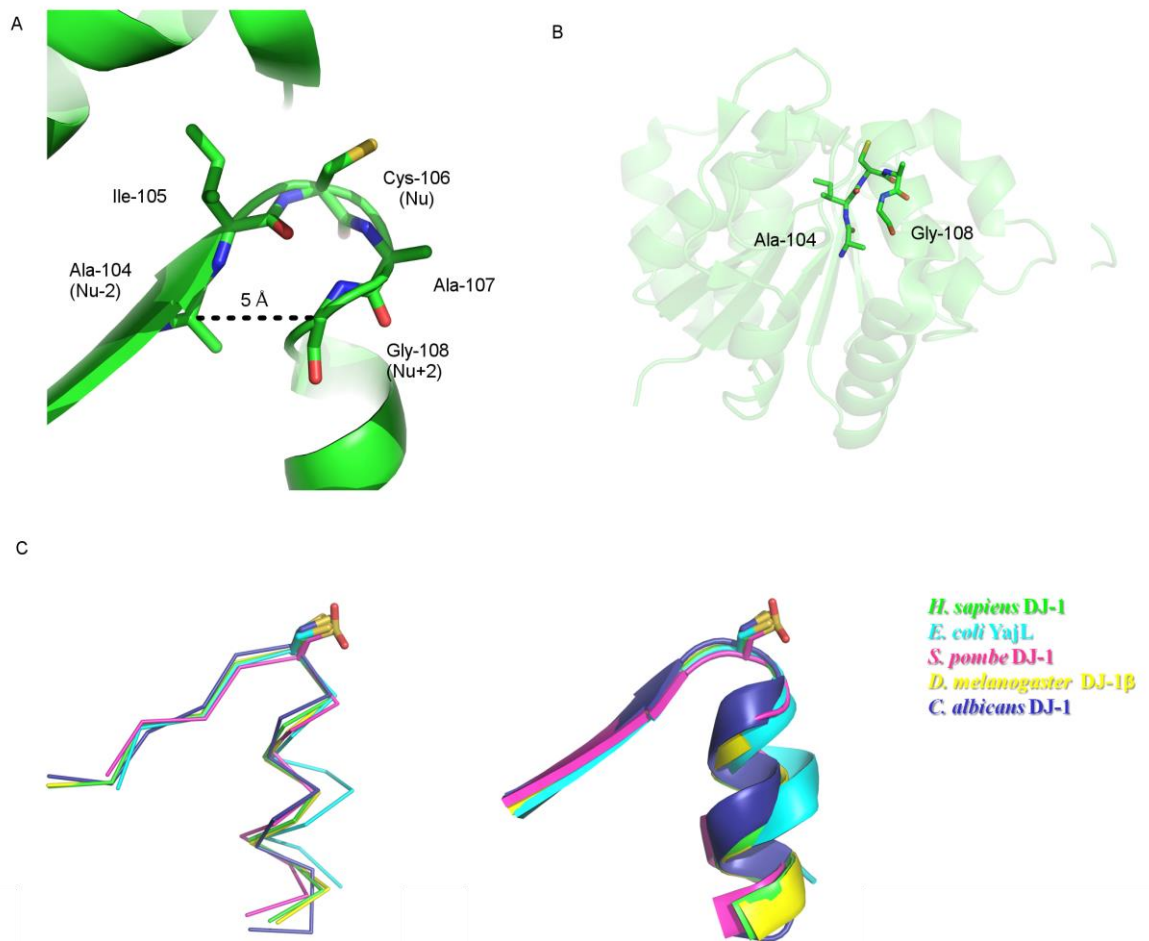


Figure 40. Structure of the human DJ-1 nucleophile elbow motif. (A) The DJ-1 structure (PDB ID code: 1PDV) is shown as a cartoon with the residues in the nucleophile elbow as sticks and the distance between the C_{α} of Ala-104 and Gly-108 is indicated in Angstroms. (B) Cartoon representation of human DJ-1 with the transparency increased to 80% to show the side chains of Ala-104 and Gly-108 pointing to the hydrophobic core of the protein. (C) Helical conformation of the residues succeeding the nucleophilic residue in DJ-1 homologues. Backbone traces (right panel) and cartoon representations (left panel) of the nucleophile elbow motifs in various DJ-1 homologues are shown with the side chain of the nucleophilic residue as sticks. Structures were rendered using PyMol (Delano, 2002).

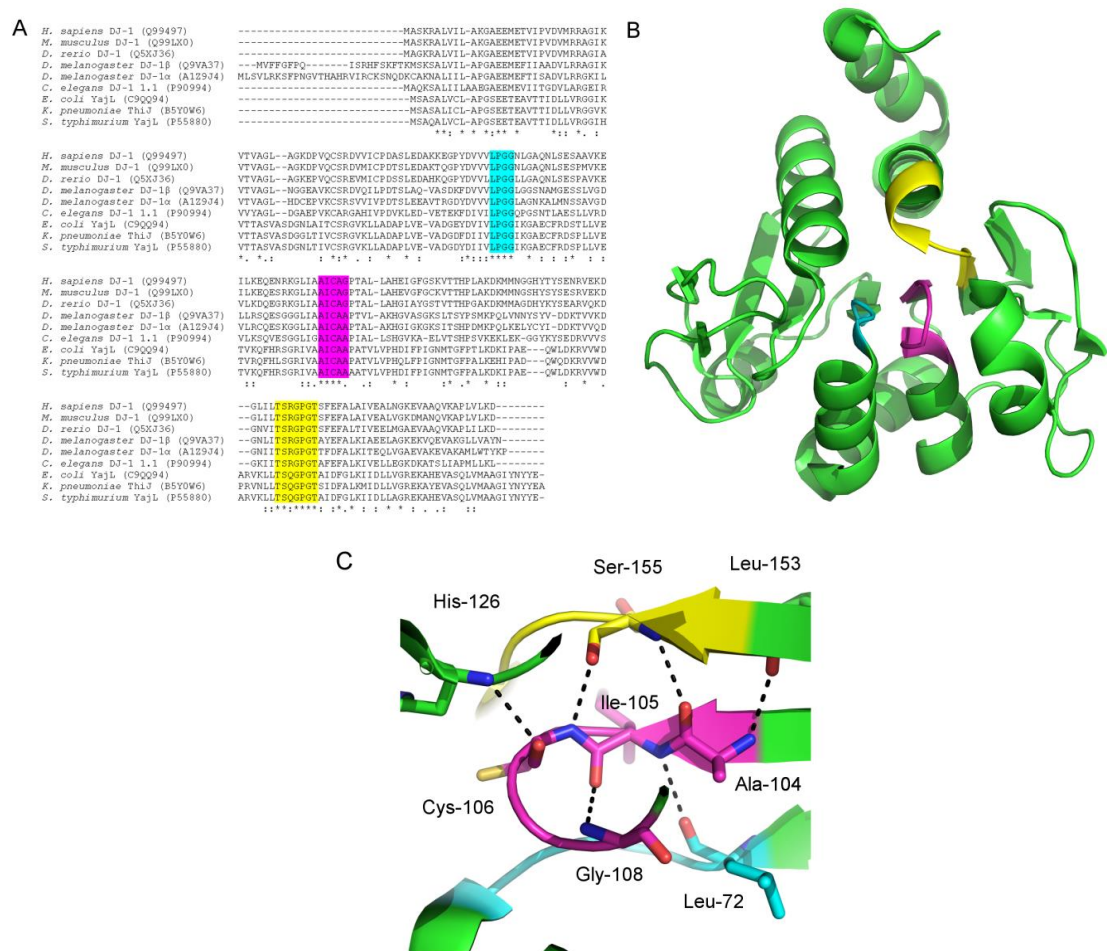


Figure 41. Conserved motifs interacting with the nucleophile elbow motif in DJ-1. (A) Multiple sequence alignment showing the conservation of two strand-loop-helix regions in prokaryotic and eukaryotic homologues of DJ-1. Motifs I and III are highlighted in cyan and yellow, respectively. The nucleophile elbow motif (motif II) is highlighted in magenta. Uniprot accession numbers are shown in parentheses. (B) Positions of motifs I, II, III in the crystal structure of DJ-1 (PDB ID code: 1PDV). (C) Interaction between the residues of the nucleophile elbow motif (motif II) and residues in motif I and III. Structures were rendered using PyMol (Delano, 2002).

4.4 Crystal structure of DJ-1 C106S bound to a sulphate anion and glycerol illuminates the mechanism of substrate recruitment and hemithioacetal intermediate formation

The initial step in the glyoxalase reaction mechanism of DJ-1 involves a nucleophilic addition reaction whereby the S-thiolate moiety of Cys-106 attacks the aldehydic carbonyl carbon (C1) of the α -oxoaldehyde *e.g.* methylglyoxal, giving rise to a hemithioacetal (Kwon *et al.*, 2013). The crystal structure of the DJ-1 C106S variant bound to a sulphate anion and glycerol in the active site provides molecular clues on how this initial step takes place (Figure 42). We found glycerol to be hydrogen bonded to the side chain of Arg-28' (of subunit B). I posit that glycerol mimics an α -oxoaldehyde being recruited by Arg-28' into the active site. Unlike glycerol with sp³ hybridised carbons, the α -oxoaldehyde carbons are sp² hybridised and therefore would be coplanar with Arg-28' sidechain guanidium moiety. This positions the substrate to an orientation favourable for nucleophilic attack. Arg-28' is anchored to subunit A via guanidium stacking with Arg-48 (Witt *et al.*, 2008). I envision that these two highly conserved arginine residues work together to guide the substrate into the active site. Consequently, homodimerisation is required to create a substrate recruitment site. PD-linked mutations that impair DJ-1 dimerisation could therefore affect the ability of DJ-1 to detoxify α -oxoaldehydes.

Thus far, I have produced a recombinant DJ-1 with an R28Q mutation to test the crucial role of this residue in substrate recruitment and catalysis. This mutation has been chosen over R28A because it has been shown to retain dimerisation and does not affect the pKa of Cys-106 (Herrera *et al.*, 2007; Witt *et al.*, 2008), hence avoiding a compounding effect. I posit that this mutation will reduce the ability of DJ-1 to catalyse glyoxal detoxification. However, the R28Q mutant exhibits a catalytic turnover constant similar to the catalytically inactive C106S mutant (Figure 43). This suggests that Arg-28' may play catalytic roles other than substrate recruitment and optimal orientation of the

substrate for nucleophilic addition reaction. Interaction of Arg-28' guanidinium group may increase the dipole moment of the α -oxoaldehyde substrate thereby further activating the aldehydic carbon for nucleophilic attack. Additionally, I have also shown that aspartic acid substitution of Glu-18 does not support catalysis (Figure 43), consistent with a previous report (Lee *et al.*, 2012)

When Cys-106 attacks the aldehydic carbonyl carbon of the α -oxoaldehyde, a tetrahedral transition state will form with an oxyanion moiety. The stabilisation of the oxyanion influences the efficiency of the reaction in many enzymes (Byran *et al.*, 1986; Menard and Storer, 1992; Li *et al.*, 2000; Lee *et al.*, 2006). Dedicated residues within the active site form an oxyanion hole to stabilise the transition state. Sulphate, a monomeric oxyanion, occupied the active site pocket in the crystal structure. The sulphate oxyanion was mainly held by the amide NH moieties of Gly-75 and Ala-107 (Figure 42). I envision that the sulphate ion mimics the tetrahedral transition state during nucleophilic addition with the backbone amide NH of Gly-75 and Ala-107 forming an oxyanion hole. Gly-75 and Ala-107 are highly conserved residues in DJ-1 homologues. The role of Ala-107 in forming an oxyanion hole is supported by a report of Buller and Townsend (2013) on the geometric rules governing the reaction mechanism of enzymes with a nucleophile elbow.

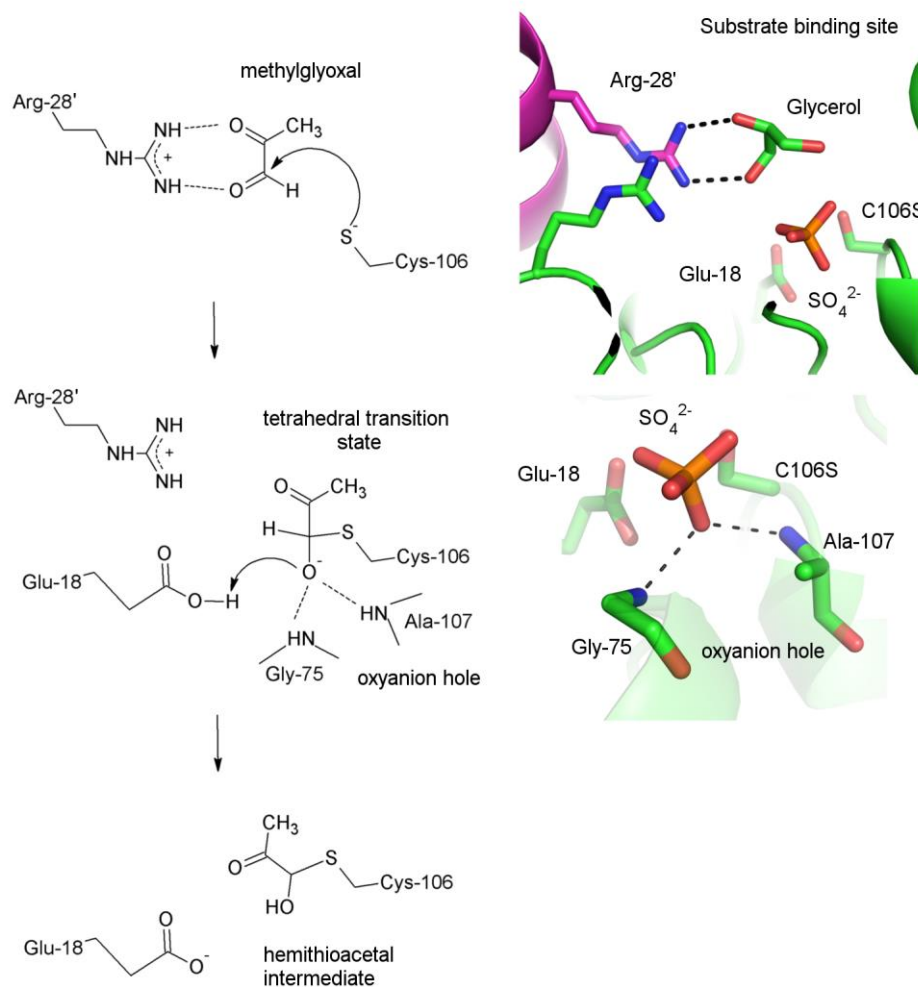


Figure 42. Proposed mechanism of the hemithioacetal intermediate formation of the DJ-1 glyoxalase reaction. Reaction mechanism (left panel) of the nucleophilic addition step of DJ-1 glyoxalase. The glycerol and sulphate in the active site mimic the substrate and transition state, respectively (right panel). Cartoon representations of subunits A and B of the DJ-1 homodimer are coloured green and magenta, respectively. Structures were rendered using PyMol (Delano, 2002).

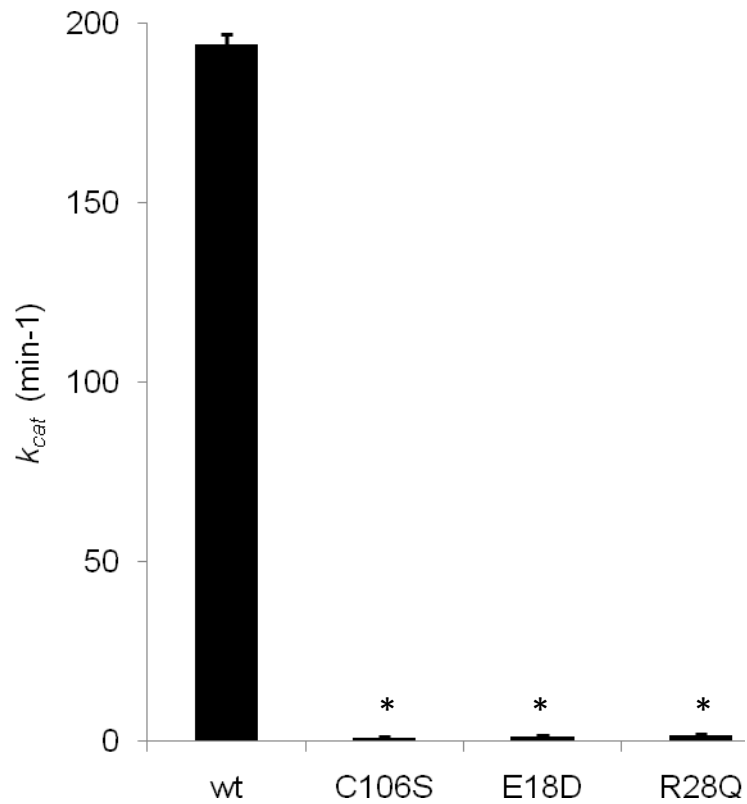


Figure 43. Glyoxalase catalytic turnover constants of DJ-1 variants. k_{cat} values were estimated using a DNPH-based quantitative assay using glyoxal as substrate. Data are presented as mean \pm SEM obtained from data ($n = 3$) from three repeats. (*) denotes $p < 0.0001$ in an unpaired t-test when compared with the k_{cat} values of the wild-type protein.

4.5 Future work

The results presented in this thesis point to several research opportunities to advance our molecular understanding of the multifaceted cellular function of DJ-1. The following future directions for further work are recommended:

Can DJ-1 prevent α -synuclein aggregation induced by copper?

α -Synuclein aggregation has been linked to the development of PD (Conway *et al.*, 1998; Eriksen *et al.*, 2005). Copper accelerates the formation of neurotoxic oligomers of α -synuclein (Wright *et al.*, 2009). It therefore raises question of whether DJ-1, through its subfemtomolar affinity for copper, is capable of sequestering the copper from α -synuclein. DJ-1 has already been shown to inhibit the inherent ability of α -synuclein to aggregate (Shendelman *et al.*, 2004; Zhou *et al.*, 2006). It would be interesting to test whether DJ-1 can also protect against accelerated α -synuclein aggregation induced by copper *in vivo* and whether mutations that disrupt the copper binding site perturb such capability.

How does copper binding affect the glyoxalase activity of DJ-1?

The copper binding site and the glyoxalase active site are found in distinct locations in DJ-1. This exemplifies the multifaceted nature of the cellular function of DJ-1. Yet it also raises interesting questions on whether the two biological activities are related. Does copper binding regulate the ability of DJ-1 to act as a glyoxalase? Perhaps it is unlikely given the spatial distance between the two sites. However, the copper site null C53A mutant has been suggested to promote Cys-106 oxidation (Waak *et al.*, 2009), which would inactivate the glyoxalase activity of DJ-1.

Reaction mechanism of DJ-1 glyoxalase activity

So far, our crystal structure of DJ-1 bound to glycerol and sulphate provided molecular clues on the mechanism of substrate binding and the initial step of the glyoxalase activity of DJ-1. However, a crystal structure of DJ-1 bound to a real substrate and/or engaged in catalysis will prove to be invaluable in determining the complete reaction mechanism and regioselectivity of insofar the only eukaryal glyoxalase that does not require a glutathione cofactor. In prokaryotes, the cofactor-independent glyoxalase (Hsp31 in *E. coli*) converts methylglyoxal into D-lactate (Subedi *et al.*, 2011). It would be interesting to know whether the same enantiomer of lactate is produced by human DJ-1 given the differences in the architecture of the active sites between the two enzymes.

Chapter 5

Materials and Methods

5.1 Bacterial strains

Table 5. *E. coli* strains for cloning and protein expression.

Strain	Genotype	Source
TOP10	<i>F</i> ⁻ <i>mcrA</i> Δ (<i>mrr-hsdRMS-mcrBC</i>) <i>φ80lacZAM15 ΔlacX74 nupG recA1</i> <i>araD139 Δ(ara-leu)7697 galE15</i> <i>galK16 rpsL(Str^R) endA1 λ⁻</i>	Life Technologies
BL21 (DE3)	<i>F</i> ⁻ <i>ompT gal dcm lon hsdS_B(r_B⁻ m_B⁻)</i> <i>λ(DE3 [lacI lacUV5-T7 gene 1 ind1</i> <i>sam7 nin5])</i>	Stratagene
BL21 (DE3) pLysS	<i>F</i> ⁻ <i>ompT hsdSB (rB-mB-)</i> <i>gal dcm</i> <i>(DE3) pLysS (CamR)</i>	Life Technologies

5.2 Plasmid constructs and primers

Table 6. Plasmid constructs.

Name	Vector	Insert	Tag	Cloning Sites	Primers
DJ-1x	pET-28a (+)	human DJ-1	-	<i>NcoI/XhoI</i>	1, 3
DJ-1-His ₆	pET-28a (+)	human DJ-1	C _T His ₆	<i>NcoI/XhoI</i>	1, 2
C53Ax	pET-28a (+)	DJ-1 C53A	-	<i>NcoI/XhoI</i>	5, 6
C106Sx	pET-28a (+)	DJ-1 C106S	-	<i>NcoI/XhoI</i>	20, 21
A107P-His ₆	pET-28a (+)	DJ-1 A107P	C _T His ₆	<i>NcoI/XhoI</i>	7, 8
C106A-His ₆	pET-28a (+)	DJ-1 C106A	C _T His ₆	<i>NcoI/XhoI</i>	9, 10
SOD1	pLEICS-03	Wild-type human SOD1	N _T His ₆	<i>NcoI/XhoI</i>	11, 12
HCV	pLEICS-03	SOD1 H46F/ C146S	N _T His ₆	<i>NcoI/XhoI</i>	13-16
pDJ-1-His ₆	pCDNA 4	human DJ-1	C _T His ₆	<i>BamHI/XhoI</i>	2, 4
pA107P-His ₆	pCDNA 4	DJ-1 A107P	C _T His ₆	<i>BamHI/XhoI</i>	2, 4
pC106A-His ₆	pCDNA 4	DJ-1 C106A	C _T His ₆	<i>BamHI/XhoI</i>	2, 4
pDJ-1x	pCDNA 4	human DJ-1	-	<i>BamHI/XhoI</i>	3, 4
pC53Ax	pCDNA 4	DJ-1 C53A	-	<i>BamHI/XhoI</i>	3, 4
His ₆ -tat-DJ-1	pLEICS-03	human DJ-1	N _T His ₆	<i>NcoI/XhoI</i>	19, 3
His ₆ -tat-C106A	pLEICS-03	DJ-1 C106A	N _T His ₆	<i>NcoI/XhoI</i>	19, 3
His ₆ -tat-A107P	pLEICS-03	DJ-1 A107P	N _T His ₆	<i>NcoI/XhoI</i>	19, 3

Table 7. Cloning and sequencing primers

No.	Primer	Sequence (5' → 3')
1	DJ-1 FWD	ATTCCATGGCTTCCAAAAGAGCTCTGGTCA
2	DJ-1 REV	AATCTCGAGCGTCTTTAAGAACAAGTGGAGCCTT
3	DJ-1 STOP REV	AATCTCGAGTTACGTCTTTAAGAACAAGTGGAGCCTT
4	DJ-1 TET FWD	ATTCCATGGCTTCCAAAAGAGCTCTGGTCA
5	DJ-1 C53A FWD	ATGTGGTCATTGCACCTGATGCCAG
6	DJ-1 C53A REV	CTGGCATCAGGTGCAATGACCACAT
7	DJ-1 A107P FWD	AGCCGCCATCTGTCCAGGTCCTACTG
8	DJ-1 A107P REV	CAGTAGGACCTGGACAGATGGCGGCT
9	DJ-1 C106A FWD	CCGCCATCGCTGCAGGTCCT
10	DJ-1 C106A REV	AGGACCTGCAGCGATGGCGG
11	SOD1 FWD	AATCCATGGCTTCCAAAAGAGCTCTGGTCA
12	SOD1 REV	ATTCTCGAGTTGGGCGATCCCAATTACA
13	SOD1 H46F FWD	CATGGATTCTTCGTTTCATGAGTTTG
14	SOD1 H46F REV	CAAATCATGAACGAAGAATCCATG
15	SOD1 C146S FWD	GTCGTTTGGCTAGCGGTGTAATTG
16	SOD1 C146S REV	CAATTACACCGCTAGCCAAACGAC
17	T7 FWD	TAATACGACTCACTATAGGG
18	T7 REV	GCTAGTTATTGCTCAGCGG
19	DJ-1 TAT FWD	ATTCCATTGGGCAGGAAGAAGCGGAGACAGCGA CGAAGAAGAGGCTCGATGGCTTCCAAAACAG
20	DJ-1 C106S FWD	GTAGGACCTGCAGATATCGCGGCTATCAG
21	DJ-1 C106S REV	CTGATAGCCGCGATATCTGCAGGTCCTAC

5.3 Media, buffers, and solutions

Table 8. Media and media supplements

Name	Composition
LB broth	1% w/v tryptone, 0.5% w/v yeast extract, 0.5% w/v NaCl
¹⁵ N -M9 medium	42 mM Na ₂ HPO ₄ , 22 mM KH ₂ PO ₄ , 86 mM NaCl, 7.6 mM ¹⁵ (NH ₄) ₂ SO ₄ , pH adjusted to 7.4
10X M9 supplement	10 mM MgSO ₄ •7H ₂ O, 10 mM thiamine, 1 mM CaCl ₂ •2H ₂ O, 40% w/v glucose, 0.01 mM FeSO ₄ •7H ₂ O

Table 9. Antibiotics

Name	Stock solution	Working Concentration
Ampicillin	200 mg/ml in ddH ₂ O	200 µg/ml
Kanamycin	50 mg/ml in ddH ₂ O	50 µg/ml
Chloramphenicol	34 mg/ml in ethanol	34 µg/ml

Table 10. General buffers and solutions

Name	Composition
TSS	10% w/v PEG 8000, 30 mM MgCl ₂ , 5% v/v DMSO
5X TBE	450 mM Tris, 450 mM boric acid, 10 mM EDTA
10X SDS-PAGE Running Buffer	250 mM Tris, 1% w/v SDS, 2.5 M glycine
4X SDS-PAGE sample buffer	250 mM Tris pH 6.8, 10 % w/v SDS, 0.008% w/v bromophenol blue, 20% v/v mercaptoethanol or 1 M DTT, 40% v/v glycerol
6X Loading dye	10 mM Tris pH 7.6, 0.0015% w/v bromphenol blue, 60% v/v glycerol, 100 mM EDTA
Coomassie stain	40% v/v methanol, 10% v/v glacial acetic acid, 0.1% Coomassie Brilliant Blue R-250
Destaining solution	10% v/v methanol, 10% v/v glacial acetic acid
Transfer Buffer	0.25 M glycine, 25 mM Tris, 20% v/v methanol
TBS	50 mM Tris pH 7.5, 150 mM NaCl
TBS-T	50 mM Tris pH 7.5, 150 mM NaCl, 0.05% v/v Tween 20
PBS	137 mM NaCl, 2.7 mM KCl, 10 mM Na ₂ HPO ₄ , 1.76 mM KH ₂ PO ₄ , pH adjusted to 7.4
PBS-T	137 mM NaCl, 2.7 mM KCl, 10 mM Na ₂ HPO ₄ , 1.76 mM KH ₂ PO ₄ , pH adjusted to 7.4, 0.1% v/v Tween 20
CD Buffer	20 mM HEPES pH 7.5, 50 mM NaCl
Microassay buffer	20 mM Tris pH 8.0, 100 mM NaCl

Table 11. Buffers used in protein purification

Name	Composition
Buffer A	50 mM Tris pH 8.0, 300 mM NaCl
Buffer B	50 mM Tris pH 8.0, 300 mM NaCl, 25 mM imidazole
Buffer C	50 mM Tris pH 8.0, 300 mM NaCl, 10 mM imidazole
Buffer D	50 mM Tris pH 8.0, 300 mM NaCl, 5% v/v glycerol, 250 mM imidazole
Buffer E	20 mM Tris pH 8.0, 100 mM NaCl
Buffer F	20 mM Tris pH 7.15, 100 mM NaCl
Buffer G	20 mM Tris pH 8.0, 100 mM NaCl, 0.5 mM TCEP

5.4 Molecular biology methods

5.4.1 Preparation of chemically competent cells

To prepare chemically competent cells, fresh LB broth was inoculated with a starter culture grown at 37°C for 18-20 hours. Cells were grown with shaking (250 rpm) at 37°C until the optical density at 595 nm (OD₅₉₅) reached 0.4 and then transferred to an ice bath to chill for 10 minutes. Cells were centrifuged at 3000 x *g* and gently resuspended in TSS buffer. The resuspended cells were further incubated on ice for at least 20 minutes prior to distribution and storage at -80°C.

5.4.2 Transformation of chemically competent cells

Plasmid DNA (10 ng) was incubated with an aliquot of thawed competent cells on ice for at least 5 minutes. Cells were heat-shock at 42°C for 45 seconds and subsequently incubated on ice for another 5 minutes. LB broth (400 µl per 50-100 µl cells) was added to the cells and incubated with shaking (180 rpm) at 37°C for an hour. Transformed cells were either grown directly in LB broth or agar plates supplemented with antibiotics as appropriate.

5.4.3 Agarose gel electrophoresis

TBE was used as the buffer system for agarose gel electrophoresis. Agarose gels were prepared using electrophoresis-grade agarose (Sigma) dissolved in 0.5X TBE. Prior to casting, ethidium bromide (1 µg/ml) was usually added to the gel solution. Samples were prepared by mixing DNA solutions with the loading dye (Qiagen). Electrophoresis was carried out in a Bio-Rad Mini-Sub Gel GT with the gel submerged in 0.5X TBE. Gels were visualised using a UVP transilluminator.

5.4.4 Molecular cloning

Wild-type human DJ-1 and human SOD1 pET-28a clones used as templates for cloning were a kind gift of Prof. Simon Moller (St. John's University, USA). Polymerase chain

reaction (PCR) was used to amplify the coding sequence of the gene of interests. Primers were designed with a 5' overhang followed by a restriction site and around 17-25 nucleotides complementary to the gene of interest. Occasionally, additional nucleotide sequences *e.g.* tat domain were added before the gene sequences. Lyophilised primers (~50 nmol) were dissolved in ddH₂O and were used at 25-50 pmol per reaction. Reaction mixtures were prepared using a ready-to-use PCR master mix (Promega) that utilises the *Taq* DNA polymerase to amplify the target sequence. Reactions were carried out using BioRad MJ Mini thermal cycler. The thermocycler programs used were customised for each target sequence. Purification of the amplified DNA was performed using the QIAquick PCR purification protocol (Qiagen).

To create the sticky ends of the target sequence, hereafter will be referred to as insert, purified PCR products were cut using restriction enzymes (New England Biolabs) following the manufacturer's protocol. Reactions were carried out for at least 2 hours. Digested products were purified using the QIAquick gel extraction kit (Qiagen). Plasmid vectors were digested using the same procedure.

Ligation was performed by incubating the mixture of linearised plasmid vector (10 ng/μl) and digested insert DNA (30 ng/μl or more) with T4 DNA ligase (New England Biolabs) for 1 hour at 16°C. Ligation products were transformed into TOP10 (Life Technologies) as described in Section 5.4.2.

To determine a positive colony *i.e.* colony that contains a plasmid vector with the insert DNA, PCR reaction mixtures containing sequencing primers were inoculated with the bacterial colony and then a PCR was carried out. Empty vector was used as negative control. PCR products were analysed for the presence of insert using agarose gel electrophoresis. Positive clones were propagated using a plasmid miniprep kit (Qiagen)

and the accuracy of the sequence was determined using the UCL DNA sequencing service.

Point mutations were introduced using the QuikChange (Stratagene) protocol. Codon changes were made in the primers that were used to amplify the entire plasmid constructs. Parent vector DNA was removed from the PCR product by treatment with *DpnI* (New England Biolabs). Subsequently, the PCR-generated mutant constructs were propagated into TOP10 and the accuracy of the sequence was determined using the UCL DNA sequencing service.

5.5 Protein production and analysis

5.5.1 Recombinant DJ-1 production in *E. coli* (applies to all DJ-1 constructs)

A day prior to protein expression, *E. coli* BL21(DE3) cells were transformed with the plasmid DNA. The transformed cells were grown in 50-ml LB broth supplemented with the selective antibiotics at 37°C overnight. The overnight cultures were then used to inoculate (4 ml culture per 400 ml fresh broth) LB broth containing appropriate antibiotics. When the OD₅₉₅ of the bacterial culture reached 0.6-0.7, IPTG was added to each broth to a final concentration of 0.4 mM and the cultures were further incubated for 4 hours to allow protein expression. Cells were harvested by centrifugation and resuspended in Buffer A. Cells were frozen at -80°C at this stage until protein extraction could be performed.

5.5.2 Preparation of ¹⁵N-labelled DJ-1 proteins

E. coli BL21(DE3) cells transformed with the DJ-1 pET-28a constructs were grown overnight (not more than 18 hours) in LB broth containing kanamycin at 37°C with shaking (200 rpm). The overnight culture was used to inoculate the pre-warmed ¹⁵N-M9 media with supplements and kanamycin; 4 ml overnight culture per 400 ml M9 media. The cells were allowed to grow at 37°C with shaking until the OD₅₉₅ reached 0.6-0.8

and then the cultures were cooled to 25°C for at least 30 minutes. IPTG was added to a final concentration of 0.2 mM. Cultures were incubated overnight at 25°C with shaking (200 rpm) prior to harvesting. Uniformly ¹⁵N-labelled proteins were purified using the same procedure as the non-labelled proteins.

5.5.3 DJ-1 protein extraction and purification (applies to all DJ-1 constructs)

To extract proteins, cells were lysed with a combination of lysozyme treatment (1 mg/ml) and 2 freeze-thaw cycles followed by sonication. The cell lysates were then clarified by ultracentrifugation (20 000 x *g* for 1 hour at 4°C).

For His₆-tagged constructs, the cleared cell lysates were loaded onto either Ni²⁺ (Qiagen) or Co²⁺ (HisPur, Pierce) affinity resins. Ni²⁺ affinity resin was preferred for pLEICS-03 derived constructs. Protein-loaded resin was washed with 100 column volumes of Buffer B for Ni²⁺ affinity resin or Buffer C for Co²⁺ affinity resin. Finally proteins were eluted with 5 column volumes of Buffer D.

Untagged DJ-1 was purified according to a method previously described (Zhou *et al.*, 2006). Briefly, ammonium sulphate was added to the cleared lysate to 60% saturation and the resulting precipitates were removed by centrifugation. The soluble fraction was applied to a phenyl-sepharose column (GE Healthcare) and fractionated by decreasing ammonium sulphate saturation. Ammonium sulphate solutions were buffered with 20 mM Tris pH 8.0. Samples of each fraction were profiled by SDS-PAGE using Coomassie R-250 as a stain. Fractions containing untagged DJ-1 were pooled and exchanged into Buffer E using a PD-10 column (GE Healthcare). When necessary, proteins were subjected to anion exchange chromatography using Q-sepharose (GE Healthcare) and/or size exclusion chromatography (SEC) using Sephacryl S-100 (GE Healthcare). Buffer F was used as the mobile phase for the SEC procedure.

5.5.4 Preparation of apo-SOD1 and variants

Using the Protex cloning service in Leicester, human *SOD1* was cloned into the pLEICS-03 vector to generate a recombinant plasmid expressing a protein with a tobacco etch virus (TEV) protease cleavable N-terminal His₆ tag. His₆ tagged SOD1 was expressed in BL21(DE3) cotransformed with pLysS plasmid (Novagen) to improve the yield of soluble proteins. Cells were grown in LB media supplemented with kanamycin and chloramphenicol to an absorbance at 595 nm of 0.5-0.7, induced with 0.4 mM IPTG, and incubated for 4 hours at 37°C before harvesting. Cells were lysed with a combination of lysozyme treatment (1 mg/ml) and 1-2 freeze-thaw cycle(s) followed by sonication. The cell lysates were cleared by ultracentrifugation at 20 000 x g for 1 hour at 4°C. His₆ tagged SOD1 was purified using HisPur cobalt(II)-affinity resin (Pierce) according to the protocol described in Section 5.5.3. To remove the tag, the HisPur eluate was buffer exchanged into Buffer G and then treated with GST-TEV protease (100 µg enzyme per 1 mg of protein; Protex, Department of Biochemistry, University of Leicester) overnight.

Apo-SOD1 was prepared as follows. Recombinant SOD1 was treated with 20 mM DTT for 10 minutes and acidified by adding 0.4% v/v Trifluoroacetic acid (Sigma) for 30 minutes on ice. The following reagents were then sequentially added: 10% v/v methanol and 15% v/v acetonitrile, 1 mM bathocuproine disulphonate (Sigma) and 1 mM EDTA. The reaction mixture was incubated for 3 hours at 4°C. Finally, the protein was buffer-exchanged into Buffer E using PD-10 chromatography.

5.5.5 Determination of protein concentration

A Bradford microassay (Bio-Rad) was used to quantify the protein concentration. BSA (Pierce) was used as a protein standard. Each protein sample was diluted in Microassay buffer to make up an 800 µl solution. To each sample, 200 µl of Bradford reagent concentrate (Bio-Rad) was added and incubated for at least 5 minutes at room

temperature. Absorbance was measured at 595 nm using a benchtop spectrophotometer. Standard curves (absorbance versus concentration, $\mu\text{g/ml}$) were plotted in Microsoft Excel 2007 and the equation of the line was used to calculate the concentration of each protein sample.

5.5.6 SDS-PAGE

SDS-PAGE was performed using the Laemmli buffer system (Laemmli, 1970). Each resolving gel used was adjusted to 12% v/v acrylamide using 30% w/v acrylamide:bisacrylamide (37.5:1) (National Diagnostics). Each protein sample was mixed with SDS-PAGE sample buffer and heated at 95°C for 5 minutes. Protein gels were electrophoresed using the Bio-Rad Mini Gel tanks filled with 1X SDS-PAGE running buffer at 180 V for 1 hour. Gels were boiled in Coomassie stain for a minute and then incubated in the destaining solution until protein bands appeared against a clear background.

5.6 Chemical and biophysical techniques

5.6.1 Electronic absorption spectroscopy

All solutions were prepared in an anaerobic glove box at room temperature. Untagged DJ-1 was pre-treated with DTT to reduce disulphide bonds and with EDTA to remove any bound metal ions. The reduced apoprotein was buffer exchanged into a degassed solution containing 25 mM Tris pH 7.5, 100 mM NaCl. The protein solution (10 μM dimer) was transferred to a sealed cuvette and titrated with a Cu(I) solution prepared by dissolving $[\text{Cu}(\text{CH}_3\text{CN})_4]\text{PF}_6$ in degassed acetonitrile. A wavelength scan was performed using an Agilent 8453 spectrophotometer. This work was performed at the Chemistry Department of University of Leicester.

5.6.2 MALDI-TOF

Proteins (1 μM) were buffer exchanged into 20 mM Tris pH 6.8 and treated with Cu(I)-GSH as required prior to analysis. Sample aliquots were then added to a nonacidified sinipinic acid/ H_2O /acetonitrile matrix solution and spotted on a sample plate. Spectra were acquired using a calibrated MALDI-TOF mass spectrometer (Applied Biosystems Voyager-DETM PRO Biospectrometry Workstation). Data were collected in the Mass Spectrometry Laboratory, The School of Pharmacy, University of London.

5.6.3 nESI-MS

Proteins (1 μM) were buffer exchanged into 50 mM ammonium acetate pH 7.5. A molar excess of Cu(I)-GSH complex was added to the protein solutions prior to analysis. Mass spectra were obtained on a QToF II MS (Waters) optimised for studying non-covalent interactions. Samples were introduced into the spectrometer using a gold-plated capillary needle (Harvard Apparatus). This work was performed at the laboratory of Prof. Carol Robinson, Department of Chemistry, University of Oxford.

5.6.4 Estimation of copper affinity

The copper affinity of DJ-1 was determined according to a previous method (Zhou *et al.*, 2008; Xiao *et al.*, 2011;). Reduced apo-DJ-1 (25 μ M dimer; untagged) in PBS was incubated with varying concentrations of $\text{Cu}^{\text{I}}(\text{Bca})_2^{3-}$ where Bca stands for bicinchoninic acid. The reaction mixtures were incubated for 10 minutes at room temperature to reach equilibrium. The equilibrium concentration of $\text{Cu}^{\text{I}}(\text{Bca})_2^{3-}$ was determined by measuring the absorbance at 562 nm using an Agilent 8453 spectrophotometer. The dissociation constant of the Cu(I)-DJ-1 complex was calculated using the equation below (Xiao *et al.*, 2011):

$$K_d \beta_2 = \frac{\left(\frac{[P]_{\text{total}}}{[CuP]}\right) - 1}{\left\{\left(\frac{[L]_{\text{total}}}{[CuL_2]}\right) - 2\right\}^2 [CuL_2]}$$

where K_d = Cu(I)-DJ-1 dissociation constant
 β_2 = $\text{Cu}^{\text{I}}(\text{Bca})_2^{3-}$ formation constant
 $[P]_{\text{total}}$ = total protein concentration as dimer
 $[CuP]$ = $\text{Cu}^{\text{I}}(\text{DJ-1})_2$ complex concentration
 $[L]_{\text{total}}$ = total Bca concentration and
 $[CuL_2]$ = $\text{Cu}^{\text{I}}(\text{Bca})_2^{3-}$ complex concentration

5.6.5 Crystallisation and structure determination of Cu(I)-bound DJ-1

His₆-tagged DJ-1 crystals were obtained by mixing one volume of protein solution (15 mg/ml) in 10 mM Tris pH 8.0, 75 mM NaCl, 3 mM DTT, 2.5% v/v glycerol with one volume of the reservoir solution (100 mM Tris pH 8.0, 10% w/v PEG 3350) using the hanging drop vapour diffusion method. The crystals were then soaked in the reservoir solution supplemented with 1 mM Cu(I)-GSH (1:3 molar ratio) complex, to get the Cu(I)-bound form of DJ-1.

X-ray diffraction data were collected at beamline I0-3 at the Diamond Light Source. To obtain optimal measurements of the anomalous signal from the copper ion, the data were collected using a 1.3772 Å radiation source with 0.1° oscillation. Diffraction data were processed using the fast_dp protocol of XDS (Kabsch, 2010), POINTLESS and SCALA (Collaborative Computational Project, 1994). Molecular replacement using

PHASER (McCoy *et al.*, 2007) was carried out using 1PDV as the search model. Refinement and model building were performed using CCP4i REFMAC (Collaborative Computational Project, 1994; Murshudov *et al.*, 1997) and COOT (Emsley P. and Cowtan K., 2004). The atomic coordinates and structure factors have been deposited in the Protein Data Bank (PDB ID: 4BTE).

5.6.6 Crystallisation and structure determination of DJ-1 C106S bound to glycerol and sulphate anion

Untagged DJ-1 C106S (phenyl-sepharose eluate) was buffer-exchanged into Buffer E once using a PD SpinTrap G-25 desalting column (GE Healthcare) and concentrated to 12 mg/ml using an Amicon Ultra-4 centrifugal filter unit with 10 KDa MWCO Ultracel-3 membrane (Millipore). Crystals were obtained by mixing one volume of the protein solution with one volume of the reservoir solution (20% v/v glycerol, 24% w/v PEG 1500) using a hanging drop vapour diffusion method. Plate-like crystals grew overnight. Diffraction data were collected at 100 K using a Rigaku RU2HB X-ray generator equipped with a copper anode, Xenocs multilayer optics and an R-Axis IV detector. Data were indexed, integrated and scaled using MOSFLM (Leslie, 1992), POINTLESS and SCALA (Collaborative Computational Project, 1994). An initial model was obtained using PHASER (McCoy *et al.*, 2007) with the 1.8 Å structure of DJ-1 (PDB ID: 1PDV; Tao and Tong, 2003) as the search model. Refinement of the model was performed using phenix.refine. Electron densities for sulphate anion and glycerol in the active site were evident from the difference Fourier map. Manual adjustment and ligand fitting were performed in COOT (Emsley and Cowtan, 2004) and the structure figures were prepared using PyMOL (Delano, 2002).

5.6.7 Single crystal spectroscopy of Cu(I)-bound DJ-1

Single crystal electronic absorption spectroscopy was performed at beamline I0-2 at the Diamond Light Source using an Andor303 imaging spectrograph with triple grating turret and Czerny-Turner geometry on an aperture setting of F/4 using a coupled aircooled Newton EM CCD and Maetel reflective lenses (Harwell, UK). Cu(I)-bound DJ-1 crystals were prepared by soaking the apo-DJ-1 crystals in reservoir solution (100 mM Tris pH 8.0 and 10% (w/v) PEG 3350) supplemented with Cu(I)-GSH complex. Data were normalised based on protein content and a difference plot was obtained. For single crystal fluorescence, apo-DJ-1 crystals were soaked in reservoir solution containing either Cu(I)-GSH or 1 mM CuSO₄ for 30 minutes. Spectra were recorded using a VortexEX fluorescence at the beamline I0-2 at Diamond Light Source.

5.6.8 Circular dichroism (CD) spectroscopy

Proteins (7.5 µM) in CD Buffer were transferred into a 0.5 – mm pathlength quartz cuvette. Far-UV CD spectra were recorded from 200-260 nm with 1 nm increments at 20°C using a Chirascan-plus CD spectrometer (Applied Photophysics) at University of Leicester.

5.6.9 Nuclear magnetic resonance (NMR) spectroscopy

Uniformly ¹⁵N labelled proteins were buffer exchanged into 25 mM sodium phosphate buffer pH 6.5. Deuterium oxide was added to each protein solution to a final concentration of 10% v/v D₂O. Heteronuclear single quantum correlation (HSQC) experiments for each protein (450 µM) were performed on a Bruker Avance III 500 MHz NMR spectrometer at 25°C. The NMR data were processed using NMRpipe (Delaglio *et al.*, 1995) and rendered using CCPNMR Analysis (Vranken *et al.*, 2005). NMR experiments were performed at the UCL Biomolecular NMR facility.

5.6.10 *In vitro* SOD1 activation assay

A SOD1 assay was performed according to a method developed by Rae *et al.* (2001). Cu(I) was loaded into wild-type DJ-1 and the C53A variant by incubating the proteins in Cu(I)-GSH (1:5) complex under anaerobic conditions. Unbound copper was removed by buffer-exchanging the protein into TN buffer using a 0.5 ml desalting column (Pharmacia) at least twice. Proteins (20 μ M) were quickly incubated with apo-SOD1 (10 μ M) for 30 minutes at 37°C. Reaction mixtures were then assayed for SOD1 activity using a kit from Sigma based on the reduction of the tetrazolium salt WST-1 by xanthine oxidase-generated superoxide to give a yellow formazan dye which absorbs at 490 nm (Figure 45).

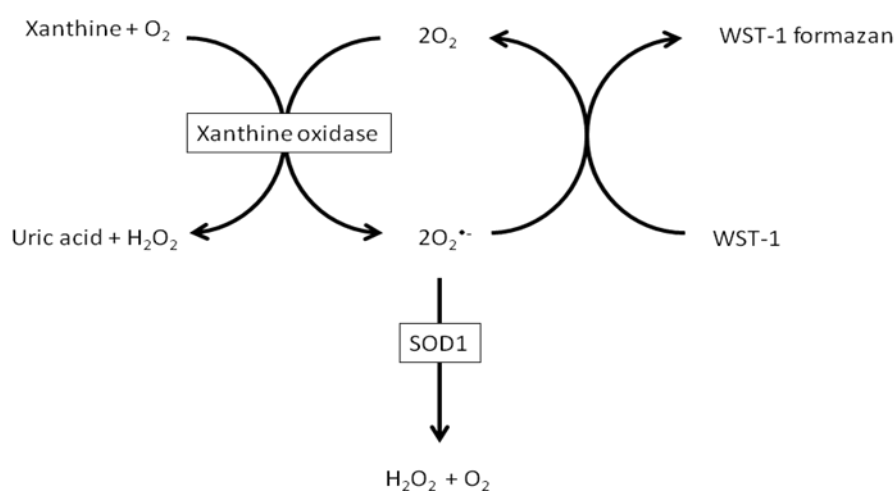


Figure 45. Chemical basis of the SOD1 activity assay.

Experiments were set up as shown in Table 12. Absorbance (A) was recorded using a VersaMax microplate reader. SOD1 activity was calculated as the percent inhibition rate of WST-1 conversion to WST-1 formazan using the equation:

$$\% \text{ SOD1 activity} = \frac{(A_{\text{blank1}} - A_{\text{blank3}}) - A_{\text{sample}} - A_{\text{blank2}}}{(A_{\text{blank1}} - A_{\text{blank3}})} \times 100$$

Data (n = 3) were collected in three independent experiments.

Table 12. Preparation of reaction mixtures for SOD1 assay.

	Sample	Blank 1	Blank 2	Blank 3
Reaction mixture	20 μ l		20 μ l	
Deionised water		20 μ l		20 μ l
WST solution	200 μ l	200 μ l	200 μ l	200 μ l
Enzyme solution	20 μ l	20 μ l		
Dilution buffer			20 μ l	20 μ l

5.6.11 *In vitro* glyoxalase activity assay

The glyoxalase activities of DJ-1 variants were determined following the procedure described in ref. 18. Proteins (2.5 nmol) in 100 mM sodium phosphate pH 6.8 were incubated with 5 mM of an aqueous solution of glyoxal at 42°C for 10 minutes. To quench the reaction, 0.1 % w/v 2,4-dinitrophenylhydrazine (DNPH) dissolved in 2 M HCl was diluted to 0.07% w/v with water and the solution was added to each reaction mixture. After 15 min incubation at room temperature, reactions were neutralized to 3.44% w/v NaOH and incubated for another 15 minutes at room temperature. Each reaction mixture was diluted with blank solution (reaction mixture without substrate and protein) and the absorbance at 570 nm ($\epsilon_{\text{glyoxal}, 570 \text{ nm}} = 2.571 \text{ mM}^{-1} \cdot \text{cm}^{-1}$) was measured. Each initial rate of reaction was measured by monitoring the decrease in substrate concentration. Initial rates of reaction were used to obtain K_{cat} values.

5.7 Cell-based assays

5.7.1 Cell culture, transfections, and transductions

Human neuroblastoma SH-SY5Y and DJ-1-null mouse embryonic fibroblasts (MEF *DJ-1*^{-/-}) cells (a kind gift from Dr. Huaibin Cai, National Institute on Aging, NIH, Bethesda, USA) were grown in DMEM (Gibco) supplemented with 10% v/v foetal calf serum (Sigma), streptomycin (100 units/ml; Gibco), penicillin (100 units/ml; Gibco) and non-essential amino acids (Gibco).

Cells were transiently transfected with DJ-1 constructs using Lipofectamine 2000 (Life Technologies) or xtremeGENE HP (Roche) using the manufacturer's procedure. Plasmid DNA (2.5 µg per 10 cm² well area) were incubated with the transfection reagent (3 µl per µg of DNA) at room temperature for 30 minutes. The transfection mixtures were then applied dropwise to each well with at least 70% cell confluency. Treated cells were incubated for at least 4 hours prior to replacement of media. Cells were assayed at least 24 hours post-transfection. The same protocol was also used for stable transfection except that stably transfected cells were selected with 100 µg/ml zeocin (Invitrogen) and subcultured for at least three weeks.

Prior to transduction, cells were grown overnight to 70% confluency. Cells were then treated with 10 µM DJ-1 protein constructs with an N-terminal tat domain for at least 2 hours at 37°C before assays were performed. Proteins were buffer exchanged into PBS and filter sterilised using a 0.22 micron syringe filter prior to application to cells. Protein transduction was confirmed using western blot analysis.

5.7.2 Cell viability assays

Cells were seeded in 96-well plates at 1×10^4 and incubated for at least 24 hours. Cells were incubated with 10 µM tat-fused proteins in PBS for 2 hours to allow transduction and then treated with 2 mM of an aqueous solution of glyoxal for 18 hours to induce

cytotoxicity (Lee *et al.*, 2012). Cell viability was measured using a PrestoBlue assay (Invitrogen).

5.7.3 Immunoblotting

Cells were lysed by adding 100 μ l of 1X SDS-PAGE sample buffer (Sigma) into each well. Lysates were transferred to a microfuge tube, sonicated and heated at 95°C for 5 minutes. Proteins were electrophoresed using SDS-PAGE and transferred onto a nitrocellulose membrane (GE Healthcare) by tank electroblotting using 1X Transfer Buffer. Each membrane was blocked with 5% w/v skimmed milk dissolved in TBS-T (Tris-buffered saline with 0.1% v/v Tween-20) for an hour and subsequently incubated with the appropriate primary antibody against DJ-1 (1 μ g/ml; Enzo Life Sciences), penta-His (1/4000 dilution; Qiagen), β -actin (1/2000 dilution; Oncogene), or CML (1 μ g/ml ; R&D systems) prepared in 3% w/v BSA in TBS-T solution for an hour. Each membrane was washed twice with TBS-T and incubated with anti-mouse IgG antibody with horseradish peroxidase (1/8000 dilution; Sigma). Membranes were developed using an enhanced chemiluminescence kit (Thermo Scientific).

5.7.4 Immunofluorescence

Cells were washed once with PBS and fixed with 4% v/v formaldehyde in PBS for 20 minutes at room temperature. Cells were then washed thrice with PBS-T. Cellular permeabilization was achieved by incubating the cells in ice cold methanol for 30 minutes and then washed thrice with PBS-T. 5% w/v BSA in PBS-T was used to block each well for 15 minutes at room temperature. Cells were then incubated with the primary antibody against human DJ-1 (1 μ g/ml; Enzo Life Sciences) for an hour followed by incubation with anti-mouse IgG antibody conjugated with Alexa Fluor 488 (Life Technologies) for another hour. To-Pro 3 (Life Technologies) was used to stain the nucleus. Micrographs were obtained using a Leica TCS SP2 confocal system (Leica Microsystems). Fluorescence was acquired using excitation wavelengths 488 nm

(Alexa Fluor 488) and 633 nm (To-Pro-3) and emission bandwidths 500-550 nm (Alexa Fluor 488) and 650-720 nm (To-Pro-3).

5.7.5 Measurement of intracellular superoxide levels and SOD1 activity

SH-SY5Y cells (1×10^5) were grown in 12-well plates for 48 hours. To induce increase the intracellular superoxide levels, cells were treated with 10 μ M menadione dissolved in serum free media for 30 minutes. Cells were stained with 20 μ M dihydroethidium (Life Technologies) for 10 minutes and analyzed using a FACScalibur flow cytometer.

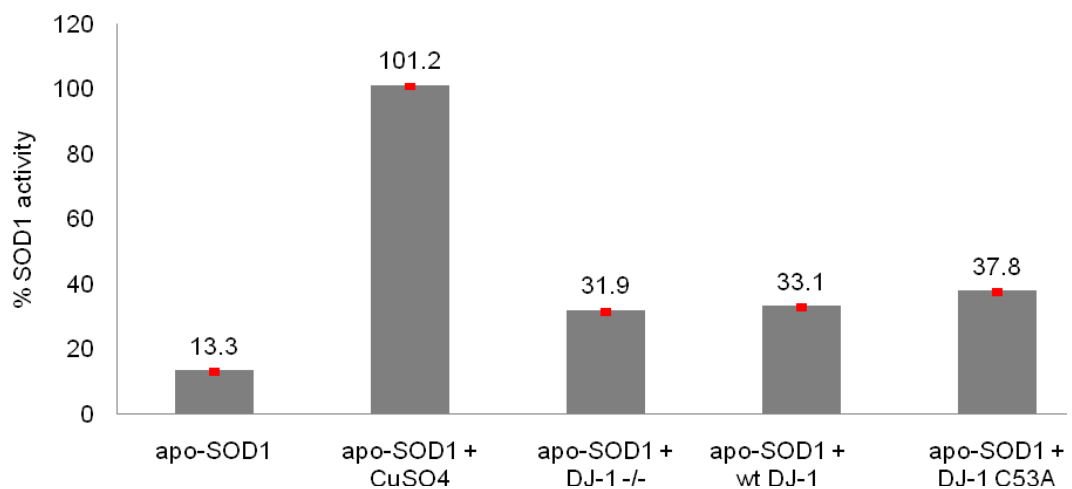
For intracellular SOD1 activity, cells were grown and treated with menadione as described above. Cytosolic extracts were prepared by lysing cells with PBS containing 1% (v/v) Triton-X-100 and 0.5 mM EDTA followed by centrifugation at 10 000 x g to remove cellular debris. SOD1 was differentiated from SOD2 by adding 800 μ l of chilled chloroform/ethanol [37.5/62.5 (v/v)] to 500 μ l of cytosolic extract and then separating the two layers by centrifuging at 2500 x g for 10 minutes. The upper aqueous layer was assayed for SOD1 activity using an SOD assay kit (Sigma).

5.7.6 Statistical analysis

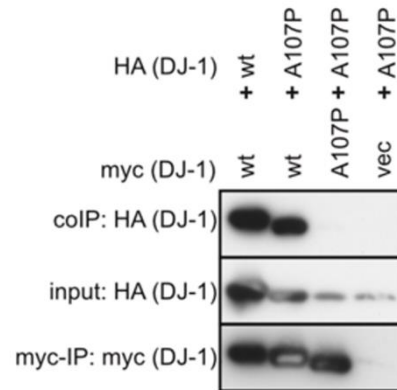
Experiments were performed at least twice independently. Statistical computations were performed using GraphPad QuickCalcs (<http://www.graphpad.com/quickcalcs/>) using continuous data analysis with unpaired t-test to compare difference between two means of independent samples. The significance limit was set to $p < 0.001$.

Appendices

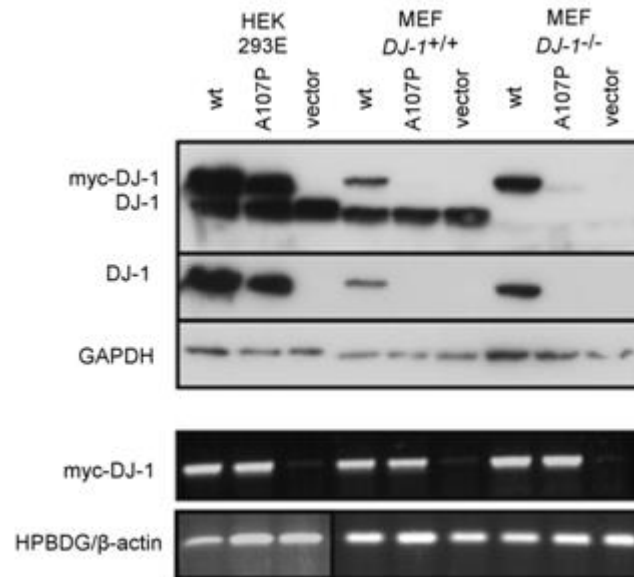
Appendix 1. *Ex vivo* SOD1 activation assay of DJ-1 ectopically expressed in MEF *DJ-1*^{-/-} cells. DJ-1 was ectopically expressed in MEF *DJ-1*^{-/-} cells and then isolated by immunoprecipitation using anti-DJ-1 antibody bound to Dynabeads. Apo-SOD1 was incubated with immunoprecipitated DJ-1 overnight at 4°C prior to measuring the SOD1 activity using an assay kit (Sigma). SOD1 activity was measured as percent inhibition rate of WST-1 conversion to WST-1 formazan by the substrate superoxide. Error bars (red) represent SEM from data, n = 3. This experiment was performed by Dr. Benny Bjorkblom (Stavanger University Hospital) under the supervision of Prof. Simon Moller (St. John's University and Stavanger University Hospital).



Appendix 2. DJ-1^{A107P} is not capable of homodimerisation but forms heterodimers with wild-type DJ-1. HEK 293E cells were transiently transfected with pCMV-myc-DJ-1 and pCMV-HA-DJ-1 mutants. Myc-tagged DJ-1 proteins were isolated using anti-myc agarose beads. Co-immunoprecipitated HA-tagged DJ-1 was detected using western blot analysis. This experiment was performed by Emmy Rannikko (University of Tuebingen) under the supervision of Prof. Philipp Kahle (Univeristy of Tuebingen).



Appendix 3. DJ-1^{A107P} has reduced protein steady state levels in HEK 293E and MEF cells. Upper panel: HEK 293E, MEF *DJ-1*^{+/+}, MEF *DJ-1*^{-/-} were transfected with pCMV-myc-DJ-1 or empty vector. Ectopically expressed DJ-1 proteins were detected by western blot analysis using DJ-1 and myc specific antibodies. GAPDH was immunodetected as a loading control. Lower panel: RT-PCR using primers specific for human *DJ-1* was performed to show equal mRNA expression levels. *β-actin* and *HPBDG* serve as controls for equal sample loading. This experiment was performed by Emmy Rannikko (University of Tuebingen) under the supervision of Prof. Philipp Kahle (University of Tuebingen).



Appendix 4. Published materials arising from this work

(page left blank for copy of publication)

References

- Abou-Sleiman, P. M., Healy, D. G., Quinn, N., Lees, A. J., and Wood, N. W. (2003) The role of pathogenic DJ-1 mutations in Parkinson's disease, *Ann Neurol* 54, 283-286.
- Afonine, P. V., Grosse-Kunstleve, R. W., Echols, N., Headd, J. J., Moriarty, N. W., Mustyakimov, M., Terwilliger, T. C., Urzhumtsev, A., Zwart, P. H., and Adams, P. D. (2012) Towards automated crystallographic structure refinement with phenix.refine, *Acta Crystallogr D Biol Crystallogr* 68, 352-367.
- Aleksandrovskii, Y. A. (1992) Antithrombin III, C1 inhibitor, methylglyoxal, and polymorphonuclear leukocytes in the development of vascular complications in diabetes mellitus, *Thromb Res* 67, 179-189.
- Aleyasin, H., Rousseaux, M. W., Marcogliese, P. C., Hewitt, S. J., Irrcher, I., Joselin, A. P., Parsanejad, M., Kim, R. H., Rizzu, P., Callaghan, S. M., Slack, R. S., Mak, T. W., and Park, D. S. (2010) DJ-1 protects the nigrostriatal axis from the neurotoxin MPTP by modulation of the AKT pathway, *Proc Natl Acad Sci U S A* 107, 3186-3191.
- Andres-Mateos, E., Perier, C., Zhang, L., Blanchard-Fillion, B., Greco, T. M., Thomas, B., Ko, H. S., Sasaki, M., Ischiropoulos, H., Przedborski, S., Dawson, T. M., and Dawson, V. L. (2007) DJ-1 gene deletion reveals that DJ-1 is an atypical peroxiredoxin-like peroxidase, *Proc Natl Acad Sci U S A* 104, 14807-14812.
- Annesi, G., Savettieri, G., Pugliese, P., D'Amelio, M., Tarantino, P., Ragonese, P., La Bella, V., Piccoli, T., Civitelli, D., Annesi, F., Fierro, B., Piccoli, F., Arabia, G., Caracciolo, M., Ciro Candiano, I. C., and Quattrone, A. (2005) DJ-1 mutations and parkinsonism-dementia-amyotrophic lateral sclerosis complex, *Ann Neurol* 58, 803-807.
- Arciello, M., Rotilio, G., and Rossi, L. (2005) Copper-dependent toxicity in SH-SY5Y neuroblastoma cells involves mitochondrial damage, *Biochem Biophys Res Commun* 327, 454-459.
- Assero, G., Lupo, G., Anfuso, C. D., Ragusa, N., and Alberghina, M. (2001) High glucose and advanced glycation end products induce phospholipid hydrolysis and phospholipid enzyme inhibition in bovine retinal pericytes, *Biochim Biophys Acta* 1533, 128-140.
- Banci, L., Bertini, I., Cantini, F., Felli, I. C., Gonnelli, L., Hadjiliadis, N., Pierattelli, R., Rosato, A., and Voulgaris, P. (2006) The Atx1-Ccc2 complex is a metal-mediated protein-protein interaction, *Nat Chem Biol* 2, 367-368.
- Batas, B., Jones, H. R., and Chaudhuri, J. B. (1997) Studies of the hydrodynamic volume changes that occur during refolding of lysozyme using size-exclusion chromatography, *J Chromatogr A* 766, 109-119.
- Batelli, S., Albani, D., Rametta, R., Polito, L., Prato, F., Pesaresi, M., Negro, A., and Forloni, G. (2008) DJ-1 modulates alpha-synuclein aggregation state in a cellular model of oxidative stress: relevance for Parkinson's disease and involvement of HSP70, *PLoS One* 3, e1884.

- Bence, N. F., Sampat, R. M., and Kopito, R. R. (2001) Impairment of the ubiquitin-proteasome system by protein aggregation, *Science* 292, 1552-1555.
- Bendor, J. T., Logan, T. P., and Edwards, R. H. (2013) The function of alpha-synuclein, *Neuron* 79, 1044-1066.
- Benesch, J. L., Ruotolo, B. T., Simmons, D. A., and Robinson, C. V. (2007) Protein complexes in the gas phase: technology for structural genomics and proteomics, *Chem Rev* 107, 3544-3567.
- Bento, C. F., Marques, F., Fernandes, R., and Pereira, P. (2010) Methylglyoxal alters the function and stability of critical components of the protein quality control, *PLoS One* 5, e13007.
- Bjorkblom, B., Adilbayeva, A., Maple-Grodem, J., Piston, D., Okvist, M., Xu, X. M., Brede, C., Larsen, J. P., and Moller, S. G. (2013) Parkinson disease protein DJ-1 binds metals and protects against metal-induced cytotoxicity, *J Biol Chem* 288, 22809-22820.
- Blackinton, J., Ahmad, R., Miller, D. W., van der Brug, M. P., Canet-Aviles, R. M., Hague, S. M., Kaleem, M., and Cookson, M. R. (2005) Effects of DJ-1 mutations and polymorphisms on protein stability and subcellular localization, *Brain Res Mol Brain Res* 134, 76-83.
- Boal, A. K., and Rosenzweig, A. C. (2009) Structural biology of copper trafficking, *Chem Rev* 109, 4760-4779.
- Bonifati, V., Rizzu, P., van Baren, M. J., Schaap, O., Breedveld, G. J., Krieger, E., Dekker, M. C., Squitieri, F., Ibanez, P., Joosse, M., van Dongen, J. W., Vanacore, N., van Swieten, J. C., Brice, A., Meco, G., van Duijn, C. M., Oostra, B. A., and Heutink, P. (2003) Mutations in the DJ-1 gene associated with autosomal recessive early-onset parkinsonism, *Science* 299, 256-259.
- Breitaud, S., Allen, C., Ingham, P. W., and Bandmann, O. (2007) p53-dependent neuronal cell death in a DJ-1-deficient zebrafish model of Parkinson's disease, *J Neurochem* 100, 1626-1635.
- Bryan, P., Pantoliano, M. W., Quill, S. G., Hsiao, H. Y., and Poulos, T. (1986) Site-directed mutagenesis and the role of the oxyanion hole in subtilisin, *Proc Natl Acad Sci U S A* 83, 3743-3745.
- Buller, A. R., and Townsend, C. A. (2013) Intrinsic evolutionary constraints on protease structure, enzyme acylation, and the identity of the catalytic triad, *Proc Natl Acad Sci U S A* 110, E653-661.
- Burre, J., Sharma, M., Tsetsenis, T., Buchman, V., Etherton, M. R., and Sudhof, T. C. (2010) Alpha-synuclein promotes SNARE-complex assembly in vivo and in vitro, *Science* 329, 1663-1667.
- Burre, J., Vivona, S., Diao, J., Sharma, M., Brunger, A. T., and Sudhof, T. C. (2013) Properties of native brain alpha-synuclein, *Nature* 498, E4-6; discussion E6-7.

- Bus, J. S., and Gibson, J. E. (1984) Paraquat: model for oxidant-initiated toxicity, *Environ Health Perspect* 55, 37-46.
- Bryan, P., Pantoliano, M. W., Quill, S. G., Hsiao, H. Y., and Poulos, T. (1986) Site-directed mutagenesis and the role of the oxyanion hole in subtilisin, *Proc Natl Acad Sci U S A* 83, 3743-3745.
- Cameron, A. D., Ridderstrom, M., Olin, B., and Mannervik, B. (1999) Crystal structure of human glyoxalase II and its complex with a glutathione thiolester substrate analogue, *Structure* 7, 1067-1078.
- Canet-Aviles, R. M., Wilson, M. A., Miller, D. W., Ahmad, R., McLendon, C., Bandyopadhyay, S., Baptista, M. J., Ringe, D., Petsko, G. A., and Cookson, M. R. (2004) The Parkinson's disease protein DJ-1 is neuroprotective due to cysteine-sulfinic acid-driven mitochondrial localization, *Proc Natl Acad Sci U S A* 101, 9103-9108.
- Carlsson, A., Lindqvist, M., and Magnusson, T. (1957) 3,4-Dihydroxyphenylalanine and 5-hydroxytryptophan as reserpine antagonists, *Nature* 180, 1200.
- Casazza, J. P., Felver, M. E., and Veech, R. L. (1984) The metabolism of acetone in rat, *J Biol Chem* 259, 231-236.
- Changela, A., Chen, K., Xue, Y., Holschen, J., Outten, C. E., O'Halloran, T. V., and Mondragon, A. (2003) Molecular basis of metal-ion selectivity and zeptomolar sensitivity by CueR, *Science* 301, 1383-1387.
- Chen, J., Li, L., and Chin, L. S. (2010) Parkinson disease protein DJ-1 converts from a zymogen to a protease by carboxyl-terminal cleavage, *Hum Mol Genet* 19, 2395-2408.
- Choi, J., Sullards, M. C., Olzmann, J. A., Rees, H. D., Weintraub, S. T., Bostwick, D. E., Gearing, M., Levey, A. I., Chin, L. S., and Li, L. (2006) Oxidative damage of DJ-1 is linked to sporadic Parkinson and Alzheimer diseases, *J Biol Chem* 281, 10816-10824.
- Ciriolo, M. R., Desideri, A., Paci, M., and Rotilio, G. (1990) Reconstitution of Cu,Zn-superoxide dismutase by the Cu(I)-glutathione complex, *J Biol Chem* 265, 11030-11034.
- Clark, L. N., Afridi, S., Mejia-Santana, H., Harris, J., Louis, E. D., Cote, L. J., Andrews, H., Singleton, A., Wavrant De-Vrieze, F., Hardy, J., Mayeux, R., Fahn, S., Waters, C., Ford, B., Frucht, S., Ottman, R., and Marder, K. (2004) Analysis of an early-onset Parkinson's disease cohort for DJ-1 mutations, *Mov Disord* 19, 796-800.
- Cleeter, M. W., Cooper, J. M., and Schapira, A. H. (1992) Irreversible inhibition of mitochondrial complex I by 1-methyl-4-phenylpyridinium: evidence for free radical involvement, *J Neurochem* 58, 786-789.
- Clements, C. M., McNally, R. S., Conti, B. J., Mak, T. W., and Ting, J. P. (2006) DJ-1, a cancer- and Parkinson's disease-associated protein, stabilizes the antioxidant transcriptional master regulator Nrf2, *Proc Natl Acad Sci U S A* 103, 15091-15096.

Cobine, P. A., George, G. N., Winzor, D. J., Harrison, M. D., Moghaddas, S., and Dameron, C. T. (2000) Stoichiometry of complex formation between Copper(I) and the N-terminal domain of the Menkes protein, *Biochemistry* 39, 6857-6863.

Cohen, G., and Heikkila, R. E. (1974) The generation of hydrogen peroxide, superoxide radical, and hydroxyl radical by 6-hydroxydopamine, dialuric acid, and related cytotoxic agents, *J Biol Chem* 249, 2447-2452.

Conway, K. A., Harper, J. D., and Lansbury, P. T. (1998) Accelerated in vitro fibril formation by a mutant alpha-synuclein linked to early-onset Parkinson disease, *Nat Med* 4, 1318-1320.

Corti, O., Lesage, S., and Brice, A. (2011) What genetics tells us about the causes and mechanisms of Parkinson's disease, *Physiol Rev* 91, 1161-1218.

Critchley, M. (1955) *James Parkinson (1755-1824): a bicentenary volume of papers dealing with Parkinson's Disease, incorporating the original 'Essay on the Shaking Palsy'*. Macmillan, London.

Culotta, V. C., Klomp, L. W., Strain, J., Casareno, R. L., Krems, B., and Gitlin, J. D. (1997) The copper chaperone for superoxide dismutase, *J Biol Chem* 272, 23469-23472.

Dauer, W., and Przedborski, S. (2003) Parkinson's disease: mechanisms and models, *Neuron* 39, 889-909.

Davis, A. V., and O'Halloran, T. V. (2008) A place for thioether chemistry in cellular copper ion recognition and trafficking, *Nat Chem Biol* 4, 148-151.

Dekker, M. C., Eshuis, S. A., Maguire, R. P., Veenma-van der Duijn, L., Pruijm, J., Snijders, P. J., Oostra, B. A., van Duijn, C. M., and Leenders, K. L. (2004) PET neuroimaging and mutations in the DJ-1 gene, *J Neural Transm* 111, 1575-1581.

Delaglio, F., Grzesiek, S., Vuister, G. W., Zhu, G., Pfeifer, J., and Bax, A. (1995) NMRPipe: a multidimensional spectral processing system based on UNIX pipes, *J Biomol NMR* 6, 277-293.

Delano, W.L., 2002. The PyMol molecular graphics system. <http://www.pymol.org/>

Dexter, D. T., Carter, C. J., Wells, F. R., Javoy-Agid, F., Agid, Y., Lees, A., Jenner, P., and Marsden, C. D. (1989) Basal lipid peroxidation in substantia nigra is increased in Parkinson's disease, *J Neurochem* 52, 381-389.

Djarmati, A., Hedrich, K., Svetel, M., Schafer, N., Juric, V., Vukosavic, S., Hering, R., Riess, O., Romac, S., Klein, C., and Kostic, V. (2004) Detection of Parkin (PARK2) and DJ1 (PARK7) mutations in early-onset Parkinson disease: Parkin mutation frequency depends on ethnic origin of patients, *Hum Mutat* 23, 525.

Domico, L. M., Zeevalk, G. D., Bernard, L. P., and Cooper, K. R. (2006) Acute neurotoxic effects of mancozeb and maneb in mesencephalic neuronal cultures are associated with mitochondrial dysfunction, *Neurotoxicology* 27, 816-825.

Dorsey, E. R., Constantinescu, R., Thompson, J. P., Biglan, K. M., Holloway, R. G., Kieburtz, K., Marshall, F. J., Ravina, B. M., Schifitto, G., Siderowf, A., and Tanner, C. M. (2007) Projected number of people with Parkinson disease in the most populous nations, 2005 through 2030, *Neurology* 68, 384-386.

Emsley, P., and Cowtan, K. (2004) Coot: model-building tools for molecular graphics, *Acta Crystallogr D Biol Crystallogr* 60, 2126-2132.

Eriksen, J. L., Wszolek, Z., and Petrucelli, L. (2005a) Molecular pathogenesis of Parkinson disease, *Arch Neurol* 62, 353-357.

Eriksen, J. L., Przedborski, S., and Petrucelli, L. (2005b) Gene dosage and pathogenesis of Parkinson's disease, *Trends Mol Med* 11, 91-96.

Fan, J., Ren, H., Jia, N., Fei, E., Zhou, T., Jiang, P., Wu, M., and Wang, G. (2008) DJ-1 decreases Bax expression through repressing p53 transcriptional activity, *J Biol Chem* 283, 4022-4030.

Faucheux, B. A., Martin, M. E., Beaumont, C., Hauw, J. J., Agid, Y., and Hirsch, E. C. (2003) Neuromelanin associated redox-active iron is increased in the substantia nigra of patients with Parkinson's disease, *J Neurochem* 86, 1142-1148.

Fearnley, J. M., and Lees, A. J. (1991) Ageing and Parkinson's disease: substantia nigra regional selectivity, *Brain* 114 (Pt 5), 2283-2301.

Ferraroni, M., Rypniewski, W., Wilson, K. S., Viezzoli, M. S., Banci, L., Bertini, I., and Mangani, S. (1999) The crystal structure of the monomeric human SOD mutant F50E/G51E/E133Q at atomic resolution. The enzyme mechanism revisited, *J Mol Biol* 288, 413-426.

Fonck, C., and Baudry, M. (2001) Toxic effects of MPP(+) and MPTP in PC12 cells independent of reactive oxygen species formation, *Brain Res* 905, 199-206.

Fukushima, T., Yamada, K., Isobe, A., Shiwaku, K., and Yamane, Y. (1993) Mechanism of cytotoxicity of paraquat. I. NADH oxidation and paraquat radical formation via complex I, *Exp Toxicol Pathol* 45, 345-349.

Gan, L., Johnson, D. A., and Johnson, J. A. (2010) Keap1-Nrf2 activation in the presence and absence of DJ-1, *Eur J Neurosci* 31, 967-977.

Ghazavi, F., Fazlali, Z., Banihosseini, S. S., Hosseini, S. R., Kazemi, M. H., Shojaee, S., Parsa, K., Sadeghi, H., Sina, F., Rohani, M., Shahidi, G. A., Ghaemi, N., Ronaghi, M., and Elahi, E. (2011) PRKN, DJ-1, and PINK1 screening identifies novel splice site mutation in PRKN and two novel DJ-1 mutations, *Mov Disord* 26, 80-89.

Gibb, W. R., and Lees, A. J. (1988) The relevance of the Lewy body to the pathogenesis of idiopathic Parkinson's disease, *J Neurol Neurosurg Psychiatry* 51, 745-752.

Giroto, S., Sturlese, M., Bellanda, M., Tessari, I., Cappellini, R., Bisaglia, M., Bubacco, L., and Mammi, S. (2012) Dopamine-derived quinones affect the structure of the redox

sensor DJ-1 through modifications at Cys-106 and Cys-53, *J Biol Chem* 287, 18738-18749.

Glomb, M. A., and Monnier, V. M. (1995) Mechanism of protein modification by glyoxal and glycolaldehyde, reactive intermediates of the Maillard reaction, *J Biol Chem* 270, 10017-10026.

Gorell, J. M., Johnson, C. C., Rybicki, B. A., Peterson, E. L., Kortsha, G. X., Brown, G. G., and Richardson, R. J. (1997) Occupational exposures to metals as risk factors for Parkinson's disease, *Neurology* 48, 650-658.

Gorner, K., Holtorf, E., Odoy, S., Nuscher, B., Yamamoto, A., Regula, J. T., Beyer, K., Haass, C., and Kahle, P. J. (2004) Differential effects of Parkinson's disease-associated mutations on stability and folding of DJ-1, *J Biol Chem* 279, 6943-6951.

Gorner, K., Holtorf, E., Waak, J., Pham, T. T., Vogt-Weisenhorn, D. M., Wurst, W., Haass, C., and Kahle, P. J. (2007) Structural determinants of the C-terminal helix-kink-helix motif essential for protein stability and survival promoting activity of DJ-1, *J Biol Chem* 282, 13680-13691.

Haass, C., and Kahle, P. J. (2001) Neuroscience. Parkin and its substrates, *Science* 293, 224-225.

Hague, S., Rogaeva, E., Hernandez, D., Gulick, C., Singleton, A., Hanson, M., Johnson, J., Weiser, R., Gallardo, M., Ravina, B., Gwinn-Hardy, K., Crawley, A., St George-Hyslop, P. H., Lang, A. E., Heutink, P., Bonifati, V., and Hardy, J. (2003) Early-onset Parkinson's disease caused by a compound heterozygous DJ-1 mutation, *Ann Neurol* 54, 271-274.

Halliwell, B. (2006) Oxidative stress and neurodegeneration: where are we now?, *J Neurochem* 97, 1634-1658.

Halliwell, B., and Gutteridge, J. M. (1990) Role of free radicals and catalytic metal ions in human disease: an overview, *Methods Enzymol* 186, 1-85.

Hardy, J., Cai, H., Cookson, M. R., Gwinn-Hardy, K., and Singleton, A. (2006) Genetics of Parkinson's disease and parkinsonism, *Ann Neurol* 60, 389-398.

Hartinger, C. G., Ang, W. H., Casini, A., Messori, L., Keppler, B. K., and Dyson, P. J. (2007) Mass spectrometric analysis of ubiquitin-platinum interactions of leading anticancer drugs: MALDI versus ESI, *Journal of Anal At Spectrom* 22, 960-967.

Hering, R., Strauss, K. M., Tao, X., Bauer, A., Voitalla, D., Mietz, E. M., Petrovic, S., Bauer, P., Schaible, W., Muller, T., Schols, L., Klein, C., Berg, D., Meyer, P. T., Schulz, J. B., Wollnik, B., Tong, L., Kruger, R., and Riess, O. (2004) Novel homozygous p.E64D mutation in DJ1 in early onset Parkinson disease (PARK7), *Hum Mutat* 24, 321-329.

Herrera, F. E., Zucchelli, S., Jezierska, A., Lavina, Z. S., Gustincich, S., and Carloni, P. (2007) On the oligomeric state of DJ-1 protein and its mutants associated with

Parkinson Disease. A combined computational and in vitro study, *J Biol Chem* 282, 24905-24914.

Hirai, K., Ikeda, K., and Wang, G. Y. (1992) Paraquat damage of rat liver mitochondria by superoxide production depends on extramitochondrial NADH, *Toxicology* 72, 1-16.

Honbou, K., Suzuki, N. N., Horiuchi, M., Niki, T., Taira, T., Ariga, H., and Inagaki, F. (2003) The crystal structure of DJ-1, a protein related to male fertility and Parkinson's disease, *J Biol Chem* 278, 31380-31384.

Huai, Q., Sun, Y., Wang, H., Chin, L. S., Li, L., Robinson, H., and Ke, H. (2003) Crystal structure of DJ-1/RS and implication on familial Parkinson's disease, *FEBS Lett* 549, 171-175.

Hulleman, J. D., Mirzaei, H., Guigard, E., Taylor, K. L., Ray, S. S., Kay, C. M., Regnier, F. E., and Rochet, J. C. (2007) Destabilization of DJ-1 by familial substitution and oxidative modifications: implications for Parkinson's disease, *Biochemistry* 46, 5776-5789.

Iguchi, M., Kujuro, Y., Okatsu, K., Koyano, F., Kosako, H., Kimura, M., Suzuki, N., Uchiyama, S., Tanaka, K., and Matsuda, N. (2013) Parkin-catalyzed Ubiquitin-Ester Transfer Is Triggered by PINK1-dependent Phosphorylation, *J Biol Chem* 288, 22019-22032.

Im, J. Y., Lee, K. W., Woo, J. M., Junn, E., and Mouradian, M. M. (2012) DJ-1 induces thioredoxin 1 expression through the Nrf2 pathway, *Hum Mol Genet* 21, 3013-3024.

Ishikawa, S., Taira, T., Takahashi-Niki, K., Niki, T., Ariga, H., and Iguchi-Ariga, S. M. (2010) Human DJ-1-specific transcriptional activation of tyrosine hydroxylase gene, *J Biol Chem* 285, 39718-39731.

Ito, G., Ariga, H., Nakagawa, Y., and Iwatsubo, T. (2006) Roles of distinct cysteine residues in S-nitrosylation and dimerization of DJ-1, *Biochem Biophys Res Commun* 339, 667-672.

Jellinger, K. A. (1991) Pathology of Parkinson's disease. Changes other than the nigrostriatal pathway, *Mol Chem Neuropathol* 14, 153-197.

Jellinger, K. A. (2001) The pathology of Parkinson's disease, *Adv Neurol* 86, 55-72.

Jenner, P., and Olanow, C. W. (1996) Oxidative stress and the pathogenesis of Parkinson's disease, *Neurology* 47, S161-170.

Johnstone, M., Gearing, A. J., and Miller, K. M. (1999) A central role for astrocytes in the inflammatory response to beta-amyloid; chemokines, cytokines and reactive oxygen species are produced, *J Neuroimmunol* 93, 182-193.

Kabsch, W. (2010) Xds, *Acta Crystallogr D Biol Crystallogr* 66, 125-132.

- Kato, I., Maita, H., Takahashi-Niki, K., Saito, Y., Noguchi, N., Iguchi-Ariga, S. M., and Ariga, H. (2013) Oxidized DJ-1 inhibits p53 by sequestering p53 from promoters in a DNA-binding affinity-dependent manner, *Mol Cell Biol* 33, 340-359.
- Kim, R. H., Smith, P. D., Aleyasin, H., Hayley, S., Mount, M. P., Pownall, S., Wakeham, A., You-Ten, A. J., Kalia, S. K., Horne, P., Westaway, D., Lozano, A. M., Anisman, H., Park, D. S., and Mak, T. W. (2005) Hypersensitivity of DJ-1-deficient mice to 1-methyl-4-phenyl-1,2,3,6-tetrahydropyridine (MPTP) and oxidative stress, *Proc Natl Acad Sci U S A* 102, 5215-5220.
- Knobbe, C. B., Revett, T. J., Bai, Y., Chow, V., Jeon, A. H., Bohm, C., Ehsani, S., Kislinger, T., Mount, H. T., Mak, T. W., St George-Hyslop, P., and Schmitt-Ulms, G. (2011) Choice of biological source material supersedes oxidative stress in its influence on DJ-1 in vivo interactions with Hsp90, *J Proteome Res* 10, 4388-4404.
- Kohen, R., and Chevion, M. (1985) Involvement of iron and copper in biological damage that is induced by oxygen free radicals, *J Free Radic Biol Med* 1, 339-340.
- Kondapalli, C., Kazlauskaitė, A., Zhang, N., Woodroof, H. I., Campbell, D. G., Gourlay, R., Burchell, L., Walden, H., Macartney, T. J., Deak, M., Knebel, A., Alessi, D. R., and Muqit, M. M. (2012) PINK1 is activated by mitochondrial membrane potential depolarization and stimulates Parkin E3 ligase activity by phosphorylating Serine 65, *Open Biol* 2, 120080.
- Kuntz, S., Kunz, C., and Rudloff, S. (2010) Carbonyl compounds methylglyoxal and glyoxal affect interleukin-8 secretion in intestinal cells by superoxide anion generation and activation of MAPK p38, *Mol Nutr Food Res* 54, 1458-1467.
- Kussmaul, L., and Hirst, J. (2006) The mechanism of superoxide production by NADH:ubiquinone oxidoreductase (complex I) from bovine heart mitochondria, *Proc Natl Acad Sci U S A* 103, 7607-7612.
- Kwon, K., Choi, D., Hyun, J. K., Jung, H. S., Baek, K., and Park, C. (2013) Novel glyoxalases from *Arabidopsis thaliana*, *FEBS J* 280, 3328-3339.
- Lakshminarasimhan, M., Maldonado, M. T., Zhou, W., Fink, A. L., and Wilson, M. A. (2008) Structural impact of three Parkinsonism-associated missense mutations on human DJ-1, *Biochemistry* 47, 1381-1392.
- Lamb, A. L., Torres, A. S., O'Halloran, T. V., and Rosenzweig, A. C. (2001) Heterodimeric structure of superoxide dismutase in complex with its metallochaperone, *Nat Struct Biol* 8, 751-755.
- Lamb, A. L., Wernimont, A. K., Pufahl, R. A., Culotta, V. C., O'Halloran, T. V., and Rosenzweig, A. C. (1999) Crystal structure of the copper chaperone for superoxide dismutase, *Nat Struct Biol* 6, 724-729.

- Langston, J. W., Irwin, I., Langston, E. B., and Forno, L. S. (1984) 1-Methyl-4-phenylpyridinium ion (MPP⁺): identification of a metabolite of MPTP, a toxin selective to the substantia nigra, *Neurosci Lett* 48, 87-92.
- Larin, D., Mekios, C., Das, K., Ross, B., Yang, A. S., and Gilliam, T. C. (1999) Characterization of the interaction between the Wilson and Menkes disease proteins and the cytoplasmic copper chaperone, HAH1p, *J Biol Chem* 274, 28497-28504.
- Lee, J. Y., Song, J., Kwon, K., Jang, S., Kim, C., Baek, K., Kim, J., and Park, C. (2012) Human DJ-1 and its homologs are novel glyoxalases, *Hum Mol Genet* 21, 3215-3225.
- Lee, L. C., Lee, Y. L., Leu, R. J., and Shaw, J. F. (2006) Functional role of catalytic triad and oxyanion hole-forming residues on enzyme activity of Escherichia coli thioesterase I/protease I/phospholipase L1, *Biochem J* 397, 69-76.
- Lee, S. J., Kim, S. J., Kim, I. K., Ko, J., Jeong, C. S., Kim, G. H., Park, C., Kang, S. O., Suh, P. G., Lee, H. S., and Cha, S. S. (2003) Crystal structures of human DJ-1 and Escherichia coli Hsp31, which share an evolutionarily conserved domain, *J Biol Chem* 278, 44552-44559.
- Leitch, J. M., Jensen, L. T., Bouldin, S. D., Outten, C. E., Hart, P. J., and Culotta, V. C. (2009) Activation of Cu,Zn-superoxide dismutase in the absence of oxygen and the copper chaperone CCS, *J Biol Chem* 284, 21863-21871.
- Lesage, S., and Brice, A. (2009) Parkinson's disease: from monogenic forms to genetic susceptibility factors, *Hum Mol Genet* 18, R48-59.
- Leslie A. G. W. (1992) *Joint CCP4 + ESF-EAMCB Newsletter on Protein Crystallography*, 26 .
- Lev, N., Barhum, Y., Ben-Zur, T., Melamed, E., Steiner, I., and Offen, D. (2013) Knocking out DJ-1 attenuates astrocytes neuroprotection against 6-hydroxydopamine toxicity, *J Mol Neurosci* 50, 542-550.
- Lev, N., Ickowicz, D., Barhum, Y., Lev, S., Melamed, E., and Offen, D. (2009) DJ-1 protects against dopamine toxicity, *J Neural Transm* 116, 151-160.
- Lewis, S. J., Caldwell, M. A., and Barker, R. A. (2003) Modern therapeutic approaches in Parkinson's disease, *Expert Rev Mol Med* 5, 1-20.
- Li, J., Ahvazi, B., Szittner, R., and Meighen, E. (2000) Mutation of the nucleophilic elbow of the Lux-specific thioesterase from *Vibrio harveyi*, *Biochem Biophys Res Commun* 275, 704-708.
- Lin, M. T., and Beal, M. F. (2006) Mitochondrial dysfunction and oxidative stress in neurodegenerative diseases, *Nature* 443, 787-795.
- Louis-Jeune, C., Andrade-Navarro, M. A., and Perez-Iratxeta, C. (2012) Prediction of protein secondary structure from circular dichroism using theoretically derived spectra, *Proteins* 80, 374-381.

- Lucking, C. B., Durr, A., Bonifati, V., Vaughan, J., De Michele, G., Gasser, T., Harhangi, B. S., Meco, G., Deneffe, P., Wood, N. W., Agid, Y., and Brice, A. (2000) Association between early-onset Parkinson's disease and mutations in the parkin gene, *N Engl J Med* 342, 1560-1567.
- Lyles, G. A., and Chalmers, J. (1992) The metabolism of aminoacetone to methylglyoxal by semicarbazide-sensitive amine oxidase in human umbilical artery, *Biochem Pharmacol* 43, 1409-1414.
- Malgieri, G., and Eliezer, D. (2008) Structural effects of Parkinson's disease linked DJ-1 mutations, *Protein Sci* 17, 855-868.
- Manning-Bog, A. B., McCormack, A. L., Li, J., Uversky, V. N., Fink, A. L., and Di Monte, D. A. (2002) The herbicide paraquat causes up-regulation and aggregation of alpha-synuclein in mice: paraquat and alpha-synuclein, *J Biol Chem* 277, 1641-1644.
- Marek, G. J., Vosmer, G., and Seiden, L. S. (1990) The effects of monoamine uptake inhibitors and methamphetamine on neostriatal 6-hydroxydopamine (6-OHDA) formation, short-term monoamine depletions and locomotor activity in the rat, *Brain Res* 516, 1-7.
- Mata, I. F., Wedemeyer, W. J., Farrer, M. J., Taylor, J. P., and Gallo, K. A. (2006) LRRK2 in Parkinson's disease: protein domains and functional insights, *Trends Neurosci* 29, 286-293.
- McCord, J. M., and Fridovich, I. (1969) Superoxide dismutase. An enzymic function for erythrocyte hemocuprein (hemocuprein), *J Biol Chem* 244, 6049-6055.
- McCormack, A. L., Thiruchelvam, M., Manning-Bog, A. B., Thiffault, C., Langston, J. W., Cory-Slechta, D. A., and Di Monte, D. A. (2002) Environmental risk factors and Parkinson's disease: selective degeneration of nigral dopaminergic neurons caused by the herbicide paraquat, *Neurobiol Dis* 10, 119-127.
- McCoy, A. J., Grosse-Kunstleve, R. W., Adams, P. D., Winn, M. D., Storoni, L. C., and Read, R. J. (2007) Phaser crystallographic software, *J Appl Crystallogr* 40, 658-674.
- Meco, G., Bonifati, V., Vanacore, N., and Fabrizio, E. (1994) Parkinsonism after chronic exposure to the fungicide maneb (manganese ethylene-bis-dithiocarbamate), *Scand J Work Environ Health* 20, 301-305.
- Menard, R., and Storer, A. C. (1992) Oxyanion hole interactions in serine and cysteine proteases, *Biol Chem Hoppe Seyler* 373, 393-400.
- Misra, K., Banerjee, A. B., Ray, S., and Ray, M. (1995) Glyoxalase III from *Escherichia coli*: a single novel enzyme for the conversion of methylglyoxal into D-lactate without reduced glutathione, *Biochem J* 305 (Pt 3), 999-1003.
- Mitsugi, H., Niki, T., Takahashi-Niki, K., Tanimura, K., Yoshizawa-Kumagaye, K., Tsunemi, M., Iguchi-Ariga, S. M., and Ariga, H. (2013) Identification of the recognition sequence and target proteins for DJ-1 protease, *FEBS Lett* 587, 2493-2499.

- Molgaard, A., Kauppinen, S., and Larsen, S. (2000) Rhamnogalacturonan acetyltransferase elucidates the structure and function of a new family of hydrolases, *Structure* 8, 373-383.
- Moore, R. Y., and Bloom, F. E. (1978) Central catecholamine neuron systems: anatomy and physiology of the dopamine systems, *Annu Rev Neurosci* 1, 129-169.
- Moore, D. J., Zhang, L., Dawson, T. M., and Dawson, V. L. (2003) A missense mutation (L166P) in DJ-1, linked to familial Parkinson's disease, confers reduced protein stability and impairs homo-oligomerization, *J Neurochem* 87, 1558-1567.
- Moore, D. J., Zhang, L., Troncoso, J., Lee, M. K., Hattori, N., Mizuno, Y., Dawson, T. M., and Dawson, V. L. (2005) Association of DJ-1 and parkin mediated by pathogenic DJ-1 mutations and oxidative stress, *Hum Mol Genet* 14, 71-84.
- Morgan, P. E., Dean, R. T., and Davies, M. J. (2002) Inactivation of cellular enzymes by carbonyls and protein-bound glycation/glycoxidation products, *Arch Biochem Biophys* 403, 259-269.
- Morimoto, R. I. (2008) Proteotoxic stress and inducible chaperone networks in neurodegenerative disease and aging, *Genes Dev* 22, 1427-1438.
- Morimoto, R. I., Driessen, A. J., Hegde, R. S., and Langer, T. (2011) The life of proteins: the good, the mostly good and the ugly, *Nat Struct Mol Biol* 18, 1-4.
- Munch, G., Westcott, B., Menini, T., and Gugliucci, A. (2012) Advanced glycation endproducts and their pathogenic roles in neurological disorders, *Amino Acids* 42, 1221-1236.
- Murshudov, G. N., Vagin, A. A., and Dodson, E. J. (1997) Refinement of macromolecular structures by the maximum-likelihood method, *Acta Crystallogr D Biol Crystallogr* 53, 240-255.
- Nagatsu, T., Levitt, M., and Udenfriend, S. (1964) Tyrosine Hydroxylase. The Initial Step in Norepinephrine Biosynthesis, *J Biol Chem* 239, 2910-2917.
- Nardini, M., and Dijkstra, B. W. (1999) Alpha/beta hydrolase fold enzymes: the family keeps growing, *Curr Opin Struct Biol* 9, 732-737.
- Narendra, D., Tanaka, A., Suen, D. F., and Youle, R. J. (2009) Parkin-induced mitophagy in the pathogenesis of Parkinson disease, *Autophagy* 5, 706-708.
- Niki, T., Takahashi-Niki, K., Taira, T., Iguchi-Arigo, S. M., and Ariga, H. (2003) DJBP: a novel DJ-1-binding protein, negatively regulates the androgen receptor by recruiting histone deacetylase complex, and DJ-1 antagonizes this inhibition by abrogation of this complex, *Mol Cancer Res* 1, 247-261.
- Nishinaga, H., Takahashi-Niki, K., Taira, T., Andreadis, A., Iguchi-Arigo, S. M., and Ariga, H. (2005) Expression profiles of genes in DJ-1-knockdown and L 166 P DJ-1 mutant cells, *Neurosci Lett* 390, 54-59.

Olivieri, G., Brack, C., Muller-Spahn, F., Stahelin, H. B., Herrmann, M., Renard, P., Brockhaus, M., and Hock, C. (2000) Mercury induces cell cytotoxicity and oxidative stress and increases beta-amyloid secretion and tau phosphorylation in SHSY5Y neuroblastoma cells, *J Neurochem* 74, 231-236.

Ollis, D. L., Cheah, E., Cygler, M., Dijkstra, B., Frolow, F., Franken, S. M., Harel, M., Remington, S. J., Silman, I., Schrag, J., and et al. (1992) The alpha/beta hydrolase fold, *Protein Eng* 5, 197-211.

Olzmann, J. A., Brown, K., Wilkinson, K. D., Rees, H. D., Huai, Q., Ke, H., Levey, A. I., Li, L., and Chin, L. S. (2004) Familial Parkinson's disease-associated L166P mutation disrupts DJ-1 protein folding and function, *J Biol Chem* 279, 8506-8515.

Olzmann, J. A., Bordelon, J. R., Muly, E. C., Rees, H. D., Levey, A. I., Li, L., and Chin, L. S. (2007) Selective enrichment of DJ-1 protein in primate striatal neuronal processes: implications for Parkinson's disease, *J Comp Neurol* 500, 585-599.

Ordentlich, A., Barak, D., Kronman, C., Ariel, N., Segall, Y., Velan, B., and Shafferman, A. (1998) Functional characteristics of the oxyanion hole in human acetylcholinesterase, *J Biol Chem* 273, 19509-19517.

Paik, S. R., Shin, H. J., Lee, J. H., Chang, C. S., and Kim, J. (1999) Copper(II)-induced self-oligomerization of alpha-synuclein, *Biochem J* 340 (Pt 3), 821-828.

Parker, W. D., Jr., Parks, J. K., and Swerdlow, R. H. (2008) Complex I deficiency in Parkinson's disease frontal cortex, *Brain Res* 1189, 215-218.

Pasinelli, P., Belford, M. E., Lennon, N., Bacskai, B. J., Hyman, B. T., Trotti, D., and Brown, R. H., Jr. (2004) Amyotrophic lateral sclerosis-associated SOD1 mutant proteins bind and aggregate with Bcl-2 in spinal cord mitochondria, *Neuron* 43, 19-30.

Pettersen, E. F., Goddard, T. D., Huang, C. C., Couch, G. S., Greenblatt, D. M., Meng, E. C., and Ferrin, T. E. (2004) UCSF Chimera--a visualization system for exploratory research and analysis, *J Comput Chem* 25, 1605-1612.

Perry, T. L., Godin, D. V., and Hansen, S. (1982) Parkinson's disease: a disorder due to nigral glutathione deficiency?, *Neurosci Lett* 33, 305-310.

Pezzoli, G., and Cereda, E. (2013) Exposure to pesticides or solvents and risk of Parkinson disease, *Neurology* 80, 2035-2041.

Phillips, S. A., and Thornalley, P. J. (1993) The formation of methylglyoxal from triose phosphates. Investigation using a specific assay for methylglyoxal, *Eur J Biochem* 212, 101-105.

Polymeropoulos, M. H., Lavedan, C., Leroy, E., Ide, S. E., Dehejia, A., Dutra, A., Pike, B., Root, H., Rubenstein, J., Boyer, R., Stenroos, E. S., Chandrasekharappa, S., Athanassiadou, A., Papapetropoulos, T., Johnson, W. G., Lazzarini, A. M., Duvoisin, R. C., Di Iorio, G., Golbe, L. I., and Nussbaum, R. L. (1997) Mutation in the alpha-synuclein gene identified in families with Parkinson's disease, *Science* 276, 2045-2047.

The PyMOL Molecular Graphics System, Version 1.5.0.4 Schrödinger, LLC.

Que, L. (2000) *Physical methods in bioinorganic chemistry : spectroscopy and magnetism*, University Science Books, Sausalito, CA.

Queisser, M. A., Yao, D., Geisler, S., Hammes, H. P., Lochnit, G., Schleicher, E. D., Brownlee, M., and Preissner, K. T. (2010) Hyperglycemia impairs proteasome function by methylglyoxal, *Diabetes* 59, 670-678.

Rae, T. D., Torres, A. S., Pufahl, R. A., and O'Halloran, T. V. (2001) Mechanism of Cu,Zn-superoxide dismutase activation by the human metallochaperone hCCS, *J Biol Chem* 276, 5166-5176.

Rae, T. D., Schmidt, P. J., Pufahl, R. A., Culotta, V. C., and O'Halloran, T. V. (1999) Undetectable intracellular free copper: the requirement of a copper chaperone for superoxide dismutase, *Science* 284, 805-808.

Rahman, A., Shahabuddin, and Hadi, S. M. (1990) Formation of strand breaks and interstrand cross-links in DNA by methylglyoxal, *J Biochem Toxicol* 5, 161-166.

Ralle, M., Lutsenko, S., and Blackburn, N. J. (2003) X-ray absorption spectroscopy of the copper chaperone HAH1 reveals a linear two-coordinate Cu(I) center capable of adduct formation with exogenous thiols and phosphines, *J Biol Chem* 278, 23163-23170.

Ralle, M., Lutsenko, S., and Blackburn, N. J. (2004) Copper transfer to the N-terminal domain of the Wilson disease protein (ATP7B): X-ray absorption spectroscopy of reconstituted and chaperone-loaded metal binding domains and their interaction with exogenous ligands, *J Inorg Biochem* 98, 765-774.

Ramasamy, R., Yan, S. F., and Schmidt, A. M. (2006) Methylglyoxal comes of AGE, *Cell* 124, 258-260.

Ramasamy, R., Vannucci, S. J., Yan, S. S., Herold, K., Yan, S. F., and Schmidt, A. M. (2005) Advanced glycation end products and RAGE: a common thread in aging, diabetes, neurodegeneration, and inflammation, *Glycobiology* 15, 16R-28R.

Ramirez, A., Heimbach, A., Grundemann, J., Stiller, B., Hampshire, D., Cid, L. P., Goebel, I., Mubaidin, A. F., Wriekat, A. L., Roeper, J., Al-Din, A., Hillmer, A. M., Karsak, M., Liss, B., Woods, C. G., Behrens, M. I., and Kubisch, C. (2006) Hereditary parkinsonism with dementia is caused by mutations in ATP13A2, encoding a lysosomal type 5 P-type ATPase, *Nat Genet* 38, 1184-1191.

Ramonet, D., Podhajska, A., Stafa, K., Sonnay, S., Trancikova, A., Tsika, E., Pletnikova, O., Troncoso, J. C., Glauser, L., and Moore, D. J. (2012) PARK9-associated ATP13A2 localizes to intracellular acidic vesicles and regulates cation homeostasis and neuronal integrity, *Hum Mol Genet* 21, 1725-1743.

Ramsey, C. P., and Giasson, B. I. (2010) L10p and P158DEL DJ-1 mutations cause protein instability, aggregation, and dimerization impairments, *J Neurosci Res* 88, 3111-3124.

- Rannikko, E. H., Vesterager, L. B., Shaik, J. H., Weber, S. S., Cornejo Castro, E. M., Fog, K., Jensen, P. H., and Kahle, P. J. (2012) Loss of DJ-1 protein stability and cytoprotective function by Parkinson's disease-associated proline-158 deletion, *J Neurochem*.
- Repici, M., Straatman, K. R., Balduccio, N., Enguita, F. J., Outeiro, T. F., and Giorgini, F. (2013) Parkinson's disease-associated mutations in DJ-1 modulate its dimerization in living cells, *J Mol Med (Berl)* 91, 599-611.
- Roat-Malone, R. M. (2007) *Bioinorganic chemistry : a short course*, 2nd ed. ed., Wiley; Chichester: John Wiley, Hoboken, N.J.
- Rochet, J. C. (2012) New insights into lysosomal dysfunction in Parkinson's disease: an emerging role for ATP13A2, *Mov Disord* 27, 1092.
- Rodriguez-Granillo, A., and Wittung-Stafshede, P. (2009) Differential roles of Met10, Thr11, and Lys60 in structural dynamics of human copper chaperone Atox1, *Biochemistry* 48, 960-972.
- Ross, C. A., and Poirier, M. A. (2004) Protein aggregation and neurodegenerative disease, *Nat Med* 10 Suppl, S10-17.
- Saito, Y., Nishio, K., Ogawa, Y., Kinumi, T., Yoshida, Y., Masuo, Y., and Niki, E. (2007) Molecular mechanisms of 6-hydroxydopamine-induced cytotoxicity in PC12 cells: involvement of hydrogen peroxide-dependent and -independent action, *Free Radic Biol Med* 42, 675-685.
- Schapira, A. H. (1993) Mitochondrial complex I deficiency in Parkinson's disease, *Adv Neurol* 60, 288-291.
- Schapira, A. H., Cooper, J. M., Dexter, D., Clark, J. B., Jenner, P., and Marsden, C. D. (1990) Mitochondrial complex I deficiency in Parkinson's disease, *J Neurochem* 54, 823-827.
- Schmidt, P. J., Rae, T. D., Pufahl, R. A., Hamma, T., Strain, J., O'Halloran, T. V., and Culotta, V. C. (1999) Multiple protein domains contribute to the action of the copper chaperone for superoxide dismutase, *J Biol Chem* 274, 23719-23725.
- Schneider, S. A., Paisan-Ruiz, C., Quinn, N. P., Lees, A. J., Houlden, H., Hardy, J., and Bhatia, K. P. (2010) ATP13A2 mutations (PARK9) cause neurodegeneration with brain iron accumulation, *Mov Disord* 25, 979-984.
- Schweitzer, K. J., Brussel, T., Leitner, P., Kruger, R., Bauer, P., Voitalla, D., Tomiuk, J., Gasser, T., and Berg, D. (2007) Transcranial ultrasound in different monogenetic subtypes of Parkinson's disease, *J Neurol* 254, 613-616.
- Shaikh, S., and Nicholson, L. F. (2008) Advanced glycation end products induce in vitro cross-linking of alpha-synuclein and accelerate the process of intracellular inclusion body formation, *J Neurosci Res* 86, 2071-2082.

- Shendelman, S., Jonason, A., Martinat, C., Leete, T., and Abeliovich, A. (2004) DJ-1 is a redox-dependent molecular chaperone that inhibits alpha-synuclein aggregate formation, *PLoS Biol* 2, 1764-1773.
- Shimizu, K., Ohtaki, K., Matsubara, K., Aoyama, K., Uezono, T., Saito, O., Suno, M., Ogawa, K., Hayase, N., Kimura, K., and Shiono, H. (2001) Carrier-mediated processes in blood--brain barrier penetration and neural uptake of paraquat, *Brain Res* 906, 135-142.
- Smythies, J., and Galzigna, L. (1998) The oxidative metabolism of catecholamines in the brain: a review, *Biochim Biophys Acta* 1380, 159-162.
- Soper, J. H., Kehm, V., Burd, C. G., Bankaitis, V. A., and Lee, V. M. (2011) Aggregation of alpha-synuclein in *S. cerevisiae* is associated with defects in endosomal trafficking and phospholipid biosynthesis, *J Mol Neurosci* 43, 391-405.
- Spillantini, M. G., Schmidt, M. L., Lee, V. M., Trojanowski, J. Q., Jakes, R., and Goedert, M. (1997) Alpha-synuclein in Lewy bodies, *Nature* 388, 839-840.
- Subedi, K. P., Choi, D., Kim, I., Min, B., and Park, C. (2011) Hsp31 of *Escherichia coli* K-12 is glyoxalase III, *Mol Microbiol* 81, 926-936.
- Sun, S. Y., An, C. N., and Pu, X. P. (2012) DJ-1 protein protects dopaminergic neurons against 6-OHDA/MG-132-induced neurotoxicity in rats, *Brain Res Bull* 88, 609-616.
- Taira, T., Saito, Y., Niki, T., Iguchi-Ariga, S. M., Takahashi, K., and Ariga, H. (2004) DJ-1 has a role in antioxidative stress to prevent cell death, *EMBO Rep* 5, 213-218.
- Taira, T., Takahashi, K., Kitagawa, R., Iguchi-Ariga, S. M., and Ariga, H. (2001) Molecular cloning of human and mouse DJ-1 genes and identification of Sp1-dependent activation of the human DJ-1 promoter, *Gene* 263, 285-292.
- Takahashi, R. N., Rogerio, R., and Zanin, M. (1989) Maneb enhances MPTP neurotoxicity in mice, *Res Commun Chem Pathol Pharmacol* 66, 167-170.
- Takahashi, K., Taira, T., Niki, T., Seino, C., Iguchi-Ariga, S. M., and Ariga, H. (2001) DJ-1 positively regulates the androgen receptor by impairing the binding of PIASx alpha to the receptor, *J Biol Chem* 276, 37556-37563.
- Takahashi-Niki, K., Niki, T., Taira, T., Iguchi-Ariga, S. M., and Ariga, H. (2004) Reduced anti-oxidative stress activities of DJ-1 mutants found in Parkinson's disease patients, *Biochem Biophys Res Commun* 320, 389-397.
- Tanaka, N., Smith, P., and Shuman, S. (2010) Structure of the RNA 3'-phosphate cyclase-adenylate intermediate illuminates nucleotide specificity and covalent nucleotidyl transfer, *Structure* 18, 449-457.
- Tang, B., Xiong, H., Sun, P., Zhang, Y., Wang, D., Hu, Z., Zhu, Z., Ma, H., Pan, Q., Xia, J. H., Xia, K., and Zhang, Z. (2006) Association of PINK1 and DJ-1 confers digenic inheritance of early-onset Parkinson's disease, *Hum Mol Genet* 15, 1816-1825.

- Tao, X., and Tong, L. (2003) Crystal structure of human DJ-1, a protein associated with early onset Parkinson's disease, *J Biol Chem* 278, 31372-31379.
- Tawara, T., Fukushima, T., Hojo, N., Isobe, A., Shiwaku, K., Setogawa, T., and Yamane, Y. (1996) Effects of paraquat on mitochondrial electron transport system and catecholamine contents in rat brain, *Arch Toxicol* 70, 585-589.
- Thiruchelvam, M., Prokopenko, O., Cory-Slechta, D. A., Buckley, B., and Mirochnitchenko, O. (2005) Overexpression of superoxide dismutase or glutathione peroxidase protects against the paraquat + maneb-induced Parkinson disease phenotype, *J Biol Chem* 280, 22530-22539.
- Thiruchelvam, M., Richfield, E. K., Baggs, R. B., Tank, A. W., and Cory-Slechta, D. A. (2000) The nigrostriatal dopaminergic system as a preferential target of repeated exposures to combined paraquat and maneb: implications for Parkinson's disease, *J Neurosci* 20, 9207-9214.
- Thornalley, P. J. (2003) Glyoxalase I--structure, function and a critical role in the enzymatic defence against glycation, *Biochem Soc Trans* 31, 1343-1348.
- Thornalley, P. J., Langborg, A., and Minhas, H. S. (1999) Formation of glyoxal, methylglyoxal and 3-deoxyglucosone in the glycation of proteins by glucose, *Biochem J* 344 Pt 1, 109-116.
- Thornalley, P. J. (1990) The glyoxalase system: new developments towards functional characterization of a metabolic pathway fundamental to biological life, *Biochem J* 269, 1-11.
- Tsuboi, Y., Munemoto, H., Ishikawa, S., Matsumoto, K., Iguchi-Arigo, S. M., and Ariga, H. (2008) DJ-1, a causative gene product of a familial form of Parkinson's disease, is secreted through microdomains, *FEBS Lett* 582, 2643-2649.
- Uversky, V. N., Li, J., and Fink, A. L. (2001) Metal-triggered structural transformations, aggregation, and fibrillation of human alpha-synuclein. A possible molecular link between Parkinson's disease and heavy metal exposure, *J Biol Chem* 276, 44284-44296.
- Valente, E. M., Abou-Sleiman, P. M., Caputo, V., Muqit, M. M., Harvey, K., Gispert, S., Ali, Z., Del Turco, D., Bentivoglio, A. R., Healy, D. G., Albanese, A., Nussbaum, R., Gonzalez-Maldonado, R., Deller, T., Salvi, S., Cortelli, P., Gilks, W. P., Latchman, D. S., Harvey, R. J., Dallapiccola, B., Auburger, G., and Wood, N. W. (2004) Hereditary early-onset Parkinson's disease caused by mutations in PINK1, *Science* 304, 1158-1160.
- van der Brug, M. P., Blackinton, J., Chandran, J., Hao, L. Y., Lal, A., Mazan-Mamczarz, K., Martindale, J., Xie, C., Ahmad, R., Thomas, K. J., Beilina, A., Gibbs, J. R., Ding, J., Myers, A. J., Zhan, M., Cai, H., Bonini, N. M., Gorospe, M., and Cookson, M. R. (2008) RNA binding activity of the recessive parkinsonism protein DJ-1 supports involvement in multiple cellular pathways, *Proc Natl Acad Sci U S A* 105, 10244-10249.

- Vranken, W. F., Boucher, W., Stevens, T. J., Fogh, R. H., Pajon, A., Llinas, M., Ulrich, E. L., Markley, J. L., Ionides, J., and Laue, E. D. (2005) The CCPN data model for NMR spectroscopy: development of a software pipeline, *Proteins* 59, 687-696.
- Vives-Bauza, C., Zhou, C., Huang, Y., Cui, M., de Vries, R. L., Kim, J., May, J., Tocilescu, M. A., Liu, W., Ko, H. S., Magrane, J., Moore, D. J., Dawson, V. L., Grailhe, R., Dawson, T. M., Li, C., Tieu, K., and Przedborski, S. (2010) PINK1-dependent recruitment of Parkin to mitochondria in mitophagy, *Proc Natl Acad Sci U S A* 107, 378-383.
- Wang, L. K., Lima, C. D., and Shuman, S. (2002) Structure and mechanism of T4 polynucleotide kinase: an RNA repair enzyme, *EMBO J* 21, 3873-3880.
- Wang, H., Liu, J., and Wu, L. (2009) Methylglyoxal-induced mitochondrial dysfunction in vascular smooth muscle cells, *Biochem Pharmacol* 77, 1709-1716. Wang, C., Liu, L., Zhang,
- Wang, C., Liu, L., Zhang, L., Peng, Y., and Zhou, F. (2010) Redox reactions of the alpha-synuclein-Cu(2+) complex and their effects on neuronal cell viability, *Biochemistry* 49, 8134-8142.
- Webber, P. J., and West, A. B. (2009) LRRK2 in Parkinson's disease: function in cells and neurodegeneration, *FEBS J* 276, 6436-6444.
- Wells-Knecht, K. J., Zyzak, D. V., Litchfield, J. E., Thorpe, S. R., and Baynes, J. W. (1995) Mechanism of autoxidative glycosylation: identification of glyoxal and arabinose as intermediates in the autoxidative modification of proteins by glucose, *Biochemistry* 34, 3702-3709.
- Wernimont, A. K., Huffman, D. L., Lamb, A. L., O'Halloran, T. V., and Rosenzweig, A. C. (2000) Structural basis for copper transfer by the metallochaperone for the Menkes/Wilson disease proteins, *Nat Struct Biol* 7, 766-771.
- Willis, A. W., Evanoff, B. A., Lian, M., Galarza, A., Wegrzyn, A., Schootman, M., and Racette, B. A. (2010) Metal emissions and urban incident Parkinson disease: a community health study of Medicare beneficiaries by using geographic information systems, *Am J Epidemiol* 172, 1357-1363.
- Wilson, M. A., Collins, J. L., Hod, Y., Ringe, D., and Petsko, G. A. (2003) The 1.1-Å resolution crystal structure of DJ-1, the protein mutated in autosomal recessive early onset Parkinson's disease, *Proc Natl Acad Sci U S A* 100, 9256-9261.
- Wilson, M. A. (2011) The role of cysteine oxidation in DJ-1 function and dysfunction, *Antioxid Redox Signal* 15, 111-122.
- Witt, A. C., Lakshminarasimhan, M., Remington, B. C., Hasim, S., Pozharski, E., and Wilson, M. A. (2008) Cysteine pKa depression by a protonated glutamic acid in human DJ-1, *Biochemistry* 47, 7430-7440.

- Wong, P. C., Waggoner, D., Subramaniam, J. R., Tessarollo, L., Bartnikas, T. B., Culotta, V. C., Price, D. L., Rothstein, J., and Gitlin, J. D. (2000) Copper chaperone for superoxide dismutase is essential to activate mammalian Cu/Zn superoxide dismutase, *Proc Natl Acad Sci U S A* 97, 2886-2891.
- Woo, H. A., Jeong, W., Chang, T. S., Park, K. J., Park, S. J., Yang, J. S., and Rhee, S. G. (2005) Reduction of cysteine sulfinic acid by sulfiredoxin is specific to 2-cys peroxiredoxins, *J Biol Chem* 280, 3125-3128.
- Wood, Z. A., Schroder, E., Robin Harris, J., and Poole, L. B. (2003) Structure, mechanism and regulation of peroxiredoxins, *Trends Biochem Sci* 28, 32-40.
- Wright, J. A., Wang, X., and Brown, D. R. (2009) Unique copper-induced oligomers mediate alpha-synuclein toxicity, *FASEB J* 23, 2384-2393.
- Wu, D. C., Teismann, P., Tieu, K., Vila, M., Jackson-Lewis, V., Ischiropoulos, H., and Przedborski, S. (2003) NADPH oxidase mediates oxidative stress in the 1-methyl-4-phenyl-1,2,3,6-tetrahydropyridine model of Parkinson's disease, *Proc Natl Acad Sci U S A* 100, 6145-6150.
- Xiao, Z., Brose, J., Schimo, S., Ackland, S. M., La Fontaine, S., and Wedd, A. G. (2011) Unification of the copper(I) binding affinities of the metallo-chaperones Atx1, Atox1, and related proteins: detection probes and affinity standards, *J Biol Chem* 286, 11047-11055.
- Xiao, Z., and Wedd, A. G. (2010) The challenges of determining metal-protein affinities, *Nat Prod Rep* 27, 768-789.
- Xu, X. M., Lin, H., Maple, J., Bjorkblom, B., Alves, G., Larsen, J. P., and Moller, S. G. (2010) The Arabidopsis DJ-1a protein confers stress protection through cytosolic SOD activation, *J Cell Sci* 123, 1644-1651.
- Xu, J., Zhong, N., Wang, H., Elias, J. E., Kim, C. Y., Woldman, I., Piffl, C., Gygi, S. P., Geula, C., and Yankner, B. A. (2005) The Parkinson's disease-associated DJ-1 protein is a transcriptional co-activator that protects against neuronal apoptosis, *Hum Mol Genet* 14, 1231-1241.
- Yamashita, S., Mori, A., Kimura, E., Mita, S., Maeda, Y., Hirano, T., and Uchino, M. (2010) DJ-1 forms complexes with mutant SOD1 and ameliorates its toxicity, *J Neurochem* 113, 860-870.
- Yang, D. J., Shi, S., Zheng, L. F., Yao, T. M., and Ji, L. N. (2010) Mercury(II) promotes the in vitro aggregation of tau fragment corresponding to the second repeat of microtubule-binding domain: Coordination and conformational transition, *Biopolymers* 93, 1100-1107.
- Yang, W., Chen, L., Ding, Y., Zhuang, X., and Kang, U. J. (2007) Paraquat induces dopaminergic dysfunction and proteasome impairment in DJ-1-deficient mice, *Hum Mol Genet* 16, 2900-2910.

Zhong, N., Kim, C. Y., Rizzu, P., Geula, C., Porter, D. R., Pothos, E. N., Squitieri, F., Heutink, P., and Xu, J. (2006) DJ-1 transcriptionally up-regulates the human tyrosine hydroxylase by inhibiting the sumoylation of pyrimidine tract-binding protein-associated splicing factor, *J Biol Chem* 281, 20940-20948.

Zhong, N., and Xu, J. (2008) Synergistic activation of the human MnSOD promoter by DJ-1 and PGC-1alpha: regulation by SUMOylation and oxidation, *Hum Mol Genet* 17, 3357-3367.

Zhou, L., Singleton, C., and Le Brun, N. E. (2008) High Cu(I) and low proton affinities of the CXXC motif of Bacillus subtilis CopZ, *Biochem J* 413, 459-465.

Zhou, W., Zhu, M., Wilson, M. A., Petsko, G. A., and Fink, A. L. (2006) The oxidation state of DJ-1 regulates its chaperone activity toward alpha-synuclein, *J Mol Biol* 356, 1036-1048.

Zhou, W., and Freed, C. R. (2005) DJ-1 up-regulates glutathione synthesis during oxidative stress and inhibits A53T alpha-synuclein toxicity, *J Biol Chem* 280, 43150-43158.

Zimprich, A., Biskup, S., Leitner, P., Lichtner, P., Farrer, M., Lincoln, S., Kachergus, J., Hulihan, M., Uitti, R. J., Calne, D. B., Stoessl, A. J., Pfeiffer, R. F., Patenge, N., Carbajal, I. C., Vieregge, P., Asmus, F., Muller-Myhsok, B., Dickson, D. W., Meitinger, T., Strom, T. M., Wszolek, Z. K., and Gasser, T. (2004) Mutations in LRRK2 cause autosomal-dominant parkinsonism with pleomorphic pathology, *Neuron* 44, 601-607.